3D User Interfaces for Interventional Support and Medical Education

DISSERTATION

zur Erlangung des akademischen Grades

Doktoringenieur (Dr.-Ing.)

angenommen durch die

Fakultät für Informatik der Otto-von-Guericke-Universität Magdeburg

von Patrick Saalfeld, M. Sc.
geb. am 11.12.1987 in Quedlinburg

Gutachter:

Prof. Dr.-Ing. Bernhard Preim
Prof. Dr. rer. nat. Bernd Fröhlich
Prof. Dr. rer. nat. Torsten Wolfgang Kuhlen

Magdeburg, den 16.11.2018

ZUSAMMENFASSUNG

Räumliche Benutzungsschnittstellen haben das Potential, die Interaktion mit medizinischen Strukturen in verschiedenen medizinischen Bereichen zu verbessern. Diese Dissertation präsentiert Interaktionstechniken sowie Ein- und Ausgabegeräte, welche Ärzte bei der Durchführung von Interventionen unterstützen, Studierenden und Dozenten während der medizinischen Ausbildung helfen sowie Ärzten und Patienten ermöglichen, den Prozess der Patientenaufklärung zu verbessern.

Zur Unterstützung von Ärzten während der Durchführung von Interventionen werden Freihand-Gesten präsentiert, welche eine berührungslose und somit sterile Interaktion mit Bildgebungssoftware ermöglichen. Dies erlaubt die Analyse von Patienten-spezifischen Daten während des Eingriffs auf sterile Weise. Die Bereiche der Patientenaufklärung, medizinischen Ausbildung und Therapieplanung werden durch die natürliche Interaktionstechnik des Skizzierens unterstützt. Dazu werden Methoden präsentiert, die das echtzeitfähige Erzeugen von zwei- und dreidimensionalen vaskulären Strukturen, deren Erkrankungen und Behandlungsmethoden sowie des Blutflusses ermöglichen. Hierfür wird ein interaktives Whiteboard genutzt sowie das zSpace, welches räumliche Ein- und Ausgabegeräte verwendet.

Zusätzlich werden in dieser Dissertation Richtlinien für die Evaluierung von interaktiven medizinischen Visualisierungen vorgestellt. Hierzu werden quantitative und qualitative Methoden vorgestellt, Empfehlungen für die Erhebung von Daten, der Definition von Aufgaben und des Studiendesigns gegeben und schließlich die Auswahl geeigneter statistischer Tests unterstützt.

Die durchgeführten Studien in dieser Dissertation folgen diesen Richtlinien, wodurch es möglich ist, die entwickelten Prototypen quantitativ und qualitativ zu bewerten. Die vorgestellten Methoden zeigen das Potential der berührungslosen Interaktion mit medizinischen Bilddaten. Weiterhin ermöglichen sie, die Patientenaufklärung zu verbessern und das Verständnis für die Auswirkung verschiedener Behandlungsstrategien zu erhöhen. Schließlich erlauben die vorgestellten Methoden, Studierende beim Begreifen von Besonderheiten und räumlichen Zusammenhängen vaskulärer Strukturen zu unterstützen.

ABSTRACT

Spatial user interfaces hold the opportunity to improve the interaction with medical structures in several domains. This thesis presents spatial input and output devices as well as interaction techniques that support physicians during interventions, students and teachers in medical education, and patients and physicians during patient education.

Physicians are supported with freehand gestures that are used as a touchless interaction technique to control interventional imaging software. This enables them to investigate patient's radiographic scans during interventions in a sterile manner. Patient education, medical teaching and therapy planning are supported with the natural interaction technique of sketching. Here, approaches are presented to sketch vascular structures, pathologies, treatment options and blood flow in real-time, either as 2D or 3D structures. For this purpose, an interactive whiteboard and a spatial input and output device is used (namely the zSpace).

Furthermore, this thesis presents general guidelines for the evaluation of interactive medical visualizations. This comprises quantitative and qualitative methods, directives for the collection of data, the definition of tasks and experimental designs as well as the selection of appropriate statistical tests.

The conducted evaluations within this thesis follow these guidelines, which allows to assess them with quantitative and qualitative aspects. The presented prototypes show the potential for touchless interaction with medical image data, the chance to support patients in understanding the impact of different treatment strategies, and the opportunity in helping students to learn particularities and spatial relationships of vascular configurations.

CONTENTS

ACRONYMS

3DUI 3D User Interface

ANOVA Analysis of Variance

AR Augmented Reality

CAVE Cave Automatic Virtual Environment

CPR Curved Planar Reformation

COW Circle of Willis

CT Computer Tomography

CVD Cardiovascular Diseases

DOF Degree of Freedom

FOV Field of View

FOR Field of Regard

GPU Graphics Processing Unit

GUI Graphical User Interface

HCI Human Computer Interaction

HMD Head-mounted Display

HWD Head-worn Display

IR infrared

IQR interquartile range

LMC Leap Motion Controller

MDCT multi-detector computed tomography

MPU multi-level partition unity

MRI Magnetic Resonance Imaging

NPR Non-photorealistic Rendering

NUI Natural User Interface

RBI Reality-based Interaction

SBI Sketch-based Interface

SBM Sketch-based Modeling

SDK Software Development Kit

SUS System Usability Scale

TOF Time of Flight

UI User Interface

VE Virtual Environment

VR Virtual Reality

INTRODUCTION

> Machines require us to be precise
> and accurate, things we are not
> very good at.
>
> *Donald Norman* – The Design of
> Everyday things, revised and
> expanded edition [183]

3D SPACE is familiar and natural to all of us – we spend our whole life living inside a spatial world and have learned how to navigate in it, manipulate three-dimensional objects and understand their relationships [119]. 3D User Interfaces (3DUIs) take advantage of these developed skills. They comprise different input and output devices as well as interaction techniques that allow the *direct* exploration of spatial data in real or virtual 3D space [146, 207].

In medical domains, such as interventional radiology and anatomy education, medical structures are important in their three-dimensional form. For treatment planning and during interventions, radiographic patient data are available as 2D slices and 3D volumes. In anatomy education, students learn with 3D models and illustrations that give a spatial impression. These domains are predestined for the usage of 3DUIs. However, common methods to interact with radiographic data are based on 2D input devices. Furthermore, patient-specific data is primarily visualized as image slices only on 2D displays. Here, important depth cues cannot be used to evaluate pathologies and elaborate treatment options. In medical education, the situation is similar. The primary source for learning are anatomy atlases that contain 2D illustrations of 3D anatomical structures. Natural depth cues that are obtained through binocular vision and motion parallax cannot be used on these illustrations.

1.1 CONTRIBUTIONS

This thesis presents 3DUIs comprising interaction techniques, input devices and output devices to support physicians, teachers, students, and patients in inter-

ventional radiology, treatment planning, as well as medical and patient education. For *interventional support*, freehand gestures are presented as they allow a touchless and, thus, sterile interaction with the software that controls and displays the patient's radiographic images. Typical tasks of interventional radiology such as exploration and measurement of medical image data are considered. The developed gestures focus on spatial and natural movements that mimic real-world gestures. Additionally, the physician is supported with features that facilitate the execution and memorizing of these gestures.

For medical education and treatment planning, the interaction technique of sketching is used to support physicians, patients, teachers and students. Sketching as an input modality represents an easy and natural alternative to traditional input paradigms [191]. Sketching allows to *externalize* ideas by putting thoughts on paper in the form of scribbles – although imprecise, they allow an elemental way of human communication. *Patient education* is supported with an approach usable on tablets and interactive whiteboards to sketch 2D vessels, pathologies, treatment options and blood flow. The developed prototype supports physicians to explain and patients to understand different treatment strategies for vascular pathologies. For *teaching*, a spatial input and output device is used to support anatomy and pathology education by allowing the creation of 3D vessels with integrated blood flow. This provides anatomy educators with a novel tool to create and explain complex spatial relationships of interlinked vascular structures and blood flow behavior. *Treatment planning* is facilitated with a spatial input and output device to allow physicians to explore and analyze vascular structures and sketch free-form annotations on 3D planning models. This enables the physician to illustrate various treatment options.

Interactive medical applications such as the presented prototypes of this thesis have to be evaluated to assess their value. This is primarily realized with qualitative methods [114], whereby, e.g. a low number of non-domain experts are interviewed. Based on the obtained results, a beneficial impact is deduced. However, the validity of these results is limited, since the improvement is not quantified and the generalization is restricted to the small borders of the evaluation setting. As an alternative, this thesis presents guidelines for the evaluation of interactive medical visualizations, focusing on quantitative methods that allow collecting measurable and comparable properties. These methods are applied and combined with qualitative approaches to assess the developed prototypes of this thesis.

1.2 STRUCTURE

This thesis is organized as follows:

- **Chapter 2** – This chapter gives an overview of interaction tasks, techniques and their usage in medical applications. The provided background

is the basis for advanced interaction techniques that are applied in this thesis, i.e. gestures, labeling, and sketching. A technical discussion of input and output devices for gesture recognition and sketching concludes the chapter.

- **Chapter 3** – In this chapter, foundations for the evaluation of interactive medical visualization systems are provided. Besides giving an overview of evaluation strategies, quantitative evaluation methods are investigated in detail. Furthermore, guidelines for the planning of an evaluation as well as the collection and analysis of the obtained data are discussed and summarized in a decision tree.

- **Chapter 4** – This chapter presents freehand gestures for the touchless and sterile interaction with radiologic workstation software to inspect patient-specific image data. Additionally, medical background information on interventional radiology are given and important interaction tasks during interventions are identified. The chapter concludes with a comparative evaluation of the used gestures against established interaction techniques.

- **Chapter 5** – The fifth chapter presents sketching techniques for the 2D illustration of vascular structures, pathologies, treatment options and real-time blood flow. The described techniques can be applied on whiteboards as well as graphic tablets to support physicians and patients in the process of patient education. For the understanding of vascular pathologies, background information on the cardiovascular system are provided. Additionally, the mathematical foundations on blood flow simulations are described. A mixed design evaluation is used to assess the usefulness of the developed prototype and concludes the chapter.

- **Chapter 6** – In this chapter, methods are presented to sketch a wide variety of vascular structures in different body areas and to illustrate common vascular diseases. These methods are developed to support medical education. The user is facilitated with a spatial input and output device to provide additional depth cues during 3D sketching. As background information, the chapter introduces foundations of medical education and its development. After that, the mathematical background of implicit surfaces is described and how they can be used to create vascular structures. The chapter concludes with an evaluation that uses quantitative and qualitative approaches.

- **Chapter 7** – This chapter presents techniques to spatially sketch generic annotations on dynamic 3D medical structures. These techniques are able to support physicians in the process of treatment planning. Again, a spatial input and output device is used to improve the perception of depth and to facilitate the physician in creating free-form annotations in space. As

background information, this chapter provides details on the unfolding and animation of 3D medical structures to create dynamic data. The chapter concludes with a mixed-design evaluation and a description of a possible integration of the prototype into clinical practice.

- **Chapter** 8 – The final chapter concludes the thesis by providing a summary and discussion of the contributions that were made. Furthermore, possibilities for future work are presented.

3D INTERACTION FOR INTERVENTIONAL SUPPORT & MEDICAL EDUCATION

T HIS chapter gives an overview of basic interaction tasks, techniques and their use in medical applications. On this basis, the advanced interaction tasks and techniques relevant in this thesis are discussed, i.e.:

- gestures (see Section 2.2.1)),

- labeling (see Section 2.2.2), and

- sketching (Section 2.2.3).

A technical discussion of input and output devices that are used for gestures and sketching concludes the chapter. The presented work focuses on spatial input and output. For an overview of non-spatial interaction techniques, tasks and their evaluation, the reader is referred to the survey of Chris Hand from 1997 [89] and to the more recent survey and its extension from Jankowski and Hachet (2013/2015) [119, 120]. The recent survey from Mendes et al. [162] from 2018 presents spatial object manipulation techniques realized with traditional desktop approaches, touch and mid-air interfaces and Virtual Environments (VEs). Tasks that are specialized to volume data, such as editing transfer functions or the positioning of clipping planes are not further discussed, since the majority of the data sets used in this thesis are surface models. The reader is referred to the book of Preim and Botha [203] for a detailed discussion of advanced interaction tasks with medical volumetric data.

2.1 BASIC INTERACTION

Basic 3D interaction tasks in the medical domain can be derived from interaction tasks presented in-depth in the 3DUI books from Bowman et al. [31] and LaViola Jr. et al. [146]. These tasks comprise:

- selection and manipulation,

- travel,

- wayfinding,

- system control, and

- symbolic input.

The former book from Bowman et al. dedicates a whole chapter to each task, whereby the latter reduced these to three chapters, integrating "wayfinding" into "travel" and "symbolic input" into "system control". For the interaction with medical data, the *selection* and *manipulation* of objects is most important. Thus, these aspects are discussed in detail in the following. A general look on 3DUIs, including their application and development challenges, can be found in the survey of Takala et al. [259]. Their comprehensive survey is based on data from 71 3DUI developers and 56 3DUI applications.

2.1.1 *Selection*

In interactive medical visualizations, the possibility to select points on surfaces, regions and objects plays a fundamental role [203]. For example, selecting positions is a prerequisite to interactively measure objects in treatment planning, and selecting an object by picking is essential to learn its name and purpose in computer-assisted anatomy education.

If a spatial input device is used, a way to select objects in space is beneficial. One natural and intuitive way is *grabbing*. However, only objects in the user's reach can be grabbed directly. For remote objects, either a possibility to navigate to this object is necessary or a remote grabbing technique can be used. Two categories for remote grabbing were presented and evaluated by Bowman and Hodges [30]:

- arm-extension techniques and

- ray-casting techniques.

Arm-extension means that the user's arm virtually "grows" to the desired length. These techniques make manipulation simple, because similar natural arm and hand motions can be used as for objects in close distance. With ray-casting, a virtual ray is send out from the input device and objects that got hit by the ray can be grabbed. This interaction can be performed easily, since the user only has to point in the direction of the desired object. In the mentioned study from Bowman and Hodges [30], almost all users preferred the ray-casting technique, as no arm stretching and less effort regarding precision is necessary. Therefore, mostly ray-based interaction techniques are used for selection and manipulation in this thesis.

Another important aspect for selection is *user support* that helps selecting specially formed objects, such as vascular structures that are long and thin. The necessity to support the user with such structures can be derived from *Fitts's law* [68]: based on the distance between cursor and object as well as the object's

(a)   (b)
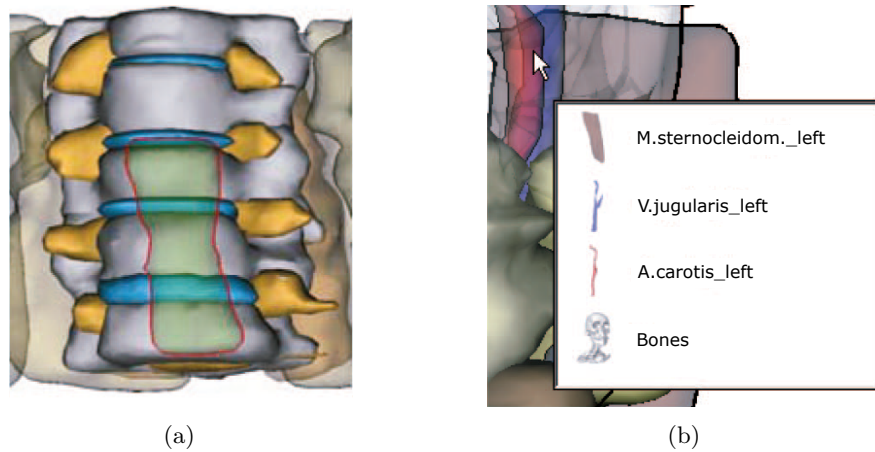
Figure 2.1: Selection support is necessary when structures overlay each other, such as the transparent esophagus in (a). Mühler et al. [172] solve this with a relevance factor calculation for each structure, based on the size and transparency of an object. If the selection is still ambiguous, a list can be shown to the user (b). Images (a) and (b) from Mühler et al. [172] © IEEE 2010.

width, the time to select the object can be predicted. According to the law, the time increases with thin objects. Another reason for user support are noisy input modalities such as free-hand gestures. One approach is to artificially increase the selection space around objects. A solution in the object domain would be to store an invisible larger bounding volume with each structure [234], which was presented by the author of this thesis. Alternatively, the problem can be transferred to image-space. Here, each structure can be rendered with a distinct color in an off-screen buffer [248]. Then, morphological operations such as repeated dilation can be applied to the image to increase the selection area (the opposite, i.e. erosion, was used by Mühler et al. [171] to find the center point of a structure). Besides enlarging the selection space of an object, the *selection volume* can be changed, e.g. from a ray to a cone [202] or all selectable objects can be placed in a miniature copy of the environment (i.e. world in miniature) [257]. A problem occurs if objects are occluded by others, e.g. the esophagus can occlude vertebras and intervertebral discs (see Figure 2.1a). Rendering all objects simultaneously, even with transparency, results in an ambiguous selection. Here, Mühler et al. [172] calculated a relevance factor per object based on its transparency and size: opaque objects are favored since this follows the user's expectation, and small objects are favored since they are more difficult to select. If the selection is still ambiguous, a list with possibilities can be shown (see Figure 2.1b). Another solution is *layer-based selection* that is inspired by the anatomic dissection course. Here, layers of structures can be *peeled off* subsequently to reveal inner structures [210]. In anatomy education applications, selection can often additionally be performed indirectly by a hierarchical list that allows the selection of single structures or whole categories such as nerves and arteries. This enables

the user to quickly show or hide groups of structures. Further ways to support the user during selection are snapping or highlighting the hit object with some form of emphasis [203].

2.1.2 *Manipulation*

Object manipulation is a key element in spatial environments as it allows users to naturally grab, translate and rotate objects similar to how it is done in the physical world [163]. This section describes different techniques for:

- translation,

- rotation,

- simultaneous and separated translation and rotation, respectively, and

- scaling.

2.1.2.1 *Translation*

The translation of objects can happen directly or indirectly, whereas direct translation transfers the movement of the input device directly to the object. This is easy and intuitive for ray-based interaction: the selected object is pinned to the hitting point of the ray and object and then follows its movement. However, the precision and movement range can be restricted. Here, the already mentioned techniques for user support for selection can be used, e.g. the objects can be manipulated in a world in miniature. Additionally, the manipulation can be supported by snapping methods, e.g. objects snap on other objects or on a grid. Besides direct methods, indirect methods such as 3D widgets or handles on objects can be used. However, Teather and Stuerzlinger [263] advise against this in their work on general guidelines for 3D positioning techniques. They state that the paradigm of direct manipulation is easier to understand. This, however, primarily relates to novice users. They further state that objects should not be allowed to interpenetrate each other. While this is beneficial for treatment planning scenarios, it can represent an unnecessary hurdle in domains such as medical education. When planning the access path of an applicator in radiofrequency ablations of vertebral metastases, the applicator should only be allowed to penetrate the vertebra at specific points [165]. Therefore, a restriction of the ability to penetrate the vertebra is helpful. In anatomy education, the learning gain is of primary importance, so a simplification of real-world behavior can be desirable. This is the case in the 3D jigsaw puzzle from Ritter et al. [219, 220]. Placing puzzle pieces is less frustrating when small inner lying pieces can be placed without moving or being obstructed by other pieces.

2.1.2.2 *Rotation*

Unrestricted rotation is an important feature for interventional tasks and education, since it allows to inspect and explore structures from different angles. However, a realization with 2D displays and 2D input devices can be tricky, which can be seen by observing medical doctors trying to adjust the viewing direction in a tedious trial-and-error process [203]. There are several rotation techniques implemented in medical applications. They differ in the way the 2D input is mapped to the resulting rotation. A simple approach is to map the x- and y-movement of the mouse directly to two rotation axes of the object. Another, more flexible approach is the *virtual trackball* [44], where the mouse position is projected onto an invisible sphere that is positioned around the object. As long as the mouse cursor moves on this sphere, the object rotates around the movement delta of the azimuth and elevation of the sphere, resulting in rotations of two axes. If the cursor leaves the invisible sphere, the object is rotated around the remaining third axis, allowing for a more controlled rotation. Chen et al. [44] compared this and three additional rotation techniques, e.g. with indirect slider-based rotation. They could show that the *virtual trackball* was superior for complex rotation tasks regarding time and accuracy. Therefore, this technique and variations of it are implemented in the majority of medical viewing software[1].

However, this approach has a major disadvantage, since a 3D rotation is not handled in a transitive manner. This means that two consecutive movements of an input device from point *A* to *B* and from *B* to *C* can result in a different final rotation as moving the device directly from *A* to *C*. This violates one of four key principles that are stated as important in radiological workstations and therapy planning systems by Bade et al. [12]. In their comparative user study, they tested extensions of the virtual trackball as well as the *Two-Axis Valuator*. This technique maps horizontal mouse movement to a rotation around the up-vector of the virtual camera. Additionally, the vertical mouse movement is mapped to a rotation around the vector perpendicular to the up-vector and the view-vector of the camera. It turned out to be the best 3D rotation technique with respect to speed and user satisfaction. Interestingly, rotations of this technique are also non-transitive and violate one of their key principles equally to Chen's original virtual trackball.

Spatial input devices allow to use more Degree of Freedom (DoF) and, thus, a more intuitive rotation. A simple rotation technique is an egocentric one, where the orientation of the input device is directly mapped to a 3D object. However, cables of input devices and anisotropic sampling (precision varies depending on the direction) make an equally precise rotation around all axes difficult. For example, a pen-shaped input device is more difficult to rotate around its longitudinal axis. Another technique that uses a spatial input device and ray-based

---

1 Examples are: Artis zeego (Siemens), OpenInventor (FEI Company), Paraview (Kitware Inc.) and 3DSlicer [62]
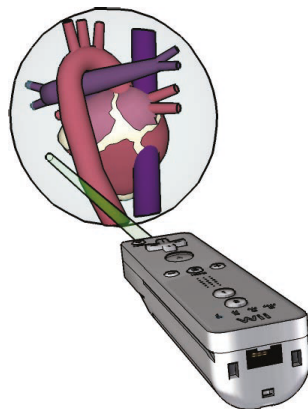
Figure 2.2: The Arcball-3D rotation technique uses a sphere that is fitted around the object. Based on the movement of the ray on the sphere, the structure is rotated [126]. Image from Katzakis et al. [126] © ACM 2013.

interaction is *Arcball-3D* [126], an extension of the mouse-based Arcball [247]. Here, a bounding sphere is fitted around the object (see Figure 2.2). The movement on this sphere is mapped to rotations. In a study conducted by Katzakis et al. [126] the Arcball-3D technique was compared to other ray-based interaction techniques. Almost all participants preferred the *Arcball-3D* rotation, although it was slightly slower than the other techniques. Besides being easy to use, the Arcball-3D technique is suitable for small thin objects, such as vascular structures.

2.1.2.3 *Separated vs. Simultaneous Translation and Rotation*

In medical applications, it is usually necessary to translate and rotate objects. The techniques presented so far can be applied as two independent repeating steps. The separation of the DoF for translation and rotation can be divided further to restrict translation and rotation to specific axes. Such separation was evaluated by Mendes et al. [163] in a VE. They could show that the separation leads to more precise manipulations at the expense of additional time for complex tasks.

The presented techniques can also be extended for simultaneous translation and rotation. An intuitive technique is the already described *pinning* technique for translation. Here, the selected object is additionally rotated around the device itself. This was realized by Baer et al. [15] to train the placement of a prosthesis implant to reconstruct the ossicular chain and, thus, a patient's hearing ability. While this technique is easy to understand, it can be impractical to use if the distance between the virtual object and input device is large. Small rotational changes around the input device's pivot point lead to large translational changes on the object. Another extension can be made to the Arcball-3D technique to allow semi-simultaneous translation and rotation. As long as the user points
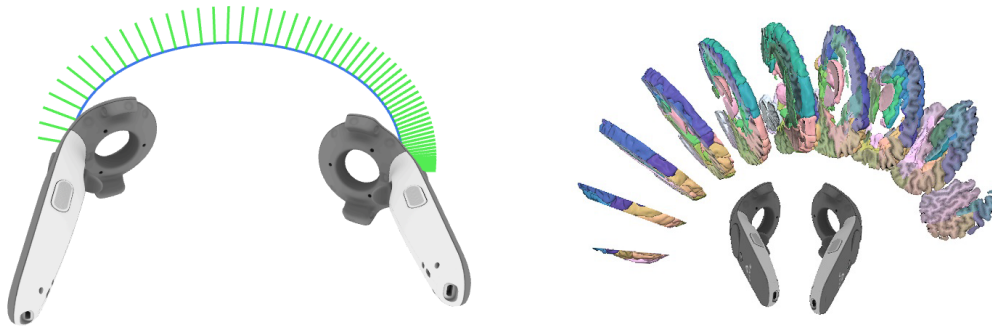
Figure 2.3: Direct object manipulation techniques are used to move and rotate multiple objects at once. A spline between both controllers is spanned to align and orient several slabs of a brain atlas dataset [94]. Images from He and Guayaquil-Sosa [94] © IEEE 2017.

onto the bounding sphere, the object is rotated as already described. If the user leaves the bounding sphere, the object is dragged behind the ray, resulting in translation. Another interesting approach for medical education was presented by He et al. [94]. Instead of manipulating the objects directly, they use two input devices to manipulate a spline that is spanned between the devices. Multiple objects are then aligned on this spline, resulting in simultaneous translation and rotation (see Figure 2.3).

2.1.2.4 *Scaling*

Scaling is also an important way to manipulate objects, since it allows users to change the lifelike size of an object. This is especially important for small structures. Scientific anatomic models of the human eye, for example, are usually available in four times or above of their actual size. An interactive medical application allows for a continuous scaling. Usually, all axes are scaled uniformly, meaning that only 1 DoF of input is necessary. Therefore, scaling is performed with widgets, sliders or with direct input similar to the mentioned ray-based translation. Instead of mapping the movement to translation, the objects are scaled depending on how much the ray is pushed towards or pulled away from it.

2.2   ADVANCED INTERACTION

This section gives an overview of advanced interaction techniques that are used in this thesis. This comprises related work on freehand gestures, labeling, and sketching.
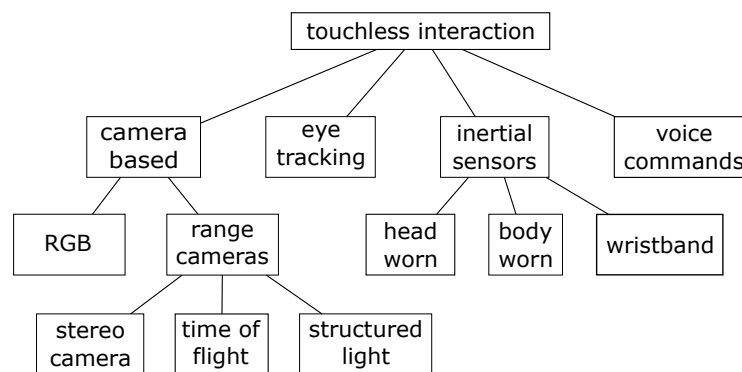
Figure 2.4: Overview of approaches for touchless interaction in interventional radiology. Image from Mewes et al. [166] © Springer International Publishing CARS 2017.

2.2.1 *Freehand Gestures*

Gestures are a crucial part of non-verbal communication. If they are executed freely in space with one or both hands, they are called freehand gestures, natural gestures, and bare hand gestures [207]. As the user's behavior and feeling during interaction is close to real-world actions, they are part of Natural User Interfaces (NUIs). Widgor and Wixon [278] state that freehand gestures are perceived as more natural compared to other interaction techniques. This was also shown in the study of van Beurden et al. [269] for hedonic qualities such as perceived fun and aesthetics. However, in the same study, gestures performed significantly worse regarding pragmatic qualities such as how effective and efficient goals can be achieved. Gestural interaction is also challenging due to the missing haptic feedback and the large space requirement. Furthermore, the accurate and reliable recognition of 3D hand poses and gestures remains a challenging research area [145]. To improve the downsides of gestural interaction, techniques to support the user memorizing and executing them are necessary. This can be achieved by showing the user available gestures and smoothing noisy input data. Such techniques are used and described later in Chapter 4.

2.2.1.1 *Usage in Medical Applications*

Freehand gestures are used in the medical domain primarily to control the display of patient's radiographic scans during interventions (see Figure 2.5b). The advantage of touchless interaction is the possibility to control the radiological software without breaking asepsis and maintaining sterility. There are several other approaches for touchless control besides gesture interaction, such as eye tracking [234] and voice commands [106] (see Figure 2.4 for an overview). Otherwise, sterility is maintained in probably problematic ways as can be seen in Figure 2.5a. There, the physician uses a surgical gown, placed between his ster-

(a)   (b)
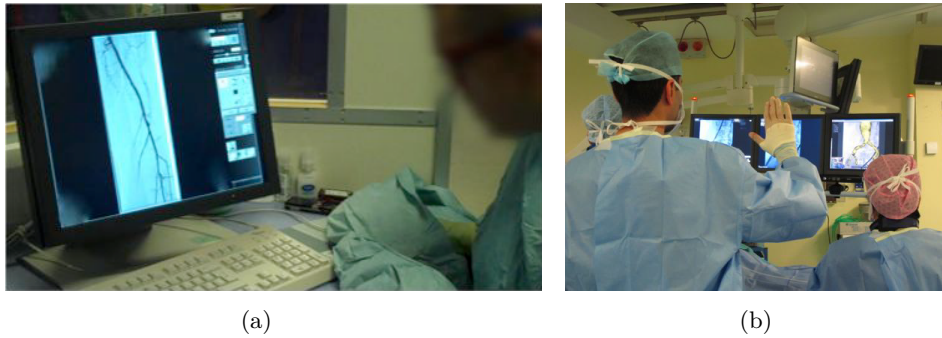
Figure 2.5: In (a), a surgical gown is used to avoid touching the non-sterile mouse with the sterile gloved hand. (b) shows the usage of gestural control for a vascular surgery. Images (a) and (b) from O'Hara et al. [185] © ACM 2014.

ile gloved hand and the non-sterile mouse. Even if sterility is maintained, the usability of mouse control is reduced.

Stevenson et al. [256] assessed the importance of gestures with ethnographic methods. They performed interviews with surgeons and observed them during interventions. Their findings comprise differences in the usefulness of freehand interaction depending on the medical domain and if the medical data is analyzed preoperatively or intraoperatively. According to their results, a simple natural gesture set is preferred, since the willingness for surgeons to invest their time and effort varies. A simple gesture set is easier to learn and, thus, increases the chance to be accepted.

Riduwan et al. [217] allowed to solve basic interaction tasks with gestures such as pointing, translation, rotation and scaling to explore 3D heart visualizations. Mauser and Burgert [160] presented a concept to support basic 2D and 3D interaction tasks and additionally, allowed radiologic image slicing. Their gesture set consisted of simple hand positioning and orientation gestures that are mapped directly onto mouse events. The mapping on mouse events allows an easy integration into existing radiological software and is understood quickly by physicians, since they can control their software in a usual manner. However, the benefits of freehand gestures and NUIs are not utilized, since gestures are only used as a mouse substitute. Thus, the interaction is indirect and eventually uses only the 2 DoF of the mouse. An alternative approach that uses natural hand gestures and metaphors from real-world interaction is presented in Chapter 4. The importance of an appropriate gesture selection and a careful use case analysis is also pointed out by Bizzotto et al. [23]. The authors emphasize the high potential for gesture interaction in intra operative situations, but also the need for an appropriate gesture selection. Because their gestures were ambiguous, they believe that a lock and an unlock gesture is mandatory. Schwarz et al. [241] tested gesture input in an operating room and pointed out that flexible and robust gesture detection helps to make the interaction and the interventional work more efficient.

Mentis et al. [164] presented fieldwork observations with touch and gesture interaction in neurosurgery theaters. Additionally, they consider spatial concerns, i.e. the distal control of medical devices with freehand gestures. Gestures are also used in the field of dental surgery by Rosa and Elizondo [222]. They presented reports on several cases to control the navigation system. Soutschek et al. [253] also developed a system to explore and navigate inside medical 3D data. Their evaluation showed a reliable recognition rate, acceptable usability as well as intuitive and efficient handling. Shen et al. [243] presented a two-handed gesture set with support for specific radiological functions such as placing cutting planes and define clipping volumes. Their evaluation confirmed that using two hands was perceived more natural and intuitive by the participants compared to one-handed systems.

There are several possibilities to obtain an appropriate gesture set. A hardware-driven approach focuses on the capabilities of the tracking hardware and uses gestures that are recognized robustly and accurately. This restricts the possible gestures. Another approach focuses on commonly used and understood gestures. Here, cultural differences have to be considered. Schwarz et al. [241] used an interesting third approach and allowed individualized gestures for physicians. With a gesture learning approach, physicians were able to create and train own gestures for different functions. This supports the adaptation to custom personal and workflow requirements.

A general problem of the presented gestures to control radiological software is a missing or unrealistic evaluation. According to the literature review of Mewes et al. [166], only 13 % of 51 investigated publications contain evaluations in real operation room settings. Even if the gestures are tested in a realistic environment, they are not compared to established techniques.

A comparative user study of gesture interaction and clinically established methods was presented by Hettig et al. [98, 99], which was co-authored by the author of this thesis. They compared different gesture input modalities with clinically established methods, such as task delegation and joystick control. Here, basic interaction tasks with a medical image viewer were executed. The gestures were used to emulate mouse control. The evaluation was conducted with radiologists and showed superiority of established methods regarding performance and usability aspects. However, they stated that by focusing on specific tasks, gesture interfaces may compete with established methods.

Freehand gestures are also used in medical education. The motivation behind this is that the natural interaction may improve the user experience and contribute to the motivation, which is eventually beneficial for learning. Hochmann et al. [101] and Smit et al. [248] used different input devices to realize 3D gesture interaction with anatomic models. However, no evaluations over long periods were conducted to assess a possible positive impact on the knowledge gain.

2.2.2 *Labeling*

Although labeling has its origin in cartography [113], complex structures also exist in several other domains such as engineering, biology and medicine. These structures are composed of many individual parts, each describable with meta-information such as their associated names. In static illustrations, these names are often depicted as textual *labels* or *annotations* (both terms are used interchangeable in this thesis). With different positioning strategies of these labels, varying objectives can be pursued. Placing the labels directly on the structures (internal labeling) allows to easily associate structures with their names at the cost of a spoiled visibility. Methods to position labels can focus on readability and place them axis-aligned [83] or they can convey topological information of the structure by projecting them onto the surface [221]. Placing the labels around the structures without overlap (external labeling) unblocks the view to the structures. However, more space is needed and the labels have to be associated with their structures. This is usually done with *leader lines* that connect the external label with an anchor point on the structure. In Figure 2.6a, an overview of the terminology of external labels is given.

The label positions can either be determined interactively or automatically. In the former case, the user selects a structure, creates a label, adds the textual description and interactively positions it. Although this approach is flexible regarding the final visualization, it has limitations in interactive scenarios where labels can disappear due to object rotations and scaling [210]. Furthermore, the process can be tedious if many labels need to be created. For the automatic calculation of label and anchor point positions, several requirements can be laid down for the external label layout algorithm, which were discussed by various authors (cf. [4, 35, 92, 208]). A minimal subset of label requirements (LR) was presented by Preim and Saalfeld [210]:

- LR1 – Anchor points should be visible.

- LR2 – Labels must not hide any graphical representation.

- LR3 – A label should be placed as close as possible to its reference object.

- LR4 – Labels must not overlap.

- LR5 – Connection lines should not cross.

- LR6 – Label placement should be coherent in dynamic and interactive illustrations, i.e. strong and sudden changes of anchor points and label positions should be avoided.

How well LR2-LR5 are fulfilled depends on the way the labels are arranged. Here, several different layout types exist such as flush layouts, where labels are placed on the sides [209], and circular layouts [93]. Both layouts can fulfill LR2, LR4
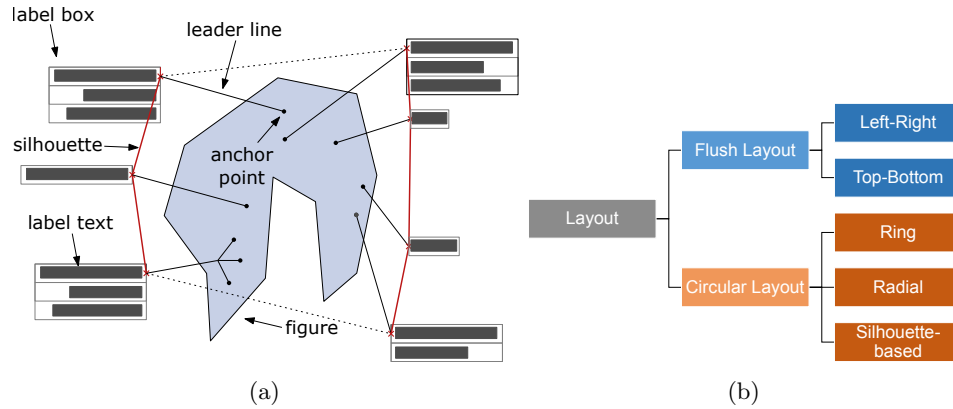
Figure 2.6: In (a), the terminology of external labels is illustrated [181]. In (b), a schematic overview of different external layouts is depicted (inspired by Ali et al. [4]). Image (a) from Niedermann et al. [181] © IEEE 2017.

and LR5. To fulfill LR3 sufficiently, circular layouts are more appropriate, since the available space around the structures is used more efficiently. Figure 2.6b gives a schematic overview of different layout types.

2.2.2.1   *Usage in Medical Applications*

The traditional usage of labels in medicine is in anatomy atlases to support education for students and educators. These books contain a large spectrum of human anatomy illustrations, divided into body regions and layers, such as muscles, vessels, nerves and bones. The third volume of the popular anatomy atlas *Sobotta* [193] contains about 1,200 figures. Most of the structures are illustrated with detailed drawings from different viewing angles and a large number of labels. These illustrations are either manually labeled by an anatomist with an artistic education, semi-automatically with computer-assistance or fully automatically (see Figure 2.7). Niedermann et al. [181] presented an automatic approach to generate high-quality label layouts for static illustrations. They generate radial layouts based on 18 layout quality criteria, which were gathered through expert interviews and an analysis of hand-made anatomical illustrations. Figure 2.7b presents an example of their approach, which is used in the aforementioned Sobotta anatomy atlas [193].

Besides anatomy education, labels also play an important role in diagnostics and treatment planning. According to Oeltze-Jafra and Preim [186], they serve to:

- record and forward diagnostic findings, e.g. to the transferring doctor or a medical specialist [37],

- focus discussions in team meetings such as tumor boards, were therapeutic strategies are discussed,

(a)   (b)
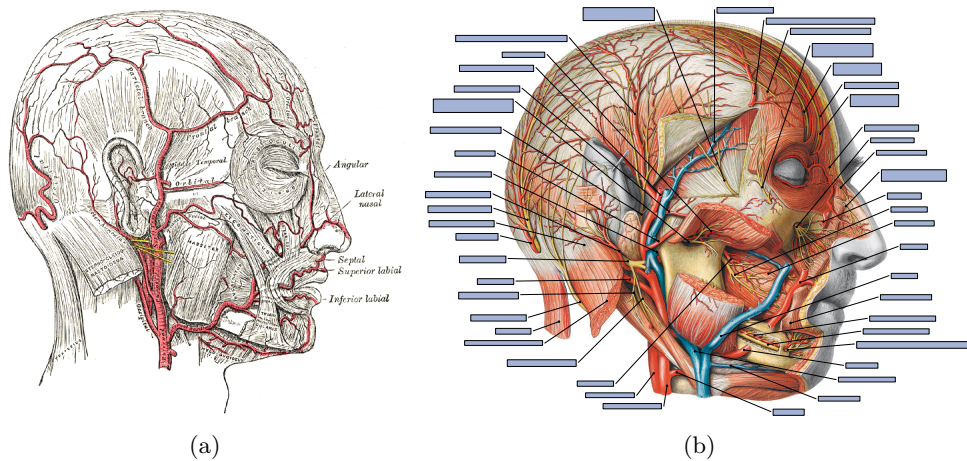
Figure 2.7: Two labeled illustrations from the same viewing direction onto the human skull. In (a), a hand-crafted illustration from Henry Vandyke Carter is depicted, containing internal and external labels (from Gray and Lewis [84]). In (b), the cross-section of a skull includes labels generated with the approach from Niedermann et al. [181] and is used in the Sobotta anatomy atlas [193]. Approximately 100 years lie between both images ((a) – 1918, (b) – 2013). Image (a) was released into the public domain and made available on Wikimedia Commons (https://commons.wikimedia.org/wiki/File:Gray508.png, last accessed: 11.06.2018). Image (b) from Niedermann et al. [181] © IEEE 2017.

- support orientation in complex views on the data, e.g. 3D views of highly branched vascular trees [203],

- explain an intervention in patient education, and

- practice an intervention in a surgery training system, such as the LiverSurgeryTrainer [170].

For a more detailed discussion of labeling for anatomy education, the reader is referred to the survey of Preim and Saalfeld [210]. See the survey of Oeltze-Jafra and Preim [186] for more examples of labeling techniques in medical visualization, including a discussion of labeling on 2D radiographic images.

2.2.2.2 *Usage in Virtual Environments*

Even for interactive 3D applications, the positioning and rendering of labels is often realized in the 2D image space. Here, the 3D models are firstly rendered, resulting in a 2D image. This image is the basis for the label layout calculation and the 2D image is enriched with 2D labels. Although this approach is appropriate for static 2D illustrations, it introduces challenges for interactive 3D applications during zooming and rotation (LR6 of the label requirements). This is even more critical in Augmented Reality (AR) and Virtual Reality (VR)

environments, where the user is part of the 3D environment – here, labels need a 3D position to be rendered in a useful way. Madsen et al. [159] tested this in an AR environment. They could show that placing annotations directly in object space instead of image space leads to the best performance for label location tasks.

The positioning of labels as 3D objects can either be performed automatically or interactively, whereby the label requirements presented in the previous section remain the same. An approach for the automatic placement on an immersive multi-screen display system is described by Pick et al. [197]. Their algorithm is based on the shadow volume technique. To calculate this volume, a point light is assumed to be at the user's head position, casting light onto all objects. This generates a shadow volume behind each object. In this area, no annotations are allowed, since they would be occluded. To prevent occlusions during interaction, a force-based approach is used to re-position the labels. This approach was used in the application *VisNest* from Nowke et al. [184] (see Figure 2.8a). VisNest allows neuroscientists to deduce functionality of the brain by inspecting neural activity linked to a geometric representation. Each brain area is provided with an annotation, showing the area's anatomical designator and neuronal activity. Tatzgern et al. [261] also presented an automatic approach for image and text annotations in an AR environment. They use poles originating from the center of each object. Labels are placed on these poles and moved along them during interaction. Additional constraints prevent the overlapping of labels and allow consistent movement on viewpoint changes.

In contrast, the *interactive positioning* of labels avoids the usage of a complex label layout algorithm, but introduces challenges regarding user interaction in the VE. An example of interactively placed annotations is presented by Assenmacher et al. [10]. They introduce the toolkit *IDEA* that allows the creation of generic annotations, including texts, images and also spoken annotations. Furthermore, they show the usage of the toolkit for data analysis at the example of air flows in the human nasal cavity.

A more fundamental investigation of annotation systems for multiple virtual reality platforms was carried out by Pick and colleagues. One of their publications focused on the creation of a framework that provides reusable and adaptable building blocks to facilitate the creation of flexible annotation systems [199]. Here, aspects ranging from data representation over persistence to the integration of new data types are discussed. In a recent work, they presented a workflow design that facilitates the most important annotation operations (creation, review, modification) [198] (see Figure 2.8b). This design is extensible to support further annotation types and interaction techniques. Furthermore, possibilities to evaluate existing annotation workflows in VEs are shown.

(a)

(b)

Figure 2.8: *VisNest* provides each brain area with *automatically placed* annotations that show their anatomical designators and maps neuronal activity to the leader line representation (a) [184]. Pick et al. [198] present a general workflow design that facilitates *interactive placement* and creation of annotations. In (b), a pie menu is used to select a view point annotation that can be placed in the Virtual Environment. Image (a) from Nowke et al. [184] © IEEE 2013. Image (b) from Pick et al. [198] © IEEE 2016.

2.2.3   *Sketching*

Problem solving is a central part in science and engineering. It is not only performed inside the researcher's mind, but also through the *externalization* in form of scribbles and sketches [152]. Sketching can be seen as a form of Reality-based Interaction (RBI) as it moves closer to real-world interaction with pen and paper [118]. Furthermore, as the input device is usually direct, e.g. a pen or touch is used, sketching can be seen as a post-WIMP (Windows, Icon, Menu, Pointer)

Figure 2.9: *Sketchpad* interprets the sketch and guesses properties such as the center and radius to draw a precise circle. Image from Sutherland [258] © ACM 1964.

User Interface (UI) [207]. The advantages of RBI are demonstrated several times, e.g. by the research of Xu et al. [286] and Naya et al. [175]. Both show that users prefer sketching over classical desktop metaphors, such as WIMP-based interaction, and are more efficient with it.

2.2.3.1 *Sketch-based Interface & Modeling*

With Sketch-based Interfaces (SBIs), it is possible to visualize and communicate ideas without the necessity to draw accurately [123]. This, however, renders challenges regarding the automatic recognition and interpretation of the sketch. Foundations to support the user during sketching were already laid by Ivan Sutherland [258] with the application *Sketchpad* (see Figure 2.9). It allows users to precisely sketch lines and circles by interpreting the 2D input.

Three major processing steps have formed in the area of SBIs that can be applied to input data:

1. resampling,

2. beautification, and

3. recognition.

The **resampling** is either performed to bring irregular and noisy input data to an equidistant form or to reduce the number of sample points. If the sampling rate of the input device is high enough, equidistant points can simply be obtained by ignoring all points that fall below a specific threshold (see Figure 2.10a). A well-known method to reduce the amount of sample points is the Douglas-Peucker algorithm [56]. This algorithm takes a curve as input and finds a similar simplified subset line. The algorithm is described in Figure 2.10b. For a comparison of different line simplification algorithms regarding accuracy and processing time, the reader is referred to the article of Shi and Cheung [246]. A
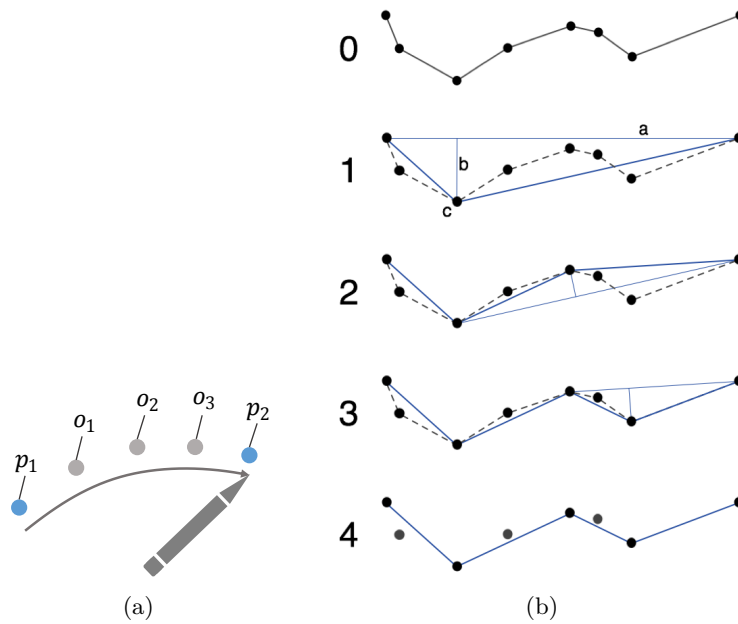
Figure 2.10: (a) A simple approach to equidistantly resample points is to omit all sampled points o_{1-3} that fall below a specified threshold between p_1 and p_2. For line simplification, the Douglas-Peucker algorithm can be used (b). The algorithm recursively divides the input line (0) into a subset with fewer points. The furthest point between the start and end point is analyzed (1). If the distance is larger than a given threshold, the point is kept, otherwise, it is omitted. If a point is kept (2), it is used as a new start/end point and the line segment is divided recursively (3) until the final simplified line is obtained (4). Image (a) from Saalfeld et al. [228] © Springer International Publishing Switzerland 2016. Image (b) from Leupold and made available on Wikimedia Commons under the Creative Commons Attribution-ShareAlike 2.0 Germany License (https://upload.wikimedia.org/wikipedia/commons/9/91/Douglas_Peucker.png, last accessed: 11.06.2018).

more complex form of resampling is called *fitting*, which either allows an equidistant resampling or line simplification. Here, parametric curves such as Bézier curves [200] and splines [18] are fitted to the input data.

One example of the **beautification** step was presented by Igarashi et al. [111]. They analyze line segments according to geometric constraints such as perpendicularity and parallelism. After that, the application recommends different options how to interpret the lines and the user can choose one.

The processing step **recognition** describes a procedure where the sketch is compared with an internal representation of symbols. The similarity is expressed with a parameter. If this parameter exceeds a threshold, the sketch is interpreted as the compared symbol [123]. A simple way to integrate recognition in an application is the usage of the *1$^\text{¢}$ Recognizer* [96].
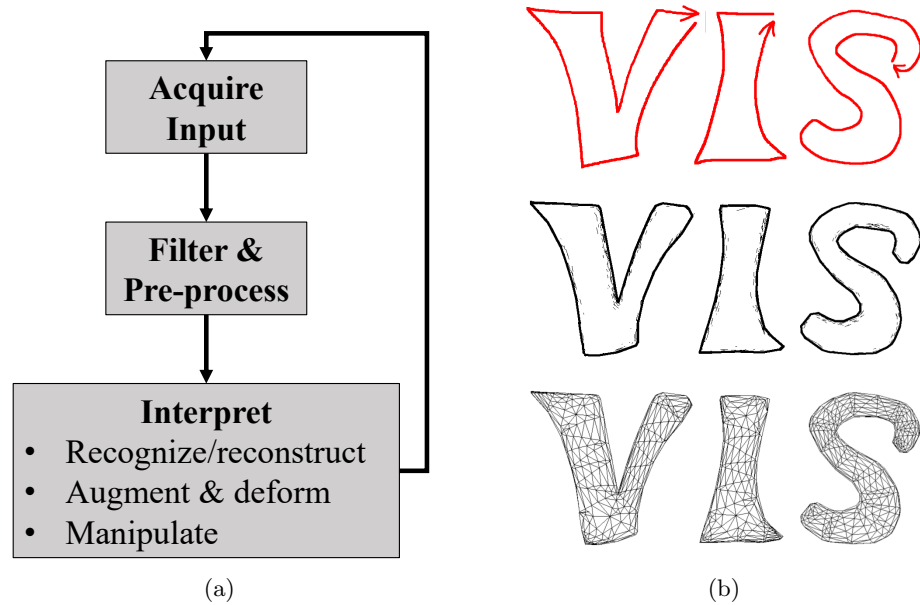
Figure 2.11: In (a), the general pipeline for Sketch-based Modeling systems is depicted (inspired by [190]). The images in (b) demonstrate this pipeline and are created with the Teddy application [112]. First, the user sketches 2D contours. This contour is then connected and smoothed. Finally, polygonization methods are used to create a 3D model out of the sketch.

SBIs are also used for geometric modeling, forming the independent research area of Sketch-based Modeling (SBM). In the focus of SBM are methods for fast and easy shape prototyping. As these methods are more accessible to non-specialist users, less learning is necessary compared to traditional modeling applications [3]. The general pipeline to create models out of sketches is depicted in Figure 2.11a. A famous application that follows this pipeline is *Teddy* [112]. In Teddy, the user sketches a closed contour. This contour is transformed to a planar polygon and the *spine* of this polygon is calculated. The vertices of the spine are elevated in proportion to the distance to the contour. Lastly, a polygonal mesh wrapping is created around the spine and contour that forms oval shapes. Figure 2.11b depicts a 3D geometry that was created with Teddy. Further details on other SBM systems can be found in the surveys of Olsen et al. [191] and Ding and Liu [54].

2.2.3.2   *Usage in Medical Applications*

In medicine, sketches are employed for a wide range of applications. For example, they are used as an intuitive interaction technique to annotate medical reports [216] or to segment structures in 2D image data [95]. In clinical practice, sketching is also a beneficial supplement for patient education and the interchange with medical staff. A versatile 2D sketching tool that can also be used
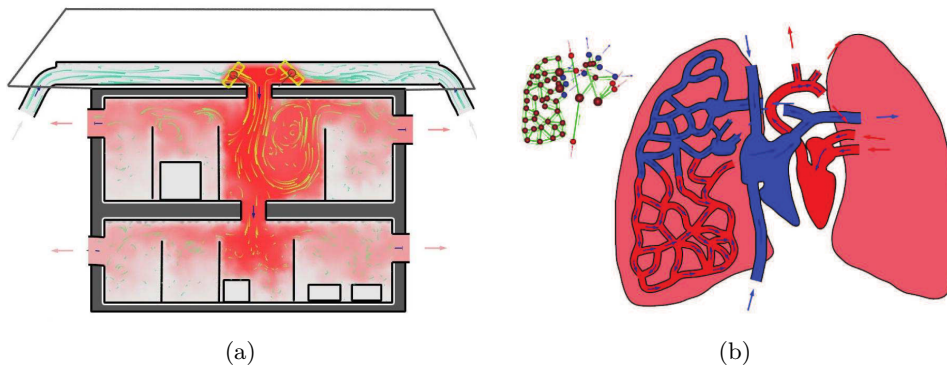
Figure 2.12: The versatile sketching tool from Zhu et al. [289] can be used to illustrate the (a) central heating system of a house and the (b) oxygen transportation in lungs. Images (a) and (b) from [289] © ACM 2011.

Figure 2.13: A model of the Aortic arch is sketched (left) and converted into a 3D model (right). Images from Pihuit et al. [201], reprinted with permission.

for medical applications was presented by Zhu et al. [289]. Their work combines methods to sketch tubular shapes and enrich them with the simulation of gas-like liquids. This allows the illustration of processes such as heat development inside a house but also of the oxygen transportation inside the lungs (see Figure 2.12).

An SBM system dedicated to support anatomy education was presented by Pihuit et al. [201]. Their work is strongly inspired by blackboard drawings performed by anatomy educators. The anatomy educators provide the system with sketches of vessels including silhouettes and hatching lines. These are transformed into 3D models of branching vessels to create vascular structures. To maintain the sketch-based look, they are visualized with Non-photorealistic Rendering (NPR) to recreate the appearance of blackboard drawings (see Figure 2.13). Different illustrative line drawing techniques that are applied to anatomical structures and a comparison how they support the shape depiction can be found in the work of Lawonn et al. [148, 149] (both co-authored from the author of this thesis).

2.2.3.3   *3D Sketching*

Apart from using 2D input for sketching, spatial environments also provide a beneficial setting for sketching. On the one hand, this involves the input devices that allow 3D sketching. On the other hand, it involves the output devices that improve the perception of the third dimension. A more technical discussion of devices is presented in the following Section 2.3.

Perkunder et al. [194] investigated differences of 2D and 3D sketching for the task of shape modeling. Their study showed that sketching in a 3D environment was perceived more stimulating and attractive than under 2D conditions. Arora et al. [7] compared traditional sketching on a physical surface against sketching with a Head-worn Display (HWD)² and investigated the accuracy. They showed that the absence of a physical surface leads to inaccuracies. Furthermore, they could show that visual guidance can compensate for the loss of accuracy in 3D sketching.

Fleisch et al. [69] presented a *3D sketching* environment and tried to close the gap between 2D sketching and 3D modeling for designers. They present techniques for creating and modifying 3D curves, such as stroke splitting and oversketching. An example of an artistic application was given by Eroglu et al. [58]. They developed methods to create 3D fluid artworks in a Cave Automatic Virtual Environment (CAVE). Here, the sketches itself are the fluid with varying characteristics in parameters such as viscosity, size and color. Wang et al. [275] and Jackson et al. [117] combined 2D sketching and a spatial environment. The former work allows freehand sketching for cartoonists on a virtual, user-definable 3D canvas, i.e. the user is restricted to a virtual plane. The latter work allows users to import existing 2D sketches and interactively *lift* 2D curves into space to create 3D structures (see Figure 2.14a). Another interesting virtual support structure was presented by Kim and Bae [130]. They tracked the user's hand that could be incorporated into the sketch environment. The user can take 3D snapshots of hand postures and use this model as a reference to aid in sketching. In a follow-up work of Kim et al. [131], the user's hand motions are tracked to approximate 3D shapes. These shapes are then used as scaffolds to support more precise 3D sketching via a pen on a tablet device. Besides supporting designers in creation processes, sketches can be used for other interaction tasks. Hagedorn and Döllner [87] use sketching to navigate inside 3D environments. The users simply sketch their navigation intentions, e.g. to follow a road on a specific path. The system interprets these sketches and starts the navigation (see Figure 2.14b).

---

2 In this thesis, the nomenclature of the 3DUI book of LaViola Jr. et al. [146] is used, i.e. the term Head-worn Display (HWD) is used instead of Head-mounted Display (HMD), since it represents the way the output device is used more accurately.

(a)

(b)
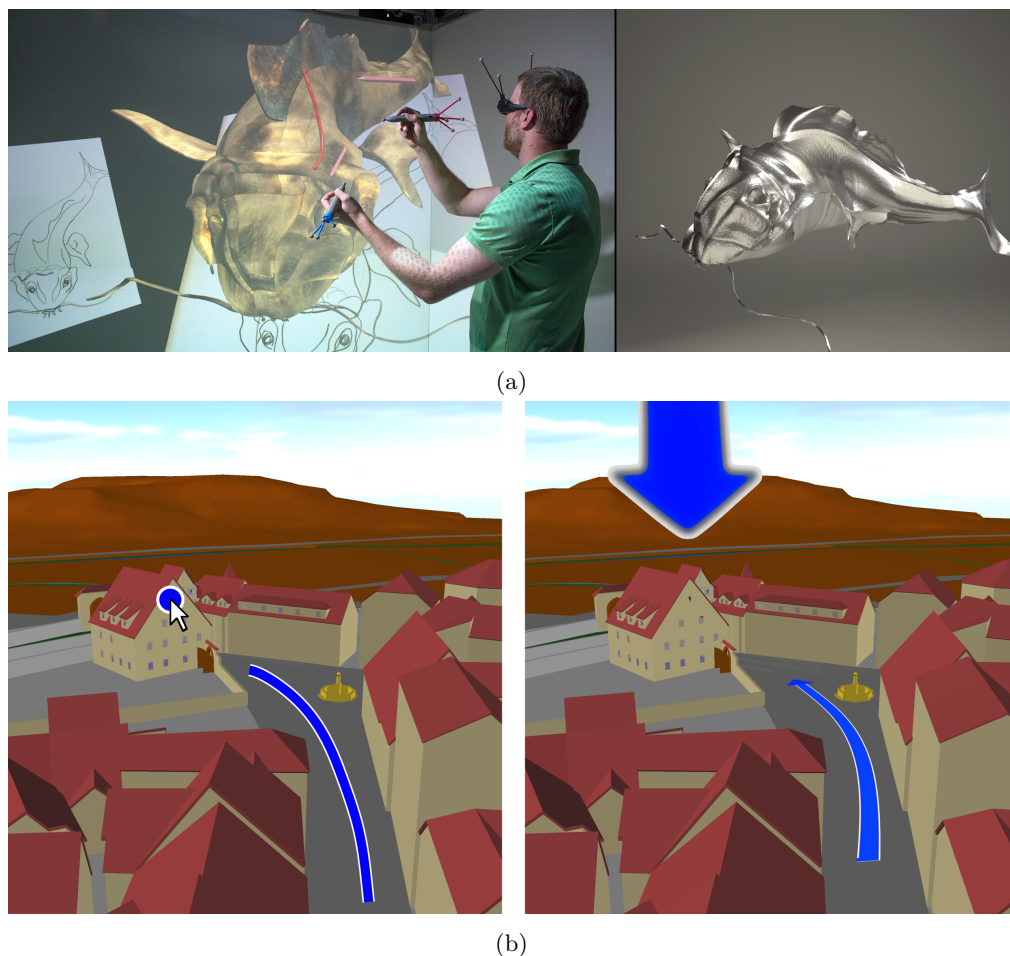
Figure 2.14: In (a), the user imports existing 2D sketches and interactively *lift* 2D curves into space to create 3D structures [117]. In (b), sketching is used to navigate inside a town. The sketch on the left is interpreted as *following the street and adjust the view to the marked house.* The interpretation is also visualized to the user (right) [87]. Image (a) from Jackson and Keefe [117] © IEEE 2016. Image (b) from Hagedorn et al. [87] © Springer-Verlag Berlin Heidelberg 2008.

2.3   DEVICES FOR FREEHAND GESTURES & SKETCHING

> "A bewildering variety of devices for communication from humans
> to computers now exists on the market" [38]

This contemporary appearing quote referring to input devices from Card et al. is actually from 1990. Since then, the variety of input devices as well as output devices has grown further according to their functionality and price. This section considers different devices that could be used for the advanced interaction techniques of freehand gestures and sketching. After discussing different devices,

the ones that are used in this dissertation are described in more detail, including their technical specifications.

2.3.1   *Input Devices for Freehand Gestures*

Freehand gestures can be recognized with several detection strategies:

- data gloves,

- myoelectric tracking,

- magnetic tracking, and

- camera-based tracking.

Data gloves use different sensors to track the movement and position of fingers and the wrist (see Figure 2.15a). One example are strain gauges that measure the curvature of fingers and enable an assessment of hand gestures. The usage of additional actuators provides tactile feedback [29]. However, data gloves have to be adjusted for each user independently and usually they only work in a restricted range of "standard hands" [207]. The freehand gestures in this thesis should be used for sterile, touchless interaction. Although data gloves would allow the touchless control of interventional software, they would disturb the physician during holding and using interventional instruments, as they reduce the freedom of movement. The time to put them on and off would also be bothersome. The survey from Dipietro et al. [55] gives an overview of glove-based systems and their applications.

Myoelectric signals are usually used to control prostheses. There, the muscle activity which create electric current is observed and used to trigger battery-driven electronic motors, e.g. for limb movement. An input device that uses these myoelectric signals is the *Myo Gesture Control Armband* (Thalmic Labs Inc., Kitchener, Canada) that is worn at the forearm (see Figure 2.15b). This device is theoretically appropriate to control interventional software since it allows touchless interaction, does not influence the hands and can be worn under surgical gowns. The developed gesture set from Hettig et al. [97] shows that the device is applicable for the exploration of 3D medical image data. However, with a reported gesture recognition accuracy of 56 %-86 % (depending on the gesture), this device is not accurate enough for the usage in clinical practice. A better gesture recognition rate is hypothetically possible with an improvement of the underlying software or the Myo Gesture Control Armband itself. However, neither the Myo Software Development Kit (SDK) (in version 0.9) nor the firmware were updated since late 2015.[3]

---

3 Checked 11.06.2018 on https://developer.thalmic.com/downloads
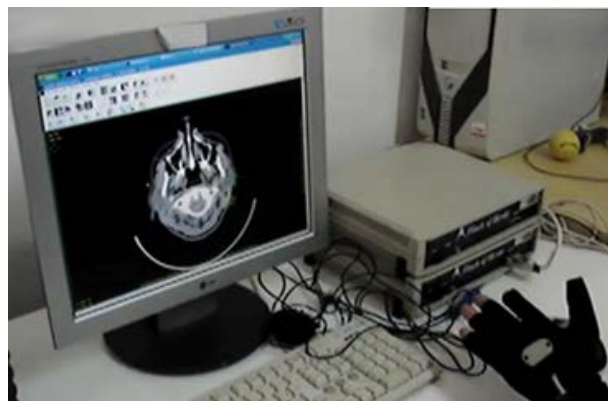
(a)
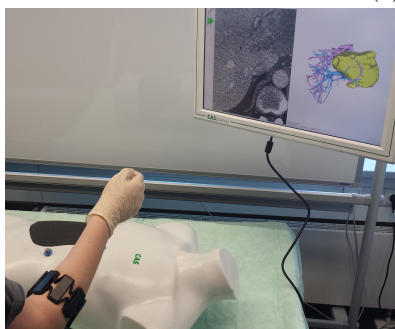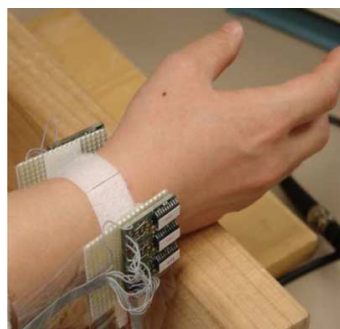
(b)   (c)

Figure 2.15: Different methods to track fingers and hand postures. (a) depicts a 5DT DataGlove5 ULTRA to control a radiological workstation [260]. In (b), the Myo Gesture Control Armband is used to control an interventional navigation system [97]. (c) shows the prototype from Ma et al. [158]. They track the hands based on magnetic tracking. Image (a) from Tani et al. [260] © IEEE 2007. Image (b) from Hettig et al. [97], reprinted with permission. Image (c) from Ma et al. [158] © IEEE 2011.

Another approach is **magnetic tracking**, where changing electromagnetic fields are tracked over time. Ma et al. [158] use this technique by attaching magnets on each fingertip and magnetic sensors on a wristband (see Figure 2.15c). The combined magnetic field allows to track the position and orientation of each fingertip and is used to calculate an estimated posture of the hand. Although this allows accurate tracking with low latency, the tracking area is small, resulting in a small interaction area. Additionally, metallic objects and unwanted external magnetic fields interfere with this tracking technique, leading to noise and artifacts. This disqualifies it for interventional radiology, since some instruments are metal-based. Using it together with Magnetic Resonance Imaging (MRI) is not possible, because this image acquisition method produces its own magnetic field.

(a)   (b)

Figure 2.16: (a) shows passive markers on the hand that aids hand tracking and grasp recognition [40]. The Microsoft Kinect v2 can be used to track hands without markers on the user's hands [287]. Image (a) from Chang et al. [40] © IEEE 2007. Image (b) from Yang et al. [287] © IEEE 2015.

Camera-based hand detection is optical and therefore, a line of sight between the user's hands and the sensor is necessary. To aid cameras, markers on the user's hands can be used to improve the tracking (see Figure 2.16a). Usually, two cameras are used to allow the trigonometric calculation of distance [207]. However, another approach is used by Time of Flight (TOF) cameras such as the *Kinect v2* (Microsoft Corporation, Redmond, Washington, USA). This device only needs one camera and calculates the distance based on the time that emitted light takes to come back to the sensor (see Figure 2.16b).

In this thesis, camera-based hand detection is used to control interventional software. In research, this is commonly realized either with the Kinect or with the Leap Motion Controller (LMC) (Leap Motion, Inc., San Francisco, USA). Several comparative studies in the medical domain have shown that the LMC is superior as it allows an improved recognition of gestures in short working distances, is more accurate [23], is less tiring and needs less widespread arm movements [222]. The LMC emits infrared (IR) light with three IR LEDs (see Figure 2.17a). This light is reflected by the user's hands and captured with two IR cameras, resulting in a grayscale stereo image (see Figure 2.17b). The cameras sample images with a rate of 39 Hz and have a viewing angle of 150° vertically and 120° horizontally. The cameras and IR LEDs are housed inside an 80 mm × 30 mm × 11 mm casing with an interaction volume of approximately 600 mm^3. Since this sensor tracks hands without markers, characteristic features of each hand have to be recognized. This is realized by the Leap Motion SDK that calculates the position and orientation for the palm, fingers, bones and joints. These information allow to define and track hand and finger gestures. The markerless tracking makes this approach less robust and prone for ambient light conditions and the color of the skin.

The accuracy in real environments was tested by Weichert et al. [277]. In static test cases, a positional accuracy of 0.2 mm was measured. For dynamic cases, however, sub-millimeter accuracy was not achieved (accuracy of 1.2 mm). Similar results were found one year later (2014) by Guna et al. [85]. Here, the

(a)   (b)
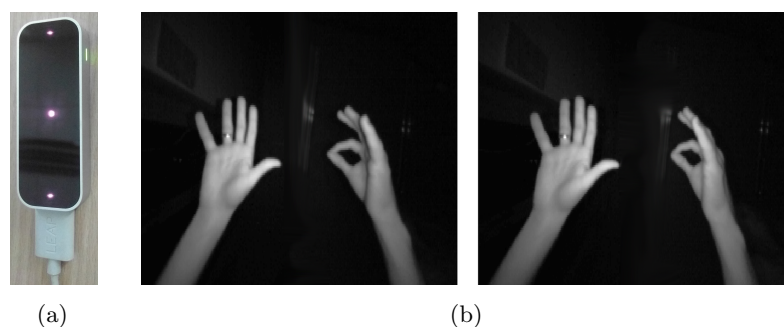
Figure 2.17: The Leap Motion Controller with visible infrared LEDs is depicted in (a). In (b), the stereoscopic grayscale images recorded from the cameras are shown.

standard deviation of the accuracy for a static test case was less than 0.5 mm. In both studies, the sensor was less accurate when the tracked object was more than 250 mm above the sensor. The reported accuracy in static cases is in the sub-millimeter range, which is sufficient to control interventional software.

2.3.2 *Input & Output Devices for Sketching*

In this thesis, sketching is used for medical education and treatment planning. Both tasks do not require sterile interaction and, thus, more options for user input and output are possible. In this thesis, the zSpace 100 (zSpace Inc., San Francisco, USA) is used for sketching (see Figure 2.20b). It combines a spatial input and output device. In the following, the zSpace and other devices are discussed in more detail and it is explained why the zSpace is suitable for sketching.

2.3.2.1 *Precise 3D Input*

Several characteristics are used to discriminate input devices. This section focuses on two of them: the way the device is held and the DoF that it allows to control. For a distinction regarding aspects such as frequency of the data generation, used sensors, and the transfer function to interpret inputs as interactions, interested readers are referred to the work of LaViola et al. [146] and Huckauf et al. [109].

The way an input device is held, restricts the possible precision. Two major holding techniques are called *power grip* and *precision grip*. Figure 2.18 gives an extensive hierarchical overview of different grasping types from Cutkosky [49]. The power grip is used for tools such as a hammer ("prismatic" grips 2/3/4/5 in Figure 2.18). Devices held this way can be moved with force. However, they can only be maneuvered with limited precision, since the movement is primarily controlled via the shoulder and arm [174]. Since sketching benefits from high precision, pen-like devices that are held with the precision grip are more ap-
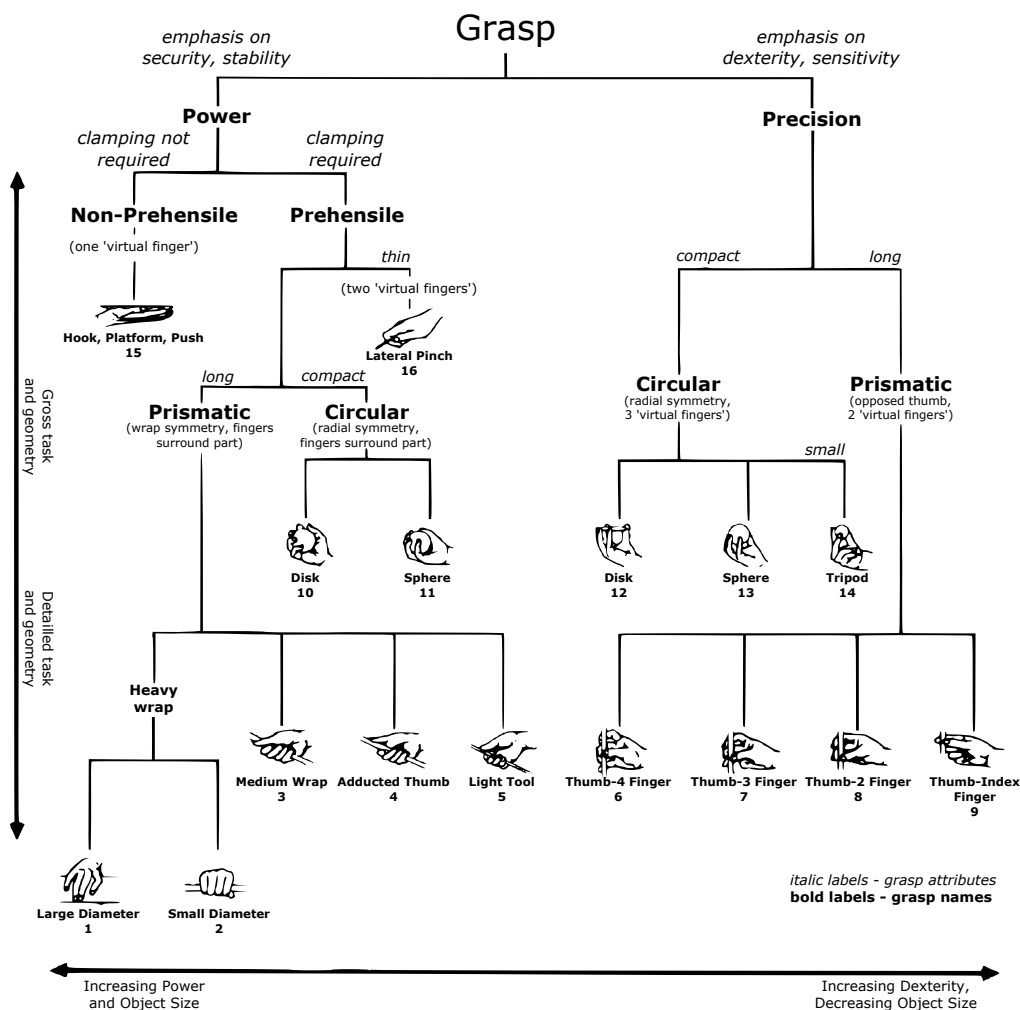
Figure 2.18: Taxonomy of grasp types adapted from Cutkosky [49]. For sketching, the input device should be held with a precision grasp type for precise input. Image from Cutkosky [49] © IEEE 1989.

propriate. Here, fine motor skills of the index finger, middle finger and thumb can be used to control the movement ("Thumb-2 Finger" grip 8 in Figure 2.18). This ability for very fine control can be illustrated by picking a raspberry from a bush: if too much pressure is applied, the raspberry is squished, otherwise, it slips away – the precision grip allows to apply the right amount of pressure [57].

There are several input devices that are held with the precision grip, e.g. pens that directly draw on a display. This has the disadvantage that the user's hand occludes content on the screen [205]. Another pen-based input device is the graphic tablet, which can be used in, e.g. surgical planning to control a virtual endoscope [137]. Here, the occlusion problem is not present.

These pen-based input devices usually only offer 2 DoF, which limits their applicability for 3D objects as they reduce the available design space for interaction

(a)   (b)
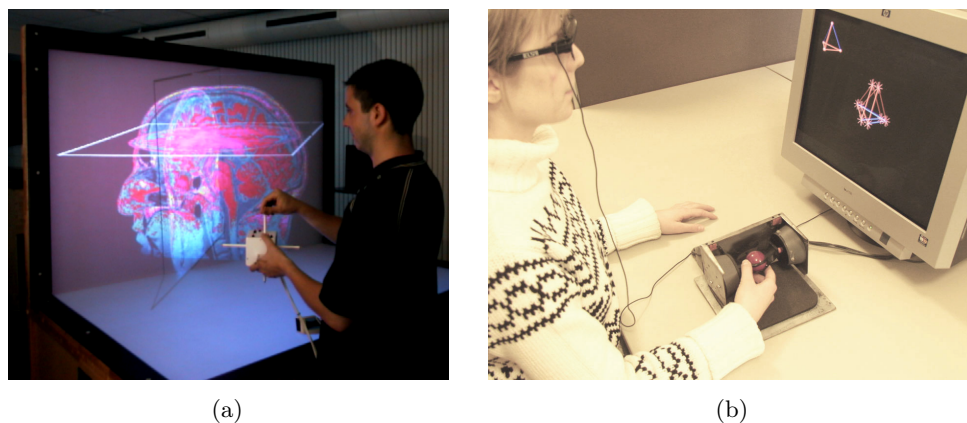
Figure 2.19: (a) The Cubic mouse used for exploring medical data [71]. (b) The Globefish device used in a 3D docking task [70, 141]. Image (a) from Fröhlich and Plate [71] © ACM 2000. Image (b) from Fröhlich et al. [70] © ACM 2006.

techniques [109]. Therefore, input devices with more DoF are used, were spatial input is beneficial. For example, Gallo et al. [72] use the Wii Remote (Nintendo Corporation, Kyoto, Japan) to manipulate 3D reconstructions of anatomical parts. This device is held with the power grip. Besides using commercially available input devices that usually try to cover a wide range of possible applications, developing own devices to solve a specific task is useful. An example is the Cubic Mouse, which allows to specify three-dimensional coordinates by pushing and pulling rods mounted on the device (see Figure 2.19a). Another example is the Globefish, which allows 3D object manipulation and navigation [141] (see Figure 2.19b). This device consists of a trackball that is retained in a spring-loaded frame (see Figure 2.19b). The trackball can be freely rotated, while a simultaneous push or pull action is possible, allowing it to be moved in any direction. Precise interaction is possible, since the trackball is held with a precision grip. Both 6 DoF devices were compared with the commercially available SpaceMouse (3Dconnexion, Munich, Germany) by Fröhlich et al. [70]. The evaluated docking task was performed faster and rated easier with the two newly developed devices.

In this thesis, the aforementioned stylus of the zSpace is used as it combines the benefits of the way it is held as well as 6 DoF for input (see Figure 2.20a). This pen-shaped device is held with a sub-category of the precision grip, i.e. with the thumb and two fingers (Grasp 8 in Figure 2.18). This is the same way a pen is held, thus it allows the precision normally used for writing and drawing [250]. Additionally, the low weight of 40 g makes it useable for longer periods of time (a standard pencil weights around 10 g), which is necessary, since a heavy input device would probably be rejected by clinicians [192]. The 6 DoF are achieved with a combination of optical tracking and an inertial sensor. IR LEDs are built in on both ends of the stylus. These are tracked by cameras of

(a)   (b)
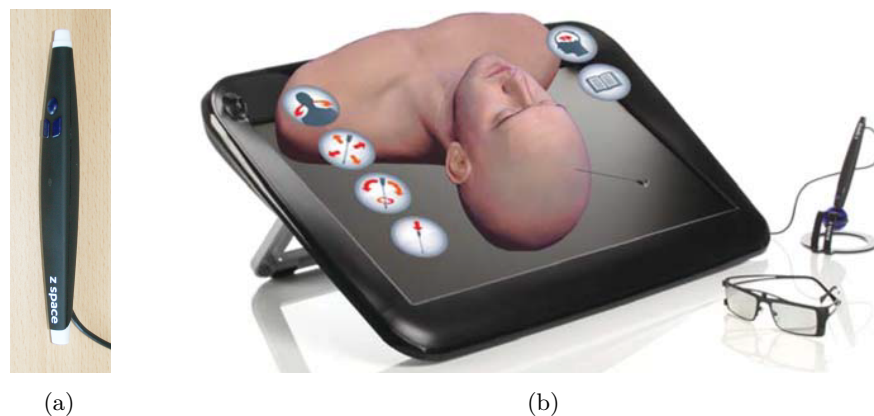
Figure 2.20: (a) shows the 6 Degrees of Freedom stylus from zSpace that is used as a precise input device for sketching [230]. In (b), the whole zSpace system is depicted, combining a stereoscopic display with tracked glasses for head tracking. The display content was inserted to illustrate the spatial capabilities of the display and shows a neurosurgery training system [122]. Image (a) from Saalfeld et al. [230]. Image (b) from John et al. [122] © Massachusetts Institute of Technology 2017.

the zSpace. Since two active markers would only allow 5 DoF, the remaining sixth DoF (rotation around the roll axis) is provided by an integrated gyroscope. As tracking resolution, zSpace documents state 2 mm in x, y and z direction and 2° for yaw, pitch and roll. The positional accuracy is reported as 3/3/5 mm for x, y, and z and the rotational accuracy with 2° for yaw, pitch, and roll. The available tracking space is limited by the viewing field of the cameras, but not further specified by zSpace documents. To take advantage of the precise tracking of the stylus, it can also be used without the actual display of the zSpace. This was presented by the author of this thesis for the exploration and measurement of medical data [237]. As the output device, an HWD was used. Since the tracking area of the stylus is restricted, the VE was limited to the area in front of the user.

2.3.2.2 *Semi-immersive & Fully Immersive Output*

To make use of the 6 DoF input device, the spatial component has to be perceivable. Here, different depth cues exist that can aid the user; the article of Preim et al. gives an overview of the different depth cues [206]. In this dissertation, the monoscopic depth cue *motion parallax* as well as the stereoscopic depth cue *binocular disparity* take an important role as they support a physician or student to estimate sizes and relationships of anatomical structures [15]. Motion parallax can be created by moving 3D objects at different amounts, resulting in the perception of different depths. Binocular disparity can be created by generating two images as they would be seen by each of our eyes. Both depth cues can be

generated with dedicated output devices. Here, different classes exist that can be further discriminated with aspects such as their:

- Field of View (FOV),

- Field of Regard (FOR),

- number of pixels, and

- degree of immersion.

The FOV describes the angle that a user is able to perceive at a given time. The FOR, on the other hand, describes the physical size of an output device. A 6-sided CAVE, for example, has a FOV equal to the FOV of the user and a FOR of 360° horizontally. The FOV that a human is able to perceive with both eyes is approximately 200° and the binocular overlap is 120°. Therefore, an output device creating a FOV of 120° is generally considered sufficient [168]. The amount of information that can be presented is limited by the number of pixels. Therefore, the pixel amount is another important factor. Current HWDs, such as the HTC Vive (HTC, Taoyuan, Taiwan), have a FOV of 110°, which almost covers the human binocular field. However, they render a low number of pixels compared to, e.g. a CAVE. This downside is especially visible if textual information is displayed in the VE. Text that is not in close proximity to the user can hardly be read on an HWD but is easily perceivable in a CAVE.

The aspect of immersion can be divided into physical and mental immersion [244]. Mental immersion describes the sensation of being engaged in an environment through involvement, physical immersion refers to the body's senses that are stimulated through a system. Here, different kinds of feedback (e.g. visual or haptic) can be induced. However, not every one of these aspects has to be considered equally for an immersive experience. Thus, weighting one over the other may be useful depending on the application scenario [107]. In general, a high immersion leads to a feeling of *presence*, i.e. the subjective experience of being in an environment, even when one is physically situated in another. Furthermore, presence leads to an improved task performance in VEs [281]. Still, the character of these aspects makes it difficult to exactly state "how immersive" a system is. A possible simplified discrimination can be made by focusing on the output device alone, where non-immersive systems use standard desktop displays and fully immersive systems make use of motion parallax, binocular disparity and allow the user a sufficient FOV. This description would apply for CAVEs and HWDs. Further, this categorization allows to label standard-sized displays as stereoscopic and motion tracking abilities as semi-immersive. Such systems were first evaluated by Arthur et al. and Ware et al. [8, 276]. They combined a stereoscopic display with mechanical head tracking for motion parallax (see Figure 2.21a). Since the immersion is restricted to the area of the display, they named this type of system "fish tank virtual reality". Their evaluation showed

(a)   (b)

Figure 2.21: In (a), an early semi-immersive *fish tank virtual reality system* is shown that combines a stereoscopic display with mechanical head tracking [8]. In (b), the *responsive workbench* is used in a collaborative scenario for anatomy education [2]. Image (a) from Arthur et al. [8] © ACM 1993. Image (b) from Agrawala et al. [2] © ACM 1997.

better performances compared to non-immersive systems, whereas motion parallax had a bigger impact and was of more value than binocular disparity. The benefit in performance of binocular disparity alone, however, was shown for simple navigation, selection and manipulation tasks [223]. Additionally, it was shown to be more preferable for complex tasks, such as playing modern video games [147]. An early pioneering semi-immersive system is the *responsive workbench*, which combines a stereoscopic image projection on a large screen and head tracking. Here, different configurations exist, for example a horizontal tabletop display [139, 140] that was later extended to allow collaborative work [2] (see Figure 2.21b).

As mentioned, in this thesis the semi-immersive zSpace is used as the output device (see Figure 2.20b). It uses a full HD 24 " display with a 120 Hz update rate. The binocular disparity is achieved with circular polarized and time-interleaved rendered images. These are filtered by glasses worn by the user. The glasses are tracked passively through IR markers and allow motion parallax through 6 DoF head tracking. The FOV and FOR depends on how close the user sits in front of the zSpace. In scientific publications, the zSpace is rarely mentioned. Its benefits for selecting, pointing and manipulation tasks were shown by Aras et al. [6] in a general comparative study. They compared the usage of the zSpace against a standard 2D display with 32 participants. Therem the usage of zSpace resulted in a faster performance of the manipulation tasks.

While semi-immersive systems lack the power of full immersion, they have advantages that make them a better choice for certain applications [276]. They allow the user to still be aware of the surroundings and are easier to integrate in everyday workspaces. Compared to an HWD, they do not block out the real-

world and are less intruding, while still providing important depth cues such as binocular disparity and motion parallax. However, this can be beneficial in some cases as Souse et al. [252] stated. They emphasize the important role of standardized illumination and ambient light conditions while radiological images are inspected as these vary depending on the physician's displays, lighting and seating position. An HWD allows to standardize these conditions. Still, semi-immersive systems involve less danger to injuries and they allow to interact with the real-world. This is especially helpful in one of the aimed use cases of this thesis – the usage of a semi-immersive system for treatment planning. This integration would not only be easier than a fully immersive system, but also more acceptable by physicians.

2.3

3

GUIDELINES FOR THE EVALUATION OF INTERACTIVE MEDICAL VISUALIZATIONS

INTERACTIVE medical visualizations are able to support diagnostic processes, therapeutic decisions and to satisfy intraoperative information needs. An evaluation of these systems is mandatory to assess existing techniques, to develop new ones as well as to generate and verify postulated hypotheses. Here, a wide variety of evaluation strategies exists that differ in several aspects. One aspect is the duration in which the evaluation is conducted. In longitudinal studies, several observations are carried out over a long period of time. The root of this type of evaluation lie in ethnographic methodologies, were researchers live in a different culture and take part in their daily activities as unobtrusive as possible [46]. Their subjective observations are recorded and evaluated in diaries. This technique was adopted in Human Computer Interaction (HCI) research as so called "diaries of use". Here, participants record their first-hand experiences over a longer time.

In contrast, cross-sectional studies analyze data of a study of one point in time. These are not unique in the context of 3DUIs, however, often an adaptation to the spatial input and output is necessary as these strategies were designed with 2D interfaces in mind [146]. An overview of different evaluation strategies and in which state of development they should be performed is described by [5].

Since medical visualization techniques are adapted to a specific application scenario, prior knowledge is often required, thus, the range of eligible participants is narrowed. For example, to assess the rupture risk of an aneurysm, different visualizations exist to assess morphological parameters such as the aneurysm volume [81] or hemodynamic parameters in form of the approximated blood flow [80, 273]. In these studies, participants have to judge, e.g. which aneurysm seems to be the larger one. Hence, they are also called "judgment studies" [39].

The medical visualizations are complex, as they rely on a fundamental understanding of different domains, e.g. in the aneurysm case a combination of anatomical knowledge as well as fluid and mechanical dynamics. As a result, only a small number of experts is available to assess the benefits of a visualization technique. The acquired results are difficult to reproduce and the generalizability is at least doubtful. An alternative approach investigated in more detail is quantitative evaluation as it can objectify research and determine whether a

37

statistically significant difference is achieved. However, statistical tests rely on a larger number of participants. Therefore, participants are selected that are as close as possible to medical experts. Here, often medical students are chosen, as they have at least a basic medical understanding. Of course, this basic understanding can compensate a completed specialized medical training only to a limited extent.

The main contributions of this chapter are comprehensive guidelines to quantitatively evaluate medical visualizations targeting computer scientists and engineers. These guidelines are summarized as a decision tree (see Figure 3.1), containing a distinction of evaluation approaches and presenting appropriate statistical tests for a variety of collected data.

This chapter is based on the publications:

- Glaßer, S., **Saalfeld**, **P.**, Berg, P., Merten, N. & Preim, B. *How to Evaluate Medical Visualizations on the Example of 3D Aneurysm Surfaces* in *Proc. of Eurographics Workshop on Visual Computing in Biology and Medicine (VCBM)* (2016), 153–162 [81], and

- **Saalfeld**, **P.**, Luz, M., Berg, P., Preim, B. & Glaßer, S. Guidelines for Quantitative Evaluation of Medical Visualizations on the Example of 3D Aneurysm Surface Comparisons. *Computer Graphics Forum (CGF)* **37,** 226–238 (2017) [233].

3.1 BACKGROUND ON EVALUATION RESEARCH

Psychophysics is the "scientific study of the relation between stimulus and sensation" [78] and is closely related to interactive medical visualizations. The findings from this discipline were incorporated into 2D and 3D visualizations [20] to enhance them and the evaluation process as well. The resulting user studies offer a scientifically sound method for the assessment of a visualization's suitability and performance [134]. However, evaluating only time and error is not enough. This is shown by the BELIV conference (**BE**yond time and errors: novel eva**L**uation methods for **I**nformation **V**isualization) that first took place in 2006. Although focusing on information visualization, the questions and problems discussed there are also highly relevant for interactive medical visualization. How trustworthy is a visualization? Does it present data in a way that shows the underlying uncertainty? If a visualization is superior to compared ones in all evaluated aspects, is this an indication of superiority, or did the study design favors this visualization technique? This so-called "boring dominance" and other problems with study designs are discussed in the work of Kim et al. [129]. Such work is important, since studies are challenging and most published research in this field only states the final and working evaluation setup, not mentioning the preceded stony path. Another example from information visualization is the work of Lam et al. [143].

They introduce and discuss seven evaluation scenarios, which are subdivided in scenarios for *understanding data analysis processes* and *visualization evaluation*.

The presented guidelines in this chapter for quantitative evaluation can be categorized into the *evaluation of user performance*, *evaluation of visualization type*, as well as *evaluation of visual data analysis and reasoning*.

Isenberg et al. took an in-depth look into evaluation practices of the IEEE Visualization community [114]. They describe several evaluation categories and recapitulate that the qualitative methods dominate the reviewed papers. However, an increasing trend to evaluate user experience and user performance was reported. Examples for this quantitative trend in the medical visualization domain are the performed studies from Gasteiger et al. [74] and the follow-up study from Baer et al. [13]. The work of Gasteiger et al. presented an aneurysm visualization and evaluated the visualization w.r.t. depth perception, flow perception and surface shape. Subsequently, Baer et al. [13] were able to determine statistically significant differences for the aneurysm visualizations compared to two other visualizations. Borkin et al. [27] determined the best suited visualization technique for the depiction of the endothelial shear stress of coronary arteries. The study provided by Díaz et al. [53] compared shading techniques for volumetric data with a quantitative statistical analysis. Preim et al. [206] provide an overview of perceptually motivated techniques for medical visualizations focusing on spatial depth and shape cues. They proposed to design study tasks generally, so that they are solvable by a broad range of users. As mentioned in the introduction of this chapter, a trade-off exists between a study with a few (often one) expert users and more participants that are as close as possible regarding the medical background knowledge. There is a high risk in creating tasks for a larger participant base: the external validity (i.e. generalizability) is reduced. In the worst case, the results are not transferable to the initial tasks and, thus, there is no added value for the initial medical application.

In the long run, interactive medical visualizations should support medical decision-making. To assess the impact on decision-making, a real-world scenario has to be tested with a system instead of an artificial situation in a lab. This was done by Lang et al. [144] with a computer assistance system for liver resection planning. Overall, 21 cases were used for a virtual tumor resection combined with computer-assisted risk analysis. In seven of these cases, the results changed the operation plan. Another example was presented by Lundstrom et al. and their evaluation of the *Medical Visualization Table* [155]. Five orthopedic surgeons should fulfill orthopedic surgery planning for two authentic cases of pelvic fractures. The overall tasks were to diagnose the fracture and plan the treatment, including the decision to treat or not. The surgeons were asked to *think aloud* during the whole treatment planning process. As a result, all orthopedic surgeons expressed that the table is a relevant and useful tool for clinical practice.

3.2 GUIDELINES FOR QUANTITATIVE EVALUATIONS

The following guidelines are based on the publication mentioned at the beginning of this chapter. More general, they are derived based on:

- the conducted evaluations of this thesis and the resulting experiences,

- discussions with different statistical experts, and

- the studies presented in Section 3.1.

The results are visualized in a condensed form with several stages as a decision tree in Figure 3.1. In the following, these stages are described in more detail.

The most general subdivision of methods is the distinction between qualitative methods, i.e. the investigation of *phenomena*, and quantitative methods, i.e. an analysis of *measurable properties* (see Figure 3.1, Stage 1).

Qualitative research is the appropriate approach for explorative research questions and allows the generation of hypotheses or provides basic information for a new application domain. For example, a novel medical visualization can be developed with this strategy by determining fundamental requirements. Also, the decision-making of a physician can be analyzed with this approach to get a deeper understanding of the process from initial data inspection to the final treatment decision. Here, the think-aloud method is a proven method to assess the influence of a new visualization technique on the interventional strategy.

On the other hand, quantitative evaluation methods can be used on all measurable properties to determine whether statistically significant differences exists or not. An important note is that *user subjective ratings*, e.g. assessed with a Likert scale, are measurable properties as well.

In interactive systems, these two types of design are seldom distinct categories, but represent different ends of a continuum. Thus, a user study usually tends to be more quantitative or qualitative [47, 178]. There also exists the explicit middle of this continuum, called mixed method research. A combination of both approaches is also possible. In the work of Lawonn et al. [148], the most common feature line techniques were applied to various surfaces, including anatomical structures. A qualitative evaluation with 129 participants was conducted to assess these techniques regarding aesthetic qualities. In a follow-up study from Baer et al. [16], the same data was used to conduct a quantitative analysis. Here, statistical tests were used to identify significant differences between the used feature line techniques. For more information on mixed method research, the interested reader is referred to the book of John Creswell [47].

By following the decision tree on the quantitative evaluation branch, the next step is to check whether all requirements for an inferential analysis are met (see Figure 3.1, Stage 2). Examples for requirements are a large enough sample size or a clearly stated hypothesis [66]. If these requirements are not met, a descriptive analysis can be performed, comprising a test of the distribution of the data and
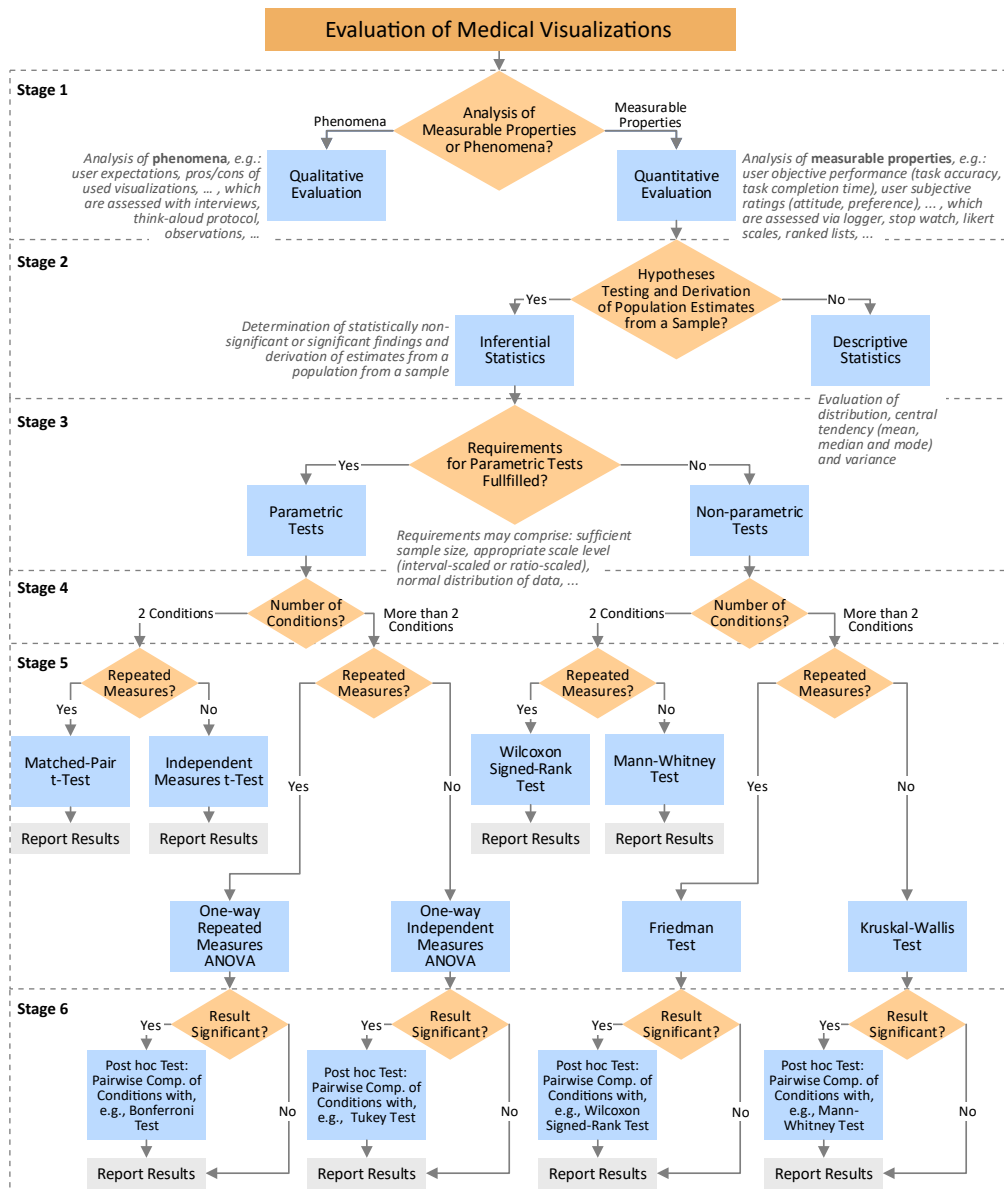
Figure 3.1: Guidelines represented as a decision tree focusing on quantitative evaluation (Stage 1). In Stage 2, the researcher decides if statistical significant or non-significant findings are useful or descriptive statistics are sufficient. The chosen statistical test depends on the type of collected data (Stage 3), the number of conditions (Stage 4) and the study design (Stage 5). Post hoc tests are possible if more than two conditions were tested (Stage 6). Image from Saalfeld et al. [233] © John Wiley and Sons 2017.

an evaluation of measures for variance and central tendency. Appropriate visualizations for this information should be provided via bar charts, boxplots, and histograms. For inferential statistics, these visualizations should be presented as well to support the interpretation of the data and allow other researchers to conduct a meta analysis and better understand the results.

The following section explains evaluation strategies for inferential statistics in more detail. Here, examples and specific problems in the medical field are investigated, followed by suggestions how to solve them. Since there exists a variety of statistical tests with differing assumptions about the sample size, distribution of the data, number of compared conditions etc., only the most common tests are pointed out and when to apply them. For a thorough discussion of probability models and a justification for the usage of a test, the reader is referred to the book of Andy Field [66].

3.2.1 *Parametric vs. Non-Parametric Tests*

Parametric tests, such as a t-test, are used to investigate differences between mean values. They have more statistical power and, thus, a higher probability to reveal possible significances than non-parametric tests. However, they are only applicable if specific requirements are met, e.g. the data is appropriately scaled, is normally distributed, and the sample size is sufficient (see Figure 3.1, Stage 3). In practice, parametric tests are frequently applied even if requirements are violated. This is justified with the argument that these tests are robust against these violations [66]. As a result, it is complicated for non-statistic professionals to decide when, e.g. a sample size is too small or a deviation from normal distribution is too strong. A general suggestion to simplify this decision is to investigate the *measure of central tendency* and the *scaling of the data*. Possible measures of central tendency are the mean, median and mode. A parametric test should only be used if the *mean* is able to represent the central tendency of the data. An illustrative example of a violation against this assumption is the usage of a forced-choice Likert scale for data acquisition. When using this type of scale, a neutral choice is missing. A calculated mean value could lie between negative and positive ratings and indicate a neutral choice. This is problematic, since the neutral choice was explicitly prohibited with the experimental design. In this example, the median would be the appropriate measure of the central tendency and would result in the usage of a non-parametric test.

The scaling of the data can have different properties. It can either be discrete (ordinal, nominal) or continuous (interval or ratio scale). For ordinal scaled data that is generated with, e.g. ranked lists, the usage of a parametric test is controversial and, if in doubt, a non-parametric test should be used. Continuous scaled data should be examined with two approaches, i.e. a test of normal distribution accompanied by a visual inspection of the histogram [66]. A feasible test for this is the Shapiro-Wilk test that examines whether the collected data
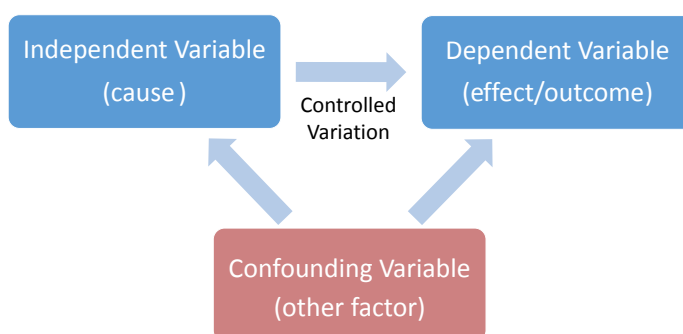
Figure 3.2: Schematic overview of the three types of variables. The independent variable is changed via a controlled variation. The result of this variation is the measurable dependent variable. All non-controlled influences are called confounding variables.

is based on a normally distributed population or not. Outliers should be considered as well, however, the definition of outliers is not definite. For example, the software *SPSS Statistics* (IBM Corporation, Armonk, New York, USA) differentiates between mild and extreme outliers. Both are defined based on the interquartile range (IQR), which describes 50 % of the data lying between the 25th and 75th percentiles. If a value differs more than 1.5 times from the IQR, it is considered as a mild outlier. If it differs more than 3 times, it is considered as an extreme outlier. An additional visual inspection of the data distribution is necessary, since the common small sample sizes in medical visualizations rarely result in normally distributed data. Through the visual inspection, a rough estimation of the distribution is possible. Again, if the data significantly deviates from a normal distribution and the visual inspection confirms this (for example if the distribution is shaped like a U), a non-parametric test is the better choice.

3.2.2 *Independent, Dependent & Confounding Variables*

The three types of variables and their interactions are depicted in Figure 3.2. In interactive medical visualization, a common independent variable is the visualization technique, whereas the different techniques are the respective conditions (see Figure 3.1, Stage 4). By using different visualization techniques, the independent variable (also called factor) is varied in a controlled way. A typical form of controlled variation is using an established visualization technique and a new one. This leads to measurable changes to the dependent variable. Examples for dependent variables are objective measures (e.g. required time) and subjective ratings (e.g. preferability).

Besides this controlled variation, unwanted influences to the dependent variable also occur. These are called confounding variables. Examples are the study duration or the participant's motivation that influence the results [48]. In inter-

active medical visualizations, differences in the perception abilities of the participants (e.g. color blindness) are important confounding variables. Furthermore, differences of the used output device can have an impact, e.g. display brightness, size and contrast. Usually, highly specialized physicians are invited to conduct the study, as they represent domain experts of the field. Their varying experience is also a confounding variable. A possibility to reduce these confounding variables is to keep them *constant*. This is easy for aspects such as display types and lighting conditions by using usability labs. However, it is more difficult for professional experience. Hence, questionnaires can be used to quantize the experience to a certain degree; then, only participants with similar experience could be asked. Another problem is the so-called *novelty bias* which occurs when a new visualization technique is compared to established ones. Here, a thorough preceding training session is necessary to reduce the bias until the initial learning curve reaches a plateau.

Overall, when keeping the confounding variables constant, every participant is equally exposed to them. Therefore, observed variations in the results are explained by the varied independent variable alone. The radical elimination of all confounding variables can have a negative impact on the evaluation as it reduces the external validity. That is due to the fact that all kinds of uncontrollable variations occur in real clinical settings. Even the same physicians differs from day to day regarding their attention span and motivation. Furthermore, the used hardware and light conditions differ and the used data sets are different from patient to patient. Researchers have to find the right balance between realism and control. Alternatively, several studies with different degrees of external validity can be performed.

3.2.3   *Tasks & Datasets*

An evaluation task should reflect the corresponding real-world task and its main challenges as realistic as possible [48]. As they create a link between the independent and dependent variable, mistakes in the task definition conclusively lead to meaningless results. For interactive medical visualizations, this assumption is a strong limiting factor for the available number of participants. This is due to the fact that tasks which imitate a real clinical scenario require the know-how that physicians gained during their whole career through education, training and experience. This is even more pronounced in cases of special medical fields, e.g. neuroradiology. Here, a smaller number of specialized surgeons and radiologists could participate. This results in less collectible data and eventually statistical analyses loose power due to the small sample size. A possible way around this dilemma is approximating the tasks such that non-expert users can provide valuable test results.

As an example related to interactive medical visualization, a physician may estimate the size of a tumor and its distance to a vessel. This could be approx-

Group 1 ⟶ Level 1

Group ⟶ Level 1 ⟶ Level 2   Group 2 ⟶ Level 2

(a) Repeated measures design   (b) Independent measures design
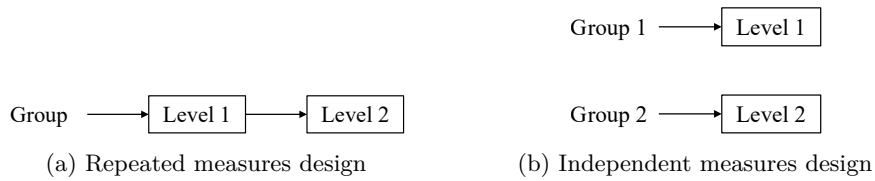
Figure 3.3: (a) Depiction of the procedure of a repeated measures design where each participant is exposed to all levels of an independent variable. In contrast, with the independent measures designs from (b), separate groups are exposed to different levels of the independent variable. Images inspired by Baer [14].

imated by representing the tumor as a sphere and the vascular structures with lines. Now, this task is solvable by non-expert users as well. However, this limits the relevance and possibility for generalization [14]. The sphere does not represent the heterogeneous shape of a tumor. Furthermore, a tumor represented as an iso-surface was segmented at some point. This segmentation has an inherent uncertainty due to possible over- or under-segmentation (thus, the tumor could be larger or smaller). Experts in this field can implicitly integrate this information in their estimation, a non-expert user would not be able to do this.

In summary, several similar tasks should be implemented to increase the result's plausibility and to improve the external validity and reliability. For pathologies such as aneurysms, different types and sizes can be shown to evaluate a single interactive aneurysm visualization. Special attention should be paid to create tasks with comparable difficulty. Otherwise, this can lead to a high variance in the results. Additionally, the aggregation of the acquired data should be analyzed either run- or participant-related, which is explained in more detail in Section 3.2.5.

3.2.4 *Experimental Design*

Experimental design can be divided into two types, illustrated in Figure 3.3:

- repeated measures design (within-subject), aiming at the variability of a particular value for the same individuals under different conditions, or

- independent measures design (between-subject), aiming at differences between groups (see Figure 3.1, Stage 5).

The choice of experimental design depends on factors such as available participants and the evaluation goal. Benefits of independent measures studies are the avoidance of sequence or learning effects. In addition, the evaluation time is shorter for each participant compared to repeated measures design. An illustrative example of a pronounced sequence effect would occur if participants are asked to estimate the water temperature by holding their hands in a water bowl.

The estimated temperature would be overestimated if the preceded temperature was very cold and vice versa.

However, a challenge is to recruit a comparable group of participants (w.r.t. age, experience, knowledge, etc.). These prerequisites are not easily met in the medical domain. Thus, independent measures studies may suffer from interpersonal differences. Repeated measures studies avoid these differences. Since learning or sequence effects may occur with a repeated measures design, particular care should be taken for the definition of tasks (e.g. the order of conditions across participants should be balanced) [48]. Although repeated measures designs are influenced by intrapersonal differences such as getting tired during the experiment, they may be superior to independent measures studies. This is due to a reduction of overall variance, allowing to reveal significant differences more easily [66].

In summary, repeated measures studies are recommended for the interactive medical visualizations due to the lower number of required participants and the reduced variance. However, certain evaluation goals cannot be achieved with this design. An example is the impact of a specific visualization on the surgical procedure of a single patient as the surgery can only be carried out once. An independent measures design should also be favored if there is a strong and hard to control influence of a learning effect. In interactive medical visualization, this can occur if only a few data sets are available that should be visualized with different techniques. A possible risk is that participants recognize the data set and answer according to their previous knowledge. An independent measures design is also mandatory if the conditions are exclusive properties of the participants, e.g. physicians are either novices or experts. These groups can only be analyzed by considering them independently.

The chosen design eventually influences the applicable statistical test. If the acquired data fulfills the requirements for a parametric test with more than two conditions and was conducted with a within-subject design, it needs to be analyzed with a repeated measures Analysis of Variance (ANOVA). A summary of when to apply which test is illustrated in the decision tree (see Figure 3.1).

3.2.5 *Data Aggregation Choices*

The acquired data of the study can either be related to *participants* or to *runs* of a study. The data should be handled related to participants if the impact on participants is investigated, e.g. the impact of a medical visualization technique on physicians. If, on the other hand, features of a technical system are tested, the results would be independent of the participants and the data sets should be related to single runs. In the participants-related case, the data should be aggregated, in the run-related case, it should be inspected individually.

The following example of the impact of a medical visualization on a physician should illustrate this distinction. The reliability of the measured results is im-

proved by conducting five runs with different data sets. Therefore, five results are obtained. A frequent mistake is to handle these results independently. However, since this evaluation scenario is focused on the physician (i.e. participant-related), the results must be aggregated to a single value. Inappropriate data aggregation can strongly bias the results of statistical tests. By ignoring the aggregation of participant-related evaluations, the sample size is artificially enlarged, which leads to an underestimation of the real data variance. This type of wrong aggregation would result in a more liberal statistical test, i.e. statistically significant results are obtained although no true effects exist [157].

3.2.6 *Using Post Hoc Tests*

The usage of post hoc tests is optional and only possible if more than two conditions were tested (see Figure 3.1, Stage 6). They allow to identify the best or worst of several conditions by reporting possible significant differences between pairs of conditions. The procedure on the usage of a post hoc test is as follows:

1. a statistical test compares all conditions simultaneously against each other (see Figure 3.1, Stage 5),

2. if a significant difference exists, a pairwise comparison of each condition is performed (see Figure 3.1, Stage 6).

A repeated measures ANOVA for three conditions may reveal a significant difference between the conditions. Now, the researcher knows that they differ significantly, but it is not possible to tell which condition performed best. Therefore, the Bonferroni post hoc test is an appropriate method. This test compares the mean values between each two conditions with t-tests, resulting in three further tests. The selection of the correct post hoc test is difficult and depends on several factors (mainly how strict or liberal the statistical test should be). This difficulty is illustrated by the amount of possibilities: in SPSS Statistics 22.0 there exist 18 selectable post hoc tests. To facilitate the selection, the decision tree (see Figure 3.1) provides the most common for each experimental design, based on the suggestions from Andy Field [66].

3.3 DISCUSSION & CONCLUSION

The ultimate goal of interactive medical visualization is the application in daily clinical practice to fulfill information needs and to support diagnosis and treatment planning. To assess whether a new technique can fulfill these needs, several evaluation strategies exist, which follow opposing approaches: from qualitative research with high realism and an observing character to quantitative research

with high precision and control. Both approaches allow the assessment of important properties, but simultaneously have immanent downsides. Qualitative evaluation is mostly used and well known in the visualization domain [114]. However, a small number of non-expert participants lead to results with a limited transferability to clinical practice. The same problem is stated in the Information Visualization community by Sheelagh Carpendale [39], where she identifies nonconvincing evaluations as a reason why new techniques are not adopted outside the research domain. The in-depth description and guidelines for quantitative evaluation given in this chapter can help designing convincing experiments with meaningful results. To cope with a possible small number of participants, tasks can be simplified to be understandable for non-expert participants. This, however, happens at the cost of external validity. Eventually, convincing evaluations need both parts: the verification that a new technique can support a physician in a realistic environment and that it achieves this in a controlled, reproducible manner. In consequence, researchers should aim at conducting mixed designs whenever possible if they are aiming for an impact to clinical practice.

4

STERILE GESTURE INTERACTION FOR INTERVENTIONAL RADIOLOGY

MANY medical interventions are not carried out in surgery, but with minimal-invasive interventions by specialized radiologists. In contrast to surgery, needles and catheters are moved through thin holes to the target anatomy. The tip of the instrument is tracked with constant imaging control to compensate for the missing direct interaction with the human tissue. Here, the physician needs to interact with interventional imaging software. To maintain the aseptic environment, this has to be sterile. Additionally, it needs to be efficient and usable, especially in critical situations. As described in Section 2.2, interaction styles such as 3DUIs and NUIs offer solutions for this. This chapter presents possibilities for sterile, gesture-based interaction on radiologic workstations using the LMC and addresses the challenges in the following ways. Due to the touchless interaction, sterility is ensured, which lowers the infection risk for the patient. Furthermore, the direct interaction with interventional imaging software without the necessity to delegate instructions to a technical assistant bears the potential for are more efficient interaction. Finally, the interaction allows more DoF compared to, e.g. mouse input and, therefore, intuitive control of spatial tasks such as the manipulation of 3D medical image data and the navigation in 3D space.

The medical background and identification of interaction tasks in the next section give an overview of a radiologist's workflow during an intervention. The tasks comprise basic and measurement tasks with 2D and 3D medical image data, such as elemental manipulations as well as performing distance measurements. After the description of these tasks, two gesture sets are presented, each evaluated with a comparative study against established input modalities. The first gesture set serves to perform basic interaction tasks, such as rotation and translation of medical data. The evaluation results showed that the developed gestures were inferior regarding task completion time and intuitiveness. Therefore, the gesture set was redesigned and extended to cover a broader range of functions and to support the physician in memorizing and executing gestures. Again, the gestures were assessed in a comparative study and shown to be inferior regarding task completion time, accuracy and usability. Considering that both gesture sets allow to solve typical tasks

49

with medical image data in a sterile manner, they are still beneficial regarding patient safety. However, it is arguable whether this can compensate for the lower efficiency and usability compared to established interaction techniques.

This chapter is based on the publications:

- **Saalfeld**, **P.**, Mewes, A., Luz, M., Preim, B. & Hansen, C. *Comparative Evaluation of Gesture and Touch Input for Medical Software* in *Proc. of Mensch & Computer* (2015), 143–152 [235] and

- **Saalfeld**, **P.**, Kasper, D., Preim, B. & Hansen, C. *Touchless Measurement of Medical Image Data for Interventional Support* in *Proc. of Mensch & Computer* (2017), 83–92 [232].

4.1   BACKGROUND ON INTERVENTIONAL RADIOLOGY

Interventional radiology combines minimal-invasive approaches and medical image guidance to treat patients. The images are acquired most significantly with Computer Tomography (CT) and MRI, which produce a series of 2D images. These images are either analyzed in its recorded form in 2D or combined to image stacks, which can be inspected with volume rendering or serve the generation of surface models. Both 2D images and 3D models are necessary in medical routine. 3D structures convey the overall shape, size and relations to other structures, but occlude potentially important details. 2D images overcome this limitation by revealing the inside.

The image data, either in 2D or 3D, is used by the physician to determine tumor locations, track surgical devices and decide, which interventions are appropriate. Besides a qualitative visual assessment, quantitative measurements are a necessity for treatment decisions [225] (recall Section 3).

In general, there exist three approaches to maintain sterility during the control of interventional software:

- A technical assistant controls the software from a non-sterile room with voice commands from the physician [108, 185]. This indirect delegated interaction method is inefficient and error-prone, since misunderstandings easily occur.

- The physician moves to a separate room with a workstation and uses mouse and keyboard interaction [108]. Besides the time for relocating, this approach is problematic due to the aspect of sterility. The physician needs to sterilize again, which not only leads to longer operation time but also increases the risk of possible infections. Additionally, the interaction with 3D visualizations by indirect mouse input is not ideal.

- The medical software in the operating room is controlled with a touchscreen device. The touchscreen is covered with a sterile transparent foil

leading to reduced usability. Furthermore, dependent on the current position of the surgeon, the touchscreen is out of reach. Therefore, the physician needs to move to it or lean over the operating table to interact with it. This is problematic due to the distraction of the workflow and the ergonomic disadvantage [90, 167, 270].

4.1.1 *Interaction Tasks*

The identification of the interaction tasks is based on:

- interviews with radiologists,

- observations during interventions, and

- the work of Hübler et al. [108].

Hübler et al. described and analyzed the workflow of interventional neuroradiology with frequent pattern mining [26]. They revealed common tasks such as controlling operating room equipment, e.g. the operating table or the C-arm, a c-shaped X-ray device. As described, the interaction with the resulting image data is necessary to retrieve information about, e.g. the contrast agent and blood flow behavior in vessels or to determine current positions of operation devices.

The two structured interviews (45 minutes each) with physicians and the two observations during interventions were conducted at the neuroradiological institute at the university hospital of Magdeburg. During the interventions, aneurysms were treated by *coiling*, i.e. a platinum wire was used to prevent blood flowing inside the aneurysm to avoid rupture. Figure 4.1 shows the setup of an interventional operation room. In the following, the identified basic interaction and measurement tasks are described.

4.1.1.1 *Basic Tasks*

During the observed interventions, the physician started by loading and observing the image data to find the relevant image slices and perspectives in 3D. Here, the physician was able to manipulate the underlying data (translation, rotation and scaling). During this navigation, rotations were most commonly used. This results in the following tasks:

- 2D tomographic images:
  - cycle through the stack of images

- 3D model:
  - rotation around arbitrary axis

- both views:

Figure 4.1: Exemplary setup of an interventional room at the neuroradiological institute at the university hospital of Magdeburg. Image from Saalfeld et al. [232] and made available in the digital library of the Gesellschaft für Informatik under the Creative Commons BY-SA 4.0 License.

– trigger button selection, e.g. to load image data, show additional information or reset the scene,

– zoom in to interesting structures such as tumors,

– zoom out to get an overview,

– translation of the image position or the object position.

4.1.1.2 *Measurement Tasks*

During treatment planning and interventions, different types of measurements are helpful. Among others, vessel diameters, lengths, aneurysm heights and volumes, boundaries, maximum and minimum extents are important. According to the interviewed physicians, distances are by far the most important type of measurement. For example, they are used to determine the distance between a tumor and essential risk structures, such as larger vessels. They are also used if volume measurements would be more appropriate, since their creation is easier in radiologic workstation software. Considering all types of measurements would lead to a complex application with an extensive gesture set. Therefore, only distance measurements are considered and requirements of these are inspected in the following.

SUPPORT FOR PRECISE POSITIONING OF MEASUREMENTS   The ability to precisely position measurements is crucial for accurate measurements [204]. This is especially difficult with freehand gestures, since hand tremble and inaccurate tracking creates noise [88]. Therefore, user support in form of smoothing and snapping should be available. To cope with possible errors during measurement creation, the physicians should be able to adjust and delete existing measurements.

VISUALIZATION OF MEASUREMENTS   The visualization of the measurement is important, since it ensures that the physician is able to associate the measurement to the correct structure. Furthermore, the depiction and alignment of the measured value affects how easy it is to read it. Depending on the task, measurements can yield more useful results on the 2D image data or on 3D planning models. For example, the heterogeneity of a tumor has to be inspected on a 2D slice, but the spatial extent can be measured more easily on a 3D model [204]. According to the physician, this also depends on the preference of the medical practitioners. Therefore, the system should show the 2D image data and its measurements in all three standard 2D image directions (sagittal, frontal, transverse).

4.2 PERFORMING BASIC TASKS WITH FREEHAND GESTURES

This section presents a gesture set to solve the basic tasks presented in the former section (see Section 4.1.1.1). The used gesture set is taken from the publication from Mewes et al. [167], which was co-authored by the author of this thesis. There, freehand gestures are used to control a radiological software prototype that is projected on the radiation shield of a multi-detector computed tomography (MDCT) scanner. A user study demonstrated that this approach is in principle useable by physicians to solve basic tasks. However, the robustness and intuitiveness of the gesture set needs to be improved. This was presented in the follow-up work of Saalfeld et al [235]. The improved gesture set was compared to touchscreen interaction in a user study. Here, the time to solve typical interaction tasks and the intuitiveness are evaluated. The results show that participants performed significantly worse with gesture interaction and rated the intuitiveness of touchscreen interaction higher. Both forms of input and the user study are described in more detail in the following.

The developed prototype uses the LMC for gesture recognition and the Leap Motion SDK V2 2.3.1[1]. It either recognizes the gestures directly or offers functions to query the position, orientation and amount of extension of each finger

---

[1] Leap Motion SDK V2.3.1: https://developer.leapmotion.com/sdk/v2, last accessed: 11.06.2018

(a)   (b)   (c)   (d)   (e)
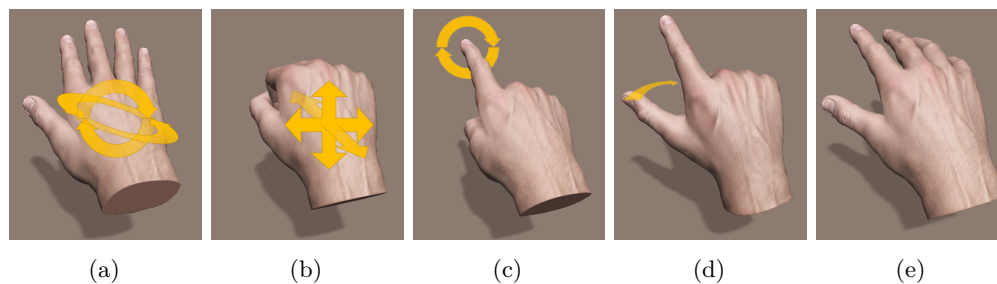
Figure 4.2: The modified freehand gesture set presented by Mewes et al. [167] with an improved rotation gesture for 3D rotation (a). Instead of rotating the object with a grab gesture, the hand can be tilted to perform 3 DoF. Image from Saalfeld et al. [235] and made available on De Gruyter under the Creative Commons Attribution-NonCommercial-NoDerivatives 3.0 License.

to develop an own gesture recognition ability. Additionally, the visualization framework VTK 5[2] and Qt 5[3] were used.

4.2.1 *Used Gestures*

As mentioned, the gesture control is realized with an improved freehand gesture set presented by Mewes et al. [167]. There, five gestures were introduced to control different interaction tasks, which are shown in Figure 4.2. Their grab gesture to rotate the 3D model was modified due to robustness problems. Instead, the object can be continuously rotated in all 3 DoF through tilting the hand with all five fingers extended (flying hand gesture, see Figure 4.2a). A dead zone guarantees that no unwanted rotation is performed. Zooming and translation is available in the 2D and 3D view and is realized by virtually grabbing the objects on the screen and translating the hand forward/backward for zooming and left/right/up/down for translation (fist gesture, see Figure 4.2b). Cycling through the 2D image stack is achieved by performing a circle gesture while the index finger is extended (see Figure 4.2c). The user can influence the step size by varying the circle's radius. A click gesture is implemented for the selection of structures or buttons (see Figure 4.2d). To select an object, the user has to extend the index finger and thumb, point to the object and move the tip of the thumb to the knuckle of the middle finger. If no action should be performed, a relaxed hand is used as a rest gesture (see Figure 4.2e).

---

2 VTK: https://www.vtk.org/, last accessed: 11.06.2018

3 Qt: https://www.qt.io/, last accessed: 11.06.2018

4.2.2 *Comparative User Study*

The following section summarizes the user study comprising the experimental setup, study design, procedure and results.

4.2.2.1 *Experimental Setup*

To recreate an interventional setting, a table with a body phantom is placed in front of the participants (see Figure 4.3a). The LMC is placed on the edge of the table within the user's arm range (see Figure 4.3a).

For touch interaction, the touchscreen of the commercial state-of-the-art surgical navigation system CAS-ONE Liver is used (CAScination AG, Bern, Switzerland). The display is a resistive medical touchscreen (ELO 2400 LM 24″, Elo Touch Solutions, Inc.) (see Figure 4.3b). The touch control is modeled after interaction with the CAS-ONE Liver system. Interestingly, the control is primarily based on pressing buttons and, thus, the advantages of the NUI aspect of touch interaction are not exploited. The cycling of 2D image data is realized with "up" and "down" buttons to change to the next or previous slice in the image stack. Discrete zooming is realized with "+" and "−" buttons. There are three exceptions on the button control: the rotation of the 3D model and the translation of the 2D position are realized with swipe movements on the touchscreen, and structures in the 3D view can be selected by touching them directly.

The developed prototype that is used for the user study can switch between gesture and touch interaction (see Figure 4.3c). It is displayed on the touchscreen, which is covered with a sterile transparent foil to recreate the interventional setting. As the test data set, 2D tomographic image slices and the reconstructed 3D model from a human liver with a hepatocellular carcinoma is used.

4.2.2.2 *Tasks & Study Design*

The participants solved five tasks (see Table 4.1). These were selected based on observations in the operating room and on subsequent discussions with clinical partners. The independent variable is the interaction modality with the two conditions *gesture-based* and *touch-based* input. As dependent variables, the task completion time and the intuitiveness are chosen. For intuitiveness, the *QUESI* is used (Questionnaire for the subjective consequences of intuitive use) [110]. It contains 14 items grouped into five sub-scales, such as subjective *mental workload* and *perceived achievement of goals*. The answer scale is a five-point Likert scale from 1 (fully disagree) to 5 (fully agree). The results of all items can be combined to a single score. Higher scores represent a higher probability of intuitive use.

The experiment is conducted with a repeated measures design, i.e. every participant fulfills the tasks with both input modalities. This prevents the influence of interpersonal differences. To avoid sequence effects, the experiment is performed as a crossover experiment (recall Chapter 3).

4.2

Table 4.1: Overview of the five tasks and the corresponding gesture or touch interaction to solve it.

Task	Description	Gesture	Touch interaction
1	Identify the range of 2D slices in which a tumor is located	Circle	Press buttons
2	Zoom the current 2D slice to factor 2.0 and center the tumor	Fist	Press buttons
3	Match the 3D rotation of the 3D model identical to a presented model	Flying hand	Drag
4	Zoom into the 3D model to zoom factor 2.0	Fist	Press buttons
5	Select the tumor in the 3D view	Click	Press buttons

4.2.2.3 *Procedure*

First, a pre-questionnaire was handed out. Besides demographic questions, it contains questions about experience with:

- interventional imaging software,

- gesture interaction,

- touchscreen interaction on smartphones and tablets, and

- touchscreen interaction in an operating room.

Every question was stated on a scale from 1 (no experience) to 5 (very much experience). The experimental setup including the touchscreen and the LMC were explained after that. Secondly, the prototype to inspect the medical data was described including its different functions. Then, the participants were asked to put on rubber gloves and started with one of the two interaction modalities with the following sequence:

1. in the instruction stage, different functions were explained based on the input modality and corresponding gestures were shown,

2. the participants could exercise the functions as long as they want until they were confident in using them,

3. the five tasks were stated subsequently, and,

4. the QUESI was handed out.

After that, the participants followed the same sequence for the second input modality.

4.2.2.4 *Results*

The study was conducted with ten medical students (7 female, 3 male). Their age ranged from 20 to 27 years ($\bar{x}$ (mean) $= 22.7$ years) and one of them was left-handed. The experience with different modalities is shown in Figure 4.4. The participants had little experience with interventional imaging software ($\bar{x} = 2.3$), with gesture interaction ($\bar{x} = 2.3$) and with touch interaction in the operating room ($\bar{x} = 2.5$). In contrast, they had much experience with touch interaction on smartphones and tablets ($\bar{x} = 4.2$).

The participants trained less than 10 min for each input modality. The task completion time was analyzed by a 2×5 repeated measures ANOVA (two conditions: gesture vs. touch $\times$ five tasks).

TASK COMPLETION TIME   The results for task completion time are shown in Figure 4.5. Compared to touch interaction ($\bar{x} = 25.4$ s, s (standard deviation) $= 35.3$ s), the participants needed almost twice as long to perform a task with freehand gestures ($\bar{x} = 48.6$ s, $s = 43.1$ s), which resulted in a significant difference ($F(1, 9) = 17.82$, $p < .01$, $\eta^2 = .66$, η^2 is the effect size, i.e. a measure of the strength of the relationship between the two variables). The rotation of the 3D model (task 3: $\bar{x} = 72.6$ s, $s = 51.8$ s) took the longest time, followed by the identification of the tumor's range of slices (task 1: $\bar{x} = 62.0$ s, $s = 44.4$ s), zooming of a 2D slice and centering the tumor (task 2: $\bar{x} = 25.0$ s, $s = 15.7$ s). In contrast, the tasks to zoom the 3D model (task 4: $\bar{x} = 12.8$ s, $s = 10.9$ s) and select the tumor (task 5: $\bar{x} = 12.6$ s, $s = 17.2$ s) were performed very fast. There was no significant interaction effect ($F(4, 36) = 2.32$, $p = .14$, $\eta^2 = .21$), although Figure 4.5 implies this: while there seems to be no difference between the two conditions for rotation of the 3D model (task 3: $\bar{x} = 68.5$ s, $s = 57.9$ s vs. $\bar{x} = 76.7$ s, $s = 47.8$ s), participants need much longer to identify the range of slices with gestures than with touch interaction (e.g. task 1: $\bar{x} = 90.9$ s, $s = 45.2$ s vs. $\bar{x} = 33.0$ s, $s = 16.0$ s).

INTUITIVENESS   The intuitiveness measured by the QUESI was analyzed with the Wilcoxon signed-rank test (see results in Figure 4.6). Overall, users found touch interaction more intuitive ($\bar{x} = 4.2$, $s = 0.5$) than gesture interaction ($\bar{x} = 3.5$, $s = 0.7$), which resulted in a significant difference (Wilcoxon-U $= -2.5$, $p < .01$). After the Bonferroni adjustment of the alpha level for the QUESI subscales, significantly higher scores emerged for touch interaction in comparison to gesture interaction only for two dimensions: *mental workload* (Wilcoxon-U $= -2.5$, $p < .01$; $\bar{x} = 4.1$, $s = 0.5$ vs. $\bar{x} = 3.2$, $s = 1.0$) and *familiarity* (Wilcoxon-U $= -2.7$, $p < .01$; $\bar{x} = 4.3$, $s = 0.6$ vs. $\bar{x} = 3.4$, $s = 0.9$). However, the data shows a trend for less perceived effort of learning for touch interaction (Wilcoxon-U $= -2.4$, $p = .01$; $\bar{x} = 4.4$, $s = 0.5$ vs. $\bar{x} = 3.4$, $s = 1.0$). There

(a) (b)

(c)
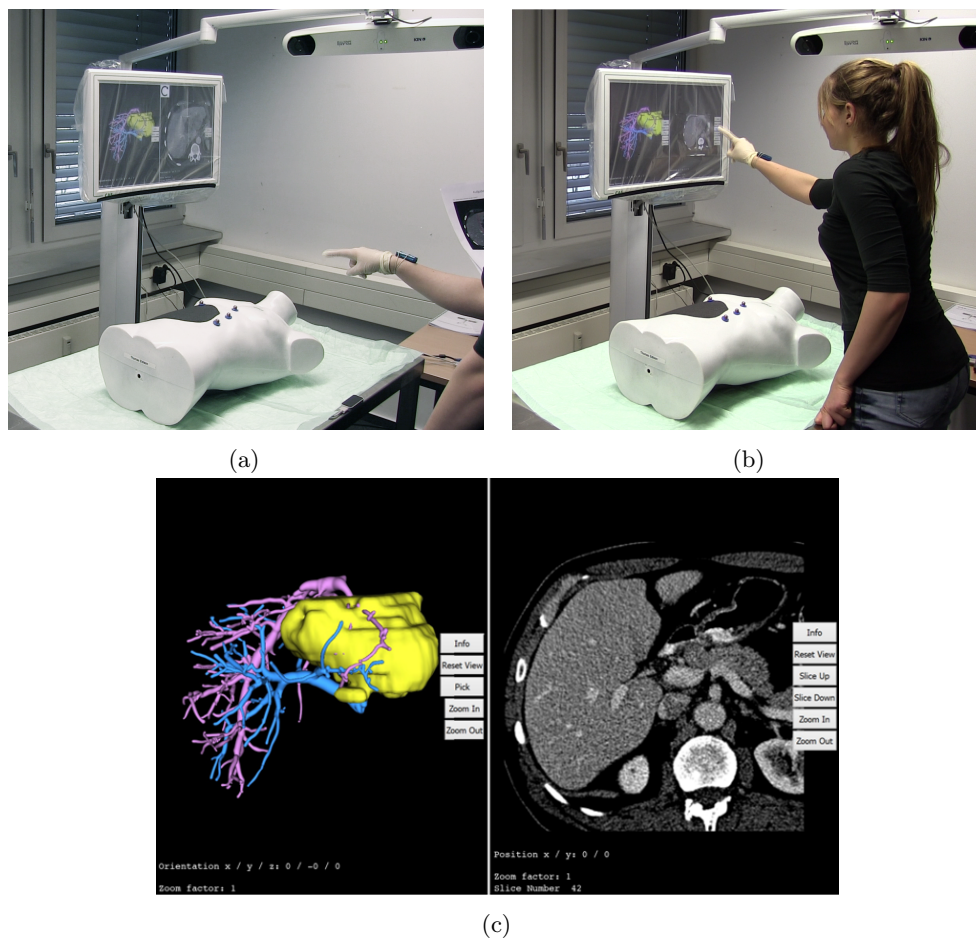
Figure 4.3: Experimental setup with touchscreen, plastic foil, surgical table and Leap Motion Controller (below hand, (a)). A user is performing tasks with free-hand gestures (a) and touchscreen interaction (b). In (c), a screenshot of the prototype used in the study is shown. Images from Saalfeld et al. [235] and made available on De Gruyter under the Creative Commons Attribution-NonCommercial-NoDerivatives 3.0 License.
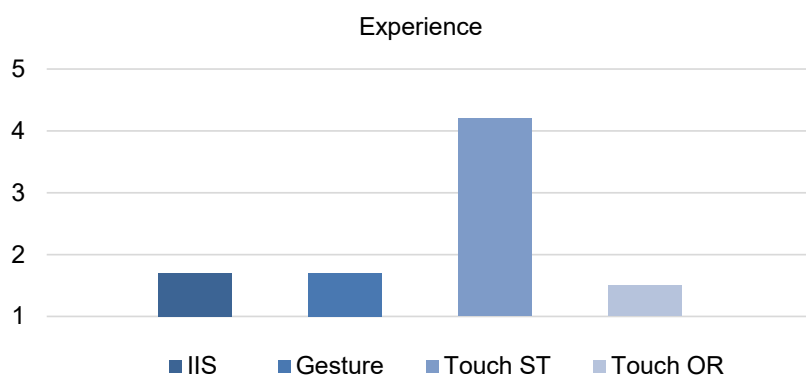
Figure 4.4: Overview of the participants' experience with different systems and input modalities on a scale from 1 (no experience) to 5 (very much experience).
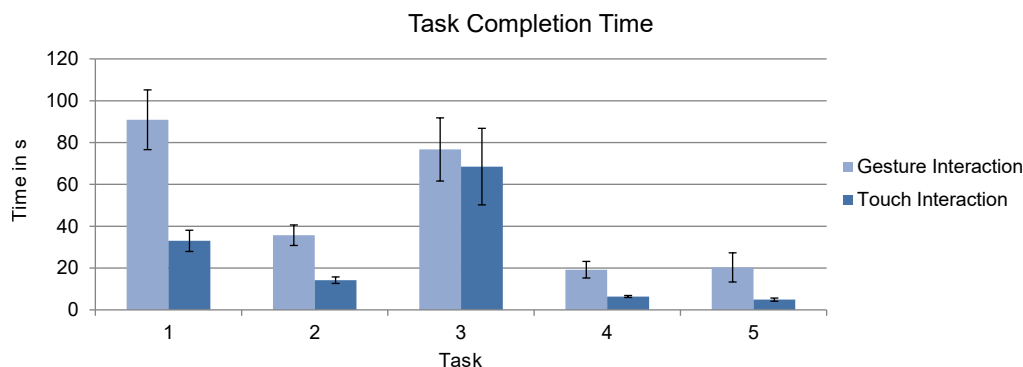
Figure 4.5: Comparison of the task completion time with freehand gesture and touch-screen interaction.
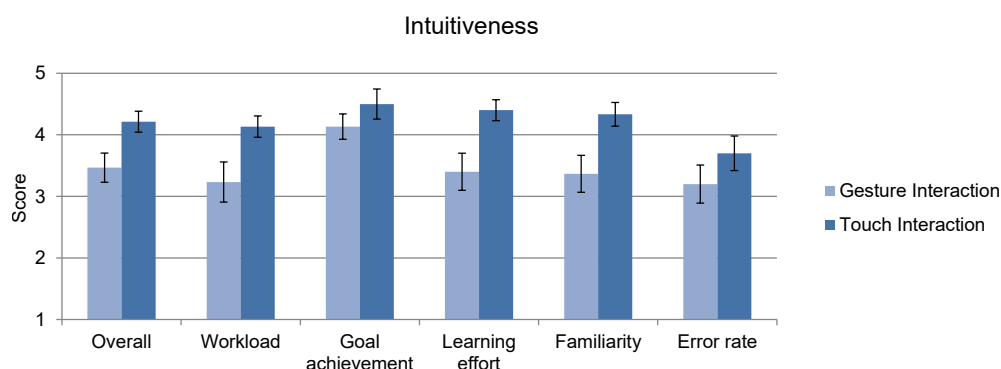
Figure 4.6: Comparison of the intuitiveness of freehand gesture and touchscreen inter-action.

was no significant effect for the sub-scales *perceived achievement of goals* and *perceived error rate*.

4.2.3 *Discussion*

This section presented a gesture set and interaction techniques to perform basic interaction tasks to control a radiological workstation software. The comparative user study showed significantly worse performance results with gestures in almost all tasks. Only for 3D rotation there was no significant difference between the two conditions regarding the task completion time. This indicates that for more complex interaction tasks higher degrees of freedom of freehand gesture interaction can compete with touch interaction. Another reason for longer task completion times was observable during the execution of gestures: some participants forgot how to correctly execute gestures. This issue could be avoided if they had more training time and if the UI shows a permanent overview of the possible gestures. The participants were medical students and, thus, had less ex-

perience in interventional settings compared to physicians. However, the medical knowledge necessary to fulfill the tasks is fairly basic.

The advantages of touch compared to gesture interaction were also found in terms of intuitiveness. This explains the significant differences of the interaction types on the sub-scales *workload*, *learning effort* and *familiarity*. Indeed, if one considers the participants' experience with interaction types (recall Figure 4.4), it stands out that the participants have much experience with touch interaction and very little experience with gesture interaction, which may also have influenced the performance. However, no significant differences emerged in terms of effectiveness (*goal achievement* and *error rate*). Freehand gesture interaction ensures sterility, enables a larger working space, provides more degrees of freedom, and compensates disadvantages of touchscreen interaction, such as the need for plastic foil and a handicap due to interaction with rubber gloves. Still, touchscreen interaction is superior regarding efficiency. To improve freehand gesture interaction, the gesture set needs to be improved regarding robustness, error tolerance and functions to support the user in executing and memorizing gestures. Furthermore, the participants need longer training times to equate lesser experience. These improvements and aspects are analyzed in the following section.

4.3   PERFORMING DISTANCE MEASUREMENTS WITH FREEHAND GESTURES

The study in the former section showed that the used gestures were inferior for basic interaction tasks in interventional radiology. However, no significant difference was shown for 3D rotation – a more complex task that benefits from more DoF input. This may also be the case for measurement tasks that can either be performed spatially on 3D models, on 2D slices, and in combination. Furthermore, the selected gestures were derived from capabilities of the LMC. Therefore, this section presents an evolved gesture set based on general results on HCI research to match the requirements of the more complex tasks of measurements. Furthermore, the physician is supported in executing and memorizing the gestures with the following features:

- a visualization of possible and currently executed gestures and

- algorithmic support to compensate for the inaccurate input due to optical tracking.

The gesture set is compared to mouse and keyboard interaction. Unfortunately, even the improvements on several aspects cannot compensate the inferiority of freehand gestures. The gesture set is inferior regarding task completion time, accuracy and usability.

The LMC was used again with the Leap Motion SDK V2 2.3.1. The prototype was developed with the game engine Unity (Unity Technologies, San Francisco,

|				
(a)	(b)	(c)	(d)	(e)
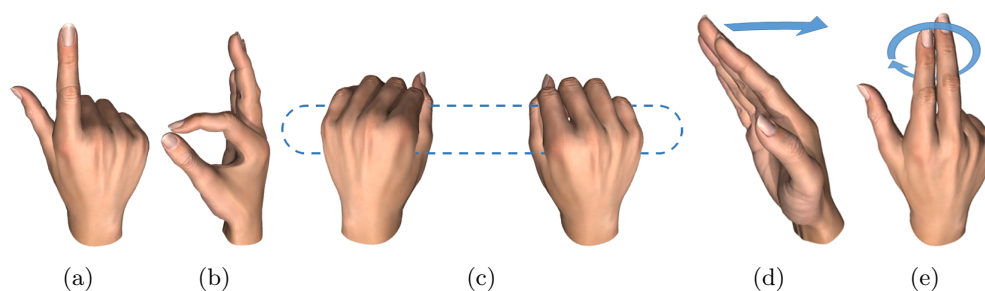
Figure 4.7: Overview of the gesture set. A measurement is created by a combination of pointing (a) and confirming the placement of measurement points with pinching (b). Object and camera manipulations are realized with a handle bar metaphor, where the objects are skewered on a virtual handle bar (c). For scrolling through medical 2D image data, a swipe gesture is used (d). For undo and redo actions, a circle gesture is used (e). All single hand gestures can be executed with either the right or the left hand. Images from Saalfeld et al. [232] and made available in the digital library of the Gesellschaft für Informatik under the Creative Commons BY-SA 4.0 License.

USA). To load the medical image data, the open source C# library *Evil DICOM*[4] was adapted for usage in Unity.

4.3.1 *Used Gestures*

Bimanual interaction allows more efficient work and an improved perception of the interaction space [100]. Thus, the presented gestures can either be used with both hands simultaneously or, if only one hand is required, with each hand interchangeable. This has the advantage that for precise tasks the dominant hand can be used. In Figure 4.7, an overview of the used gestures is depicted that are described in the following.

4.3.1.1 *Pointing*

For pointing on different views, objects and buttons, an extended index finger is used (see Figure 4.7a). By projecting the pointing direction onto the display, ray-based interaction is possible, which was found to be intuitive and minimally tiring for the hand [67].

4.3.1.2 *Pinch-to-Click*

For selecting a Graphical User Interface (GUI) element, a structure, and to create a distance measurement, a pinch gesture is used (see Figure 4.7b). This gesture is not executed with the pointing hand, but with the other one. This method was

---

4 Evil   DICOM: http://rexcardan.github.io/Evil-DICOM/index.html,   last   accessed: 11.06.2018

found to be fast, natural and unambiguous [180]. Furthermore, the kinesthetic feedback triggered by the contact of index finger and thumb generates tactile feedback, which is otherwise missing on freehand gestures.

4.3.1.3 *Translation, Rotation & Scaling*

All manipulations to transform the camera or objects start with both hands forming the same gesture next to each other. For the camera, both hands form a fist (see Figure 4.7c) and for objects, the pinch gesture is used with both hands. This mimics the metaphor of objects that are skewered on a bimanual handle bar, which was shown to be precise, efficient and intuitive [251]. Simultaneously moving both hands in any direction translates the camera or object according to the movement. Pitch and yaw rotation is triggered by rotating the handle bar around the corresponding axis. The roll rotation around the handle bar itself cannot be tracked accurately. Therefore, a pedaling motion of both hands is used [251]. Objects can be scaled uniformly by moving the hand apart or closer together. To prevent a simultaneous execution of different transformations, only one type is possible at a time. The type is determined by analyzing the initial movements of both hands. For example, if both hands are moved apart, the transformation is restricted to scaling.

4.3.1.4 *2D Medical Image Scrolling*

For changing the currently visible image slice, a swipe gesture is used. Here, one hand is vertically held over the LMC and then swiped to the left or right, which shows the previous or next slice (see Figure 4.7d). To prevent a laborious scrolling of many single images, the gesture can be held at the end of a swipe movement, allowing continuous scrolling.

4.3.1.5 *Creating & Editing Distance Measurements*

Distance measurements are created by placing single points with a consecutive usage of the pointing and pinch-to-click gesture. During creation, the measurement visualization is colored yellow (see Figure 4.8a) and after placement, colored green (see Figure 4.8b). To edit or delete an existing measurement, the physician has to change into *edit mode* by using the radial menu (see Section 4.3.3). This decision for a mandatory mode change was made to prevent ambiguities to other interactions, e.g. selecting an existing measurement and creating a new one. After selecting a measurement in edit mode, it is colored red and its end points are highlighted to show that it is editable. Now, with pointing and pinch-to-click, one end point can be repositioned. For deletion, a measurement has to be selected first. After that, an entry in the radial menu has to be selected.

(a)

(b)
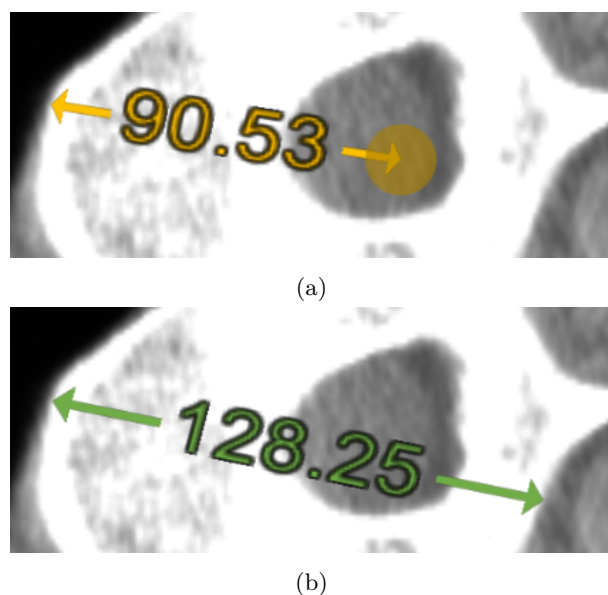
Figure 4.8: Positioning of measurements. After placing the first measurement point, the second point is positioned with the rubber band metaphor (a). If the second measurement position is placed, the finished measurement is colored green. Images were created by Saalfeld et al. [232] and made available in the digital library of the Gesellschaft für Informatik under the Creative Commons BY-SA 4.0 License.

4.3.1.6 *Undo & Redo Actions*

Besides editing measurements, the physician can cope with errors with undoing and redoing executed actions. For this purpose, a circle gesture is used. The physician holds the hand vertically over the LMC with an extended index and middle finger (see Figure 4.7e). Now, circling the hand counter-clockwise or clockwise triggers the undo and redo of an action, respectively.

4.3.2 *Support to Memorize & Execute Gestures*

4.3.2.1 *Visual Support*

The physician is supported to learn and memorize the available gestures with three different visual approaches. First, all currently possible gestures are shown with icons and informative names of their functions on the right side of the prototype application GUI (see Figure 4.9). Second, the recognized 3D hand models are visualized at the right bottom. This allows the physician to evaluate if a misrecognized gesture is caused by the LMC or by the execution. Third, the icon representing the pointing position changes according to the recognized gesture. Here, a semitransparent yellow icon is used that does not occlude content. Besides these static icons, the pointing gesture is visualized as a circle with varying

diameter depending on the movement speed. During fast movements, the diameter is increased to improve the visibility. If the hand is moved slowly, a small diameter allows higher precision for pointing. If the hands leave the tracking area of the LMC, the current gesture icon changes its colors to red. This so-called "stopper" representation [41] allows users to immediately see that further movements are not tracked anymore.

4.3.2.2 *Algorithmic Support*

Besides the visual approaches, algorithmic support is implemented to cope with the imprecise tracking of the LMC and noise introduced by hand tremble. The tracked hand positions are smoothed with *exponential smoothing*. Here, a specific amount n of previously tracked positions y_{t-i} and the current positions y_t are weighted and added, where the weight decreases with older positions. The result is a prediction of the next value, calculated with:

$$y_{t+1} = \sum_{i=0}^{n} \alpha(1-\alpha)^i y_{t-i}.$$

The parameter α is a weighting factor, resulting in less smoothing but faster reactions and with higher values. The values of α and n vary depending on the used gestures and were determined empirically.

Additionally, the physician can activate snapping [88], i.e. the pointing position snaps to nearby relevant structures. To find snapping points in the 2D image data, the *Sobel operator* is applied, which is an image processing filter that extracts edges. Every pixel that belongs to an edge is a possible 2D snapping position. For the 3D data, the vertices of the mesh are used as possible 3D snapping positions. The positions are stored inside a quadtree (edges) and octree (vertices) in a pre-processing step. During pointing, a nearest neighbor search is done inside these trees to allow for real-time performance.

4.3.3 *Graphical User Interface*

The GUI of the presented research prototype is organized in three parts: a sidebar on the left contains system options, the 2D and 3D visualizations of the medical data are positioned in the center and on the right, information about the available and recognized gestures are shown (see Figure 4.9).

Furthermore, a radial menu is available as a context menu (see Figure 4.9). A radial menu was chosen since it allows fast and efficient access to hidden functions without occupying space permanently. If the physician executes and holds the pinch gestures, it is shown and centered on the current hand position. Thus, all options can be reached within the same distance. While holding the gesture, the hand is moved to the desired function inside the menu. The function is then triggered by stopping the gesture.
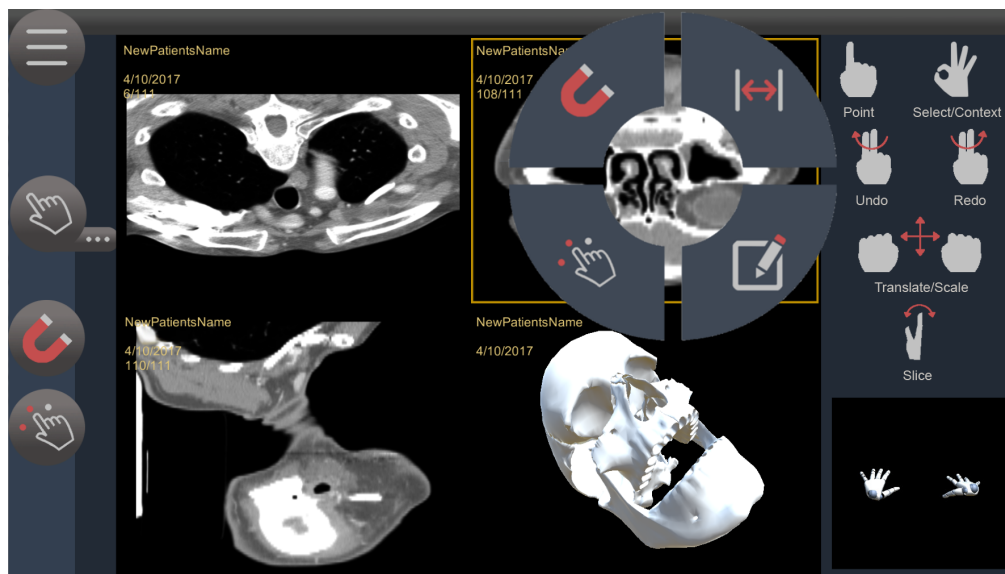
Figure 4.9: Overview of the prototype. The left bar contains menus to load image data and change measurement settings. In the center, different views on the 2D image data and 3D planning models are available and the radial menu is shown. The right side contains visualizations to support the physicians in memorizing and executing currently available gestures. Image was created by Saalfeld et al. [232] and made available in the digital library of the Gesellschaft für Informatik under the Creative Commons BY-SA 4.0 License.

4.3.4 Comparative User Study

The following section summarizes the user study comprising the experimental setup, study design, procedure and results.

4.3.4.1 Experimental Setup

The study was realized on a Sectra table (Sectra AB, Linköping, Sweden) with a 55″ display. It was tilted to a vertical position to replicate the display available in a radiological intervention room. The Sectra table is powered by a Dell Precision T5610 with an Intel Xeon CPU E5-2650 v2 with 2.60 GHz and 16 GB RAM running Windows 10. To compare the gesture set to an established interaction method, the possibility to control the prototype with a mouse and keyboard is implemented. This control was modeled after the interaction with the radiological workstation software from Sectra. Depending on the input modality, either the LMC or mouse and keyboard were placed in front of the participants (see Figure 4.10).

(a)   (b)

Figure 4.10: The evaluation setup for the gesture-based control (a) and mouse & keyboard control (b). Images were created by Saalfeld et al. [232] and made available in the digital library of the Gesellschaft für Informatik under the Creative Commons BY-SA 4.0 License.

4.3.4.2 *Tasks & Study Design*

The participants had to solve eight tasks, starting with the recreation of six predefined distance measurements (three in 2D, three in 3D). Furthermore, they were placed on various positions (directly on borders, slightly beside them or far away from them) to alter the usefulness of the snapping feature. The participants had to reproduce the start and end point of each measurement as accurate as possible. Furthermore, the participants were asked to edit two existing measurements, either in 2D or 3D. These were already created and the participants had to use the edit functions only.

The independent variable is the interaction modality with the two conditions *gesture-based* input and *mouse & keyboard*. As the dependent variable, different parametric data was collected (time, accuracy) as well as non-parametric data (usability, tiredness of the hands). For usability, the System Usability Scale (SUS) [34] was used, where several questions are stated on a five-point Likert scale ranging from 1 to 5, whereas 5 means *strongly agree*. The tiredness of fingers, wrists, arms and shoulders was assessed with questions for each body part with the same scale.

An independent measures design was chosen, i.e. each participant only uses either gesture control or mouse & keyboard input. Although this design has some disadvantages, such as interpersonal differences between participants (recall Section 3.2.4), it was necessary for this study. A pilot study showed that participants need about one hour to perform the measurements on 2D and 3D data for one input modality. Thus, a repeated measures design would result in an overall evaluation time of over two hours, which is too exhausting and time-consuming for the participants. One hour, on the other hand, would lead to acceptable signs of fatigue.

4.3.4.3 *Procedure*

The participants were alternatingly assigned to the gesture-based group and the mouse & keyboard group, respectively. For the respective input modality, each function to measure medical structures was explained. Then, a training starts, where participants could practice every interaction one by one as long as they want. After that, the tasks were stated, starting with distance measurement tasks and ending with editing of existing measurements. Finally, the participants answered the questionnaires.

4.3.4.4 *Results*

Overall, 14 participants took part in the study (8 women, 6 men) that were equally distributed on each group. On average, they were 25.7 years old. Although it was strongly attempted to acquire participants with a medical background, only three medical students took part. The other participants were students from mixed domains, including computer science and engineering. However, the recreation of existing measurements was understandable without a medical background, thus, valid results were still obtainable.

In the following, the results for the task completion time, the accuracy, and usability are presented. In contrast to the previous study, the results are presented descriptively and not with statistical tests due to the low number of participants (seven in each group).

TASK COMPLETION TIME   The task completion times that were necessary to create and edit measurements were compared. Overall, participants took 5.9 times longer with the LMC (see Figure 4.11a). This resulted in 1.8 min more time for a measurement task on average. Interestingly, there is a strong decrease of required times observable for gestures (see Figure 4.11b). This indicates that frequent usage of gesture control with longer training times can reduce the difference to mouse & keyboard control. An increase of task completion time was observable from the sixth to eighth task. The sixth task was a 3D measurement task that required the most navigation. The seventh and eighth tasks were editing tasks, which required the usage of and familiarization to different interactions and functions.

ACCURACY   The comparison of accuracy shows that participants measured 2.5 times less accurate with the LMC compared to mouse & keyboard control, which results in a deviation of 2 mm on average (see Figure 4.12a). By inspecting the accuracy regarding 2D image data and 3D planning models, the accuracy is less precise for both input modalities on 3D data. This is presumably caused by the additional dimension, which makes precise measurements more difficult.

The development of the accuracy over tasks is depicted in Figure 4.12b. The participants got more accurate over tasks with gestures and mouse & keyboard.

(a)   (b)
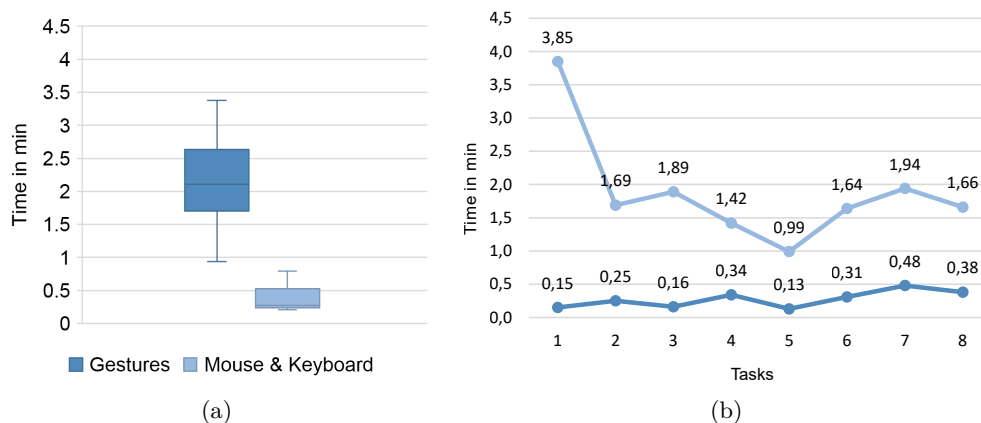
Figure 4.11: Overview of the results comparing gesture input with mouse & keyboard regarding the necessary task completion time (a) and development of task completion time by consecutive tasks (b). The whiskers show the data points that are closest to the limit of 1.5 times the interquartile range. Image (b) was created by Saalfeld et al. [232] and made available in the digital library of the Gesellschaft für Informatik under the Creative Commons BY-SA 4.0 License.

(a)   (b)
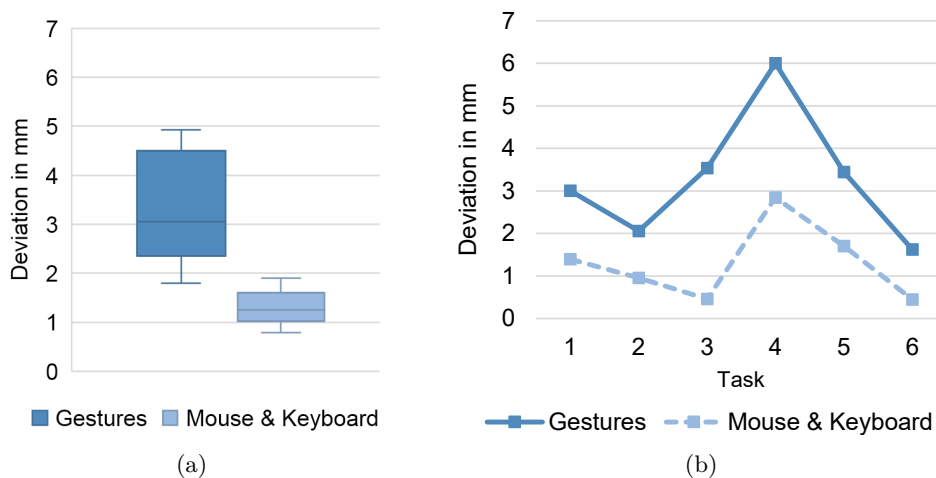
Figure 4.12: Overview of the input with mouse & keyboard regarding the deviation of measurements (a) and the development of deviation by consecutive tasks (b). Only for the first six measurements, the accuracy was measured. The whiskers show the data points that are closest to the limit of 1.5 times the interquartile range.
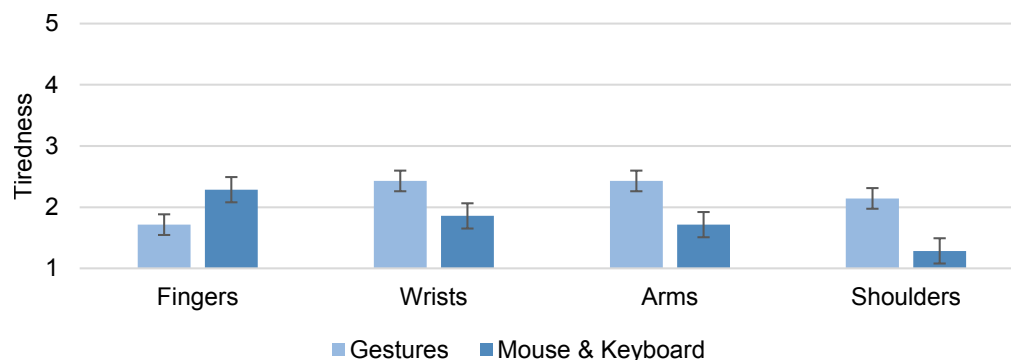
Figure 4.13: Felt tiredness for fingers, wrist, arms and shoulder with standard error. Image was created by Saalfeld et al. [232] and made available in the digital library of the Gesellschaft für Informatik under the Creative Commons BY-SA 4.0 License.

For both input modalities, a higher inaccuracy was observable for the 3D measurement tasks that also decreased from task 4 to 6, presumably due to the training.

USABILITY   The analysis of the SUS questionnaire results in an overall usability that lies between 0 and 100 [34]. The gesture input scored 51.8 points and mouse & keyboard 68.9, respectively. Both values can be interpreted as "ok" according to Bangor et al. [17]. Regarding tiredness, both input modalities lead to similar results (see Figure 4.13). The mouse & keyboard control was perceived more strenuous for the fingers, whereas gesture control led to higher tiredness for the wrists, arms and shoulders. The biggest difference according to the participants was perceived in the tiredness of the shoulders.

4.3.5 *Discussion*

This section presented interaction techniques to create an important type of measurements for interventional radiology, i.e. distances on medical 2D image data and 3D planning models. The prototype allows to perform the tasks obtained by interviews with physicians and observations of radiological interventions. The user study showed the inferiority of gestural control compared to mouse and keyboard interaction regarding task completion time and accuracy. The main reasons for this are problems with gesture recognition and an unfamiliar input method for the participants. Even the improved gesture set lacks sufficient robustness. This was especially observable for the circle and pinch gesture, which were often not recognized.

However, the gestures were rated as usable according to the SUS and the participants were able to create measurements. Furthermore, the task completion time that participants required for measurement creation shortened considerably

after the first tasks, indicating that longer training times could improve their performance.

Although three medical students participated in the evaluation, they do not represent experienced physicians. Therefore, a generalization of the results to a realistic clinical setting is not possible and an evaluation with physicians in a real environment is still necessary. This would also allow to investigate if the range of functions is sufficient.

4.4   CONCLUSION & DISCUSSION

This chapter presented background information on interventional radiology and common approaches to fulfill interaction tasks with radiological workstation software. As a possibility for sterile, touchless interaction, freehand gestures were used. Overall, two gesture sets were presented. The first one is used for basic interaction tasks such as manipulation of 2D and 3D medical image data. The second one is an improved extension of the first one to fulfill measurement tasks.

Both gesture sets were evaluated in a user study and compared to established interaction techniques, i.e. touch and mouse & keyboard control. Unfortunately, both studies showed that the freehand gestures were inferior regarding the aspects task completion time, intuitiveness, accuracy and usability. The first study indicated that for complex spatial tasks, such as 3D rotation, freehand gestures can compete with established interaction techniques. This is probably due to the higher amount of DoF. This could not be confirmed by the second study that contained complex tasks such as measuring on 3D medical data.

Although this leads to the consideration that freehand gestures were inadequate to control radiological workstations, the results have to be weighted against the advantages. Freehand gesture interaction ensures asepsis and the risk for infection on a patient is strongly reduced. Furthermore, freehand gestures allow a larger working space and provide more degrees of freedom. Compared to touchscreen interaction, the disadvantages of interacting with rubber gloves on a plastic foil are not present. Compared to mouse & keyboard, taking off and putting on gloves and scrubbing in and out is not necessary, which saves time and prevents distractions and interruptions. According to statements of the interviewed physicians, higher patient safety can justify quantitative inferiority of aspects such as longer treatment planning times.

<div style="text-align: right">

5

</div>

SKETCHING 2D VESSELS & BLOOD FLOW FOR PATIENT EDUCATION
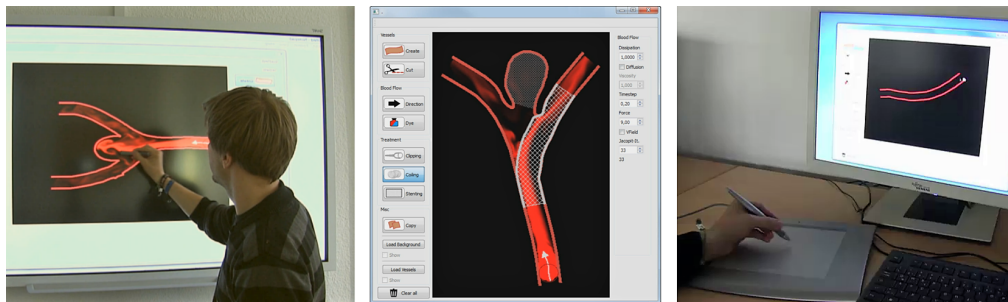
Figure 5.1: A SmartBoard and a graphic tablet are used to sketch vascular structures in 2D to explain patients their pathologies and treatment options. Images from Saalfeld et al. [228] © Springer International Publishing Switzerland 2016.

T HE process of treatment planning contains more aspects than the prevention, diagnosis, and therapy. In addition, physicians discuss treatment options not only with colleagues, but also with patients. Patients attach great importance to an understandable presentation of their disease and therapy. This results in various positive aspects [128]:

- the time of treatment may be reduced,

- patients need less medication,

- they are more active in dealing with their diseases and act more responsible, and

- they are more independent from their attending physician.

As stated in the thesis of Bram J. Keulers [128], 42 % of the patients feel not adequately informed. As discussed in Section 2.2.3, sketches are an appropriate technique to convey complex information. Patients benefit from a simplified interaction and visualization. Therefore, the approach is restricted to the 2D domain. In consequence, physicians illustrate *2D* vascular structures, treatment options and blood flow via *touch* and *pen-based* interaction.

As stated in Chapter 3, a mixed design evaluation, containing quantitative and qualitative aspects, is necessary to assess the usefulness of a prototype for medical visualization. Thus, a user study was conducted with novice users to assess the usability. Additionally, an interview was conducted with a physician. Here, the physician compared the presented approach with traditional hand-drawn sketches and discusses the benefits regarding patient education.

The prototype used on a whiteboard and graphic tablet is depicted in Figure 5.1. It was developed with the cross-platform application framework Qt (The Qt Company, Espoo, Finland).

In the following, background information on the cardiovascular system are presented, followed by background information on blood flow simulations. After that, the developed prototype is explained comprising details on the sketching of vascular structures, adding blood flow, and sketching treatment options. Then, the evaluation is described. The chapter concludes with a discussion of the presented results.

This chapter is based on the master thesis of the author of this thesis. Additionally, the fluid simulation was improved, additional treatment options can be sketched and methods for copying sketches and loading images as templates were added. These improvements are described in the following and are based on the publications:

- **Saalfeld**, **P.**, Baer, A., Preim, U., Preim, B. & Lawonn, K. *Sketching 2D Vessels and Vascular Diseases with Integrated Blood Flow* in *Proc. of Computer Graphics Theory and Applications (GRAPP)* (2015), 379–390 [227],

- **Saalfeld**, **P.**, Baer, A., Preim, U., Preim, B. & Lawonn, K. in *Computer Vision, Imaging and Computer Graphics Theory and Applications, Revised Selected Papers* 19–40 (Springer International Publishing, 2016) [228],

- **Saalfeld**, **P.**, Oeltze-Jafra, S., Saalfeld, S., Preim, U., Beuing, O. & Preim, B. *Sketching and Annotating Vascular Structures to Support Medical Teaching, Treatment Planning and Patient Education* in *Dirk Bartz Prize for Visual Computing in Medicine* (2017), 5–8 [236] and

- **Saalfeld**, **P.**, Glaßer, S., Beuing, O. & Preim, B. The FAUST Framework: Free-Form Annotations on Unfolding Vascular Structures for Treatment Planning. *Computers & Graphics* **65,** 12–21 (2017) [230]

5.1 background on the cardiovascular system, pathologies & treatment options

The cardiovascular system consists of arteries that transport blood from the heart to peripheral capillaries of the body. Veins, in contrast, carry blood back from tissue parts [245]. Pathologies of this system have a high impact on health care and economics. In Europe, Cardiovascular Diseases (CVD) lead to 3.9 million
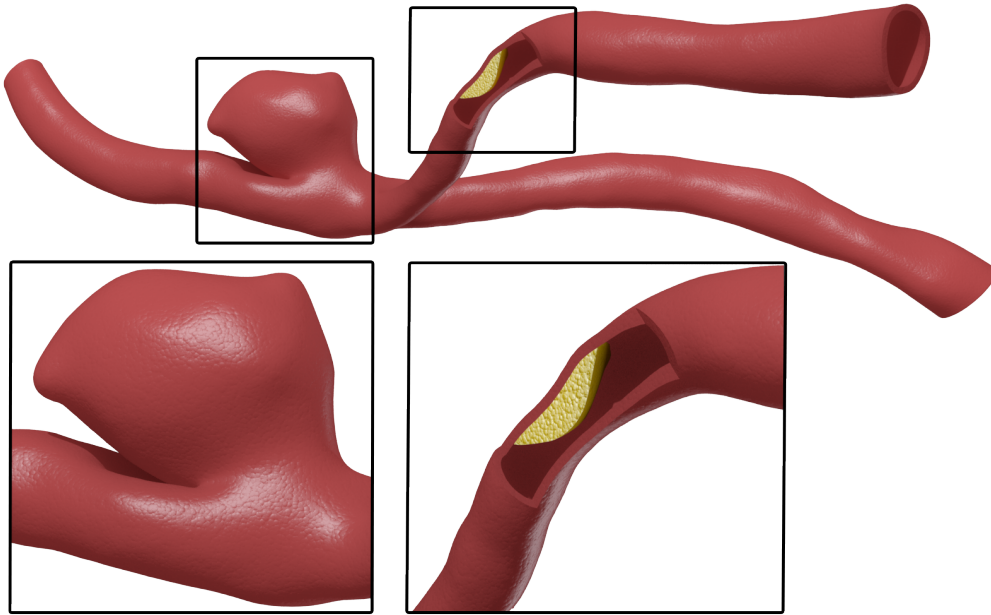
Figure 5.2: Illustration of a saccular aneurysm (left), which is the most common aneurysm type and a stenosis (right) caused by a deposit of fat inside the vessel.

deaths annually (45 %) [60]. This makes them a key threat to maintain health in the twenty-first century [215]. Due to the high number of affected people, they are responsible for yearly costs of about 210€ billion (53 % due to health care, 26 % due to productivity losses and 21 % due to informal care) [60]. Figure 5.3 gives an overview of death causes, including their overall proportion.

The cerebral vessel system and especially its central part are focused in the presented research. The central system comprises a circular combination of arteries supplying the brain and surrounding structures (see Figure 5.4). This cerebral arterial circle is often called Circle of Willis (CoW), after Thomas Willis (1621–1675), "one of the greatest neuroanatomists of all time" [267]. Its formation allows for bypassing the blood flow in case of a blocked artery. However, the anatomical manifestation of the arteries underlies strong, person-specific variations with respect to shape and length [127]. Furthermore, there are several CoW configurations where some arteries are underdeveloped or completely missing.

A common form of an arterial pathology is arteriosclerosis, which changes the vessel morphology by depositing fat, thrombi and lime inside the vessel wall [142]. Eventually, this deposition affects vessels in two problematic ways, which may cause severe consequences for the affected persons:

1. a weakening of the vessel wall and

2. a narrowing of the vessel up to complete occlusion.

Numbers of Deaths by Cause in Europe

Ischaemic Heart Disease	1,739,435
Stroke	988,573
Other CVD	1,212,657
Stomach Cancer	118,527
Colorectal Cancer	223,832
Lung Cancer	382,277
Breast Cancer	139,060
Other Cancer	1,079,059
Respiratory Disease	576,287
Injuries and Poisoning	549,174
All Other Causes	1,837,415

0%   10%   20%   30%   40%   50%   60%   70%   80%   90%   100%
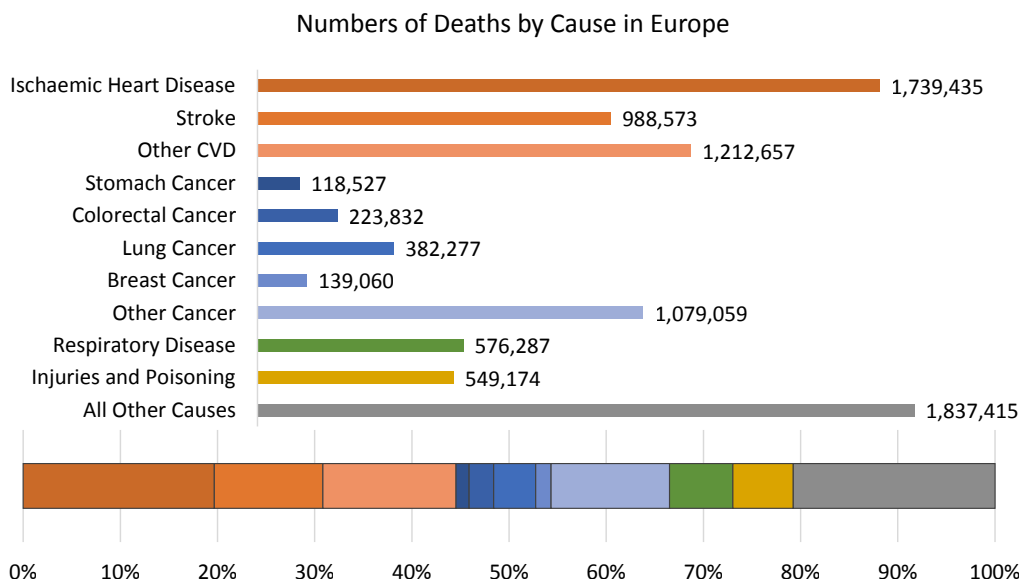
Figure 5.3: Overview of death causes based on the data from the *European Cardiovascular Disease Statistics* report from 2017 [60]. For the research prototypes within this thesis, the orange colored cardiovascular diseases (mainly strokes) are relevant.

(a)   (b)
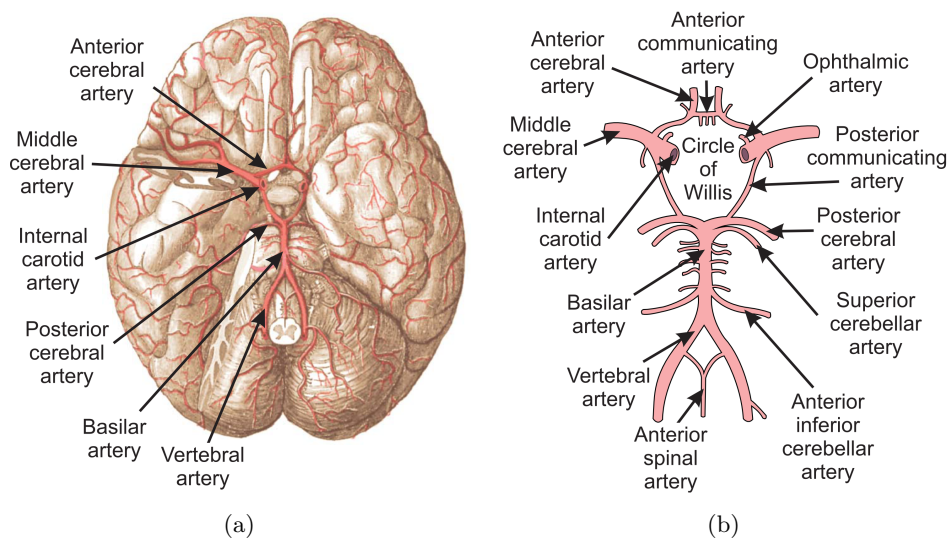
Figure 5.4: The blood supply of the brain is maintained by the (a) anterior and the posterior cerebral circulation and the (b) Circle of Willis as backup circulation (adapted from illustrations from Gray and Lewis [84]). Images adapted from images on Wikimedia Commons that were released into the public domain ((a) – https://commons.wikimedia.org/wiki/File:Arteries_beneath_brain_Gray_closer-ar.jpg, last accessed: 11.06.2018, (b) – https://commons.wikimedia.org/wiki/File:Gray519.png, last accessed: 11.06.2018).

The *weakened vessel wall* can lead to a dilation that may result in an aneurysm (see Figure 5.2). Overall, approximately 2 % to 5 % of the entire population is affected by cerebral aneurysms [266, 272]. Aneurysms can grow and displace surrounding structures, which is especially critical in the brain. Additionally, the dilated vessel can rupture, which leads to a bleeding into the surrounding tissue. Although the annual risk of rupture is low (1 % [266]), the consequences are severe, as they result in death or permanent disability in more than 40 % of the cases [21, 176]. Second, a blood clotting is possible inside the aneurysm. The blood clot can be carried away, block other arteries and may lead to a pulmonary embolism. The *narrowed vessel*, also called *stenosis* (see Figure 5.2), can lead to an undersupply of affected structures or cause a clot formation.

The choice of treatment is based on several criteria, e.g. location, shape and size of the pathology. These influence the access path and implant that can be used. Generally, therapy is carried out either:

- extravascular, i.e. from outside or

- endovascular, i.e. from inside the vessel.

Surgical clipping is an essential method for aneurysm treatment. This extravascular treatment aims at a closure of the aneurysm. The first step is a craniotomy to open the skull and disclose the aneurysm. Then, a titanium clip is placed across the aneurysm neck to stop the blood from entering into the aneurysm [75]. Endovascular therapy includes the deployment of stents and flow diverters, which redirect the cerebral blood flow yielding a decreased blood flow in the aneurysm. Another therapy is endovascular coiling, where small titanium wires are placed inside the aneurysm to induce a thrombus formation and an occlusion of the aneurysm [264]. Stenting and coiling are also commonly used in combination. Here, a stent is placed in front of the aneurysm, which stabilizes the parent artery and later prevents the coils from leaving the aneurysm. Stents can be used for the treatment of stenosis as well. This is achieved by inflating the stent with a balloon, which forces the vessel to expand. However, the placement of stents can cause local changes of the vessel morphology [42, 73], which eventually influences the blood flow. This interplay of morphologic and hemodynamic change is also subject of research [273].

Among the vascular pathologies are special cases that demand elaborate treatment planning. As an illustrative example, the treatment of unruptured aneurysms with increased neck sizes is discussed in more detail. The large neck sizes are not suited for plain or balloon-assisted coiling. They frequently require stenting to protect the parent vessels permanently. Even two stents may be necessary in aneurysms arising at a bifurcation. Here, Y-, X- or T-stenting procedures are performed (see Figure 5.5). For Y-stenting (also called *kissing stents*), two guide wires are carefully positioned such that the two stents can be released alternatingly. Therefore, the patient-individual anatomy must be analyzed, which often involves the acquisition of 3D digital subtraction images to
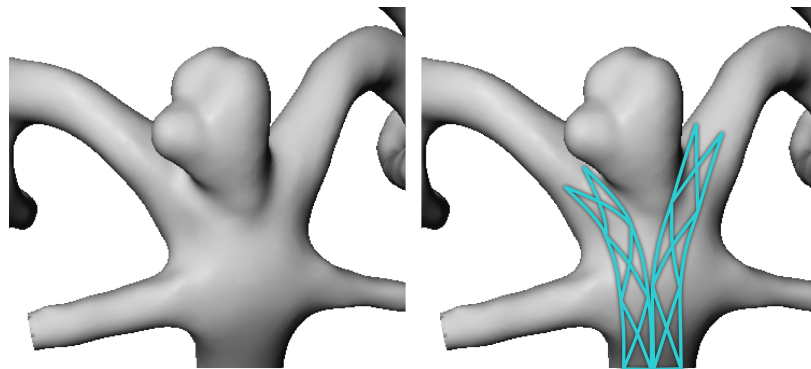
Figure 5.5: Illustration of Y-stenting, where two stents are inserted. Images from Saalfeld et al. [230].

overcome superimposition in the 2D angiography image data. Special care is required to prevent blocking branching arteries and, thus, hampering the blood supply. Furthermore, both stents should end at the same position and should also be adapted to the patient-individual vessel diameter. To further reduce the aneurysm's inflow and to promote blood clotting and a possible closure, coils are deployed after the Y-stenting. The treatment planning involves a thorough evaluation of the patient-specific CoW's anatomy. More important, the aneurysm and the direct surroundings have to be analyzed.

More examples of treatment options including a historical overview are discussed by Wong et al. [282]. Possibilities for the visualization and exploration of vascular structures and their pathologies are discussed in the thesis of Rocco Gasteiger [75].

5.2   BACKGROUND ON BLOOD FLOW SIMULATION

A visualization of blood flow behavior is used to illustrate the effect of pathological changes of the vascular structure. The blood flow is illustrated in the 2D domain, yielding a less complex representation compared to 3D, which allows the patient to follow explanations more easily. Furthermore, less computational effort is necessary for the 2D calculation, which allows a more detailed fluid simulation. This section explains the theoretical background of the used fluid simulation.

The simulation is based on the Navier-Stokes equations for *incompressible* and *homogenous* fluids (see Section 6.6), which are based on Newton's second law of fluid motion:

$$\frac{\partial u}{\partial t} = -(u \cdot \nabla)u - \frac{1}{\rho}\nabla p + v\nabla^2 u + F \,, \tag{5.1}$$

and

$$\nabla \cdot u = 0 \,. \tag{5.2}$$

Eq. 5.1 (the *momentum equation*) describes the behavior of the velocity vector field u under different influences such as advection, diffusion, pressure, and external forces for a time t. Eq. 5.2 (*continuity equation*) ensures the incompressibility by defining u as a divergence-free vector field.

The first term $-(u \cdot \nabla)u$ describes the self-advection of the fluid, which is the process of moving the velocity itself. The pressure, a force that gradually spreads from regions with high to regions with low pressure, is described with the second term $\frac{1}{\rho}\nabla p$. The factor ρ is a constant to describe the density of the fluid. Furthermore, this term ensures the incompressibility of the velocity vector field, i.e. Eq. 5.2. The third term $v\nabla^2 u$ expresses the physical process of diffusion, i.e. the property of mixing materials without external forces. Here, v is a constant that describes the viscosity. The last term F describes external forces, which allows the user to influence the simulation dynamically. Normally, such forces are steady, so the influence of the force to the fluid is constant over the time t.

5.3 SKETCHING VASCULAR SYSTEMS

The following section starts with a discussion of possible input modalities and the resulting design decisions. Furthermore, methods to create vascular structures and pathologies are presented.

5.3.1 *Touch & Pen-based Input*

The prototype should be equally usable on tablets, graphic tablets and whiteboards. Therefore, special capabilities of input methods are not utilized, e.g. pressure sensitivity, additional buttons and multi-touch. The remaining requirement on the input method is a 2D position and a discrete event, which indicates that the user starts and stops sketching. Thus, the prototype is theoretically usable with a mouse with a left button.

5.3.2 *Vessel Tree Creation*

Drawing a 2D vessel requires two lines representing the vessel walls. One possibility would be to sketch each wall separately. Although this gives the user more control over the final vessel shape, it leads to unintentional variations of the vessel thickness and longer sketching times. Therefore, the user draws only the center line and both vessel walls created around it on the fly. The width of the vessel wall is fixed. Although this reduces the flexibility of the prototype, the creation of uniform vessels is easier and faster.

There are two approaches how intersecting vessels can be handled. In the work of Zhu et al. [289], they allow 2.5D sketching. Here, sketched tubes run
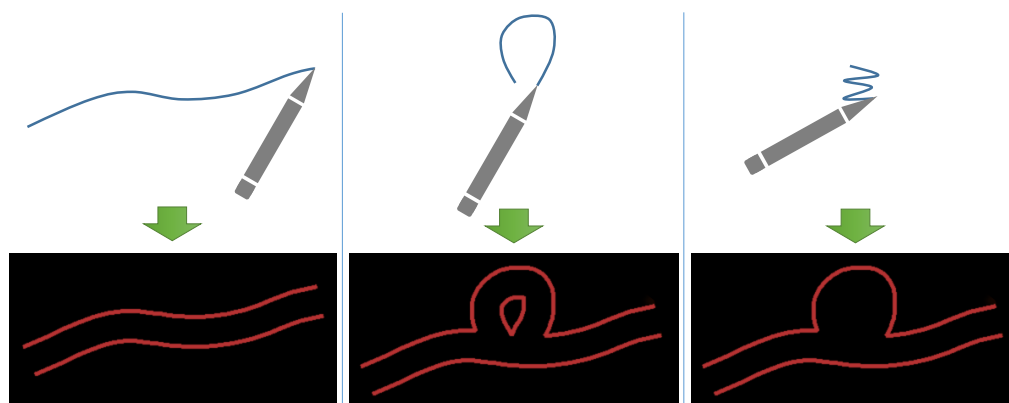
Figure 5.6: The merging approach can be used to draw a vessel containing an aneurysm by simply sketching on top of the previous drawing. Images from Saalfeld et al. [228] © Springer International Publishing Switzerland 2016.

either under or over already existing paths. In this thesis, another approach is used: the intersecting vessels are merged. While this reduces the flexibility, it simultaneously creates a powerful sketching tool. The creation of complex structures such as branching vessels and aneurysms can easily be realized without changing the drawing mode. This merging approach is illustrated in Figure 5.6.

The transformation of the input in a visualized vessel is realized by the combination of two Qt classes: the *QPainterPath* and the *QPainterPathStroker*. While the former allows to represent paths, the latter generates the outline of a given QPainterPath. First, every sketched center line is drawn with the QPainterPath with a fixed width (the vessel diameter). Then, all center lines are merged to one QPainterPath. Finally, this path is given to QPainterPathStroker to create the outline, which recreates all vessel walls.

While this approach is beneficial to easily sketch vessel trees and aneurysms, it would not allow the creation of a stenosis. Thus, the introduction of an additional cutting tool allows the creation of irregular non-symmetrical stenoses in a consistent sketch-based way. The user sketches a connected contour similar to lasso-based selection. Everything inside the contour is removed (see Figure 5.7). The illustration of the cutting area prevents ambiguity problems during cutting that are described by Heckel et al. [95].

This combination of adding and removing vessel parts gives the user a generic sketching tool, which allows the creation of a wide variety of 2D structures with the usage of only two modes. Furthermore, this flexibility enables the physician to precisely react to the needs of the patient.

To support the medical expert during the sketching process, it is possible to load images as a stencil. The physician can use this function to load a single slice of patient-specific MRI or CT data, which contains, e.g. the vessel structures of the patient. In addition, templates of frequently sketched vessels can be loaded. Figure 5.8 depicts this for a CoW. This is realized by loading a monochrome
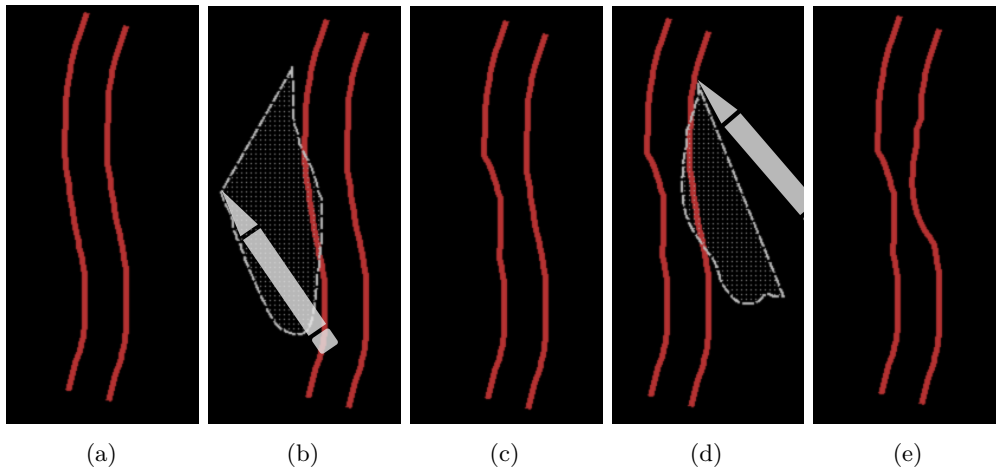
Figure 5.7: The user can sketch a cutting area. Everything inside this area is removed and allows to create a stenosis. Images from Saalfeld et al. [228] © Springer International Publishing Switzerland 2016.
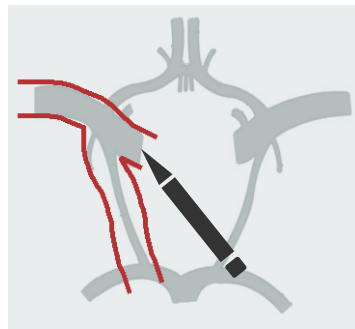
Figure 5.8: A background image of the Circle of Willis is loaded to support the sketching process. Image from Saalfeld et al. [228] © Springer International Publishing Switzerland 2016.

black and white image. Every black pixel is interpreted as a vessel and every white pixel as free space, where blood is able to flow. However, this image-based approach has disadvantages. While blood flow can be added to a loaded sketch, other functions such as cutting and sketching treatment options cannot be used. This could be avoided by implementing an object-based save and load mechanism instead of an image-based one.

5.4 ADDING PLAUSIBLE BLOOD FLOW

In the following, information on the blood flow integration are given, comprising details on the simulation, interaction techniques for creation and manipulation as well as its visualization.

5.4.1 *Simluating Blood Flow*

The most accurate but computationally expensive approach to simulate blood flow is a hemodynamic simulation that reproduces real world behavior. This can be realized by imitating several properties. In terms of fluid dynamics, blood is:

- non-Newtonian – the viscosity varies depending on the shear rate that is higher in a small vessel and

- compressible – it can be pushed together, so its density gets higher.

Such a simulation is complicated and expensive regarding calculation time, even in the 2D domain [33]. Therefore, properties such as the small compressibility of fluids are often ignored in simulations. Examples for methods to calculate non-Newtonian fluids can be found by Ciarlet et al. [45] and Ferziger and Perić [65]. However, the goal of the presented prototype is to illustrate blood flow in a plausible and informative way. Therefore, the blood in the presented simulation is considered to be an incompressible, homogeneous *Newtonian fluid*. Although this is an approximation, it allows to depict the blood flow in a plausible way, which is adequate for patient education.

To characterize the state of a fluid, two approaches can be pursued: a Lagrangian (particle-based) realization and a Eulerian (grid-based) realization. Since 2D sketches are easily transferable to a 2D grid, the Eulerian grid-based approach is used. Furthermore, the fluid simulation on a 2D grid is well suited for fragment shaders of the Graphics Processing Unit (GPU), which are used for the calculation. The grid size and resolution plays an important role. While a sparse grid accelerates the calculation time, details such as whirls may be lost. Another aspect are obstacles in the form of the vessel wall or a clip that prevent the fluid from crossing. To faithfully simulate the behavior of blood flow in the vicinity of obstacles, it is necessary to model the obstacles in the simulation grid. This is achieved by marking grid cells as occupied. Thus, the grid resolution also affects the possible level of detail of the obstacles. For the fluid simulation, the approach from the GPU Gems article from Mark J. Harris [91] is used.

The first Navier-Stokes equation can be calculated by splitting it up in several terms and compute each term separately [254]. An overview of each calculation step and their influence on the simulated flow is illustrated in Figure 5.9.

The first fragment shader pass transfers external forces into the velocity vector field of the fluid. Here, the physician is able to influence the direction of the flow. Normally, such forces are steady, so its influence is constant over time. This, however, would not represent the pulsating character of blood flow, caused by the contractions of the heart. This pulsation can be imitated by applying a factor to the force, which changes over time. For this purpose, the following heartbeat-like formula is approximated, which mimics the output of an electrocardiogram:

$$f(x) = -0.25e^{-\frac{1}{2}(1+x)^2} + 1.12e^{-\frac{x^2}{2}} - 0.75e^{-\frac{1}{2}(-\frac{1}{2}+x)^2} + 1 \ . \tag{5.3}$$
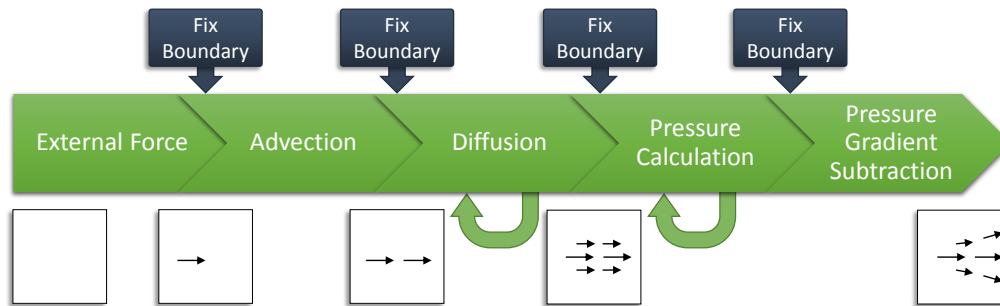
Figure 5.9: Pipeline for the fluid simulation including the influence to the underlying vector field. Each step is realized with a separate fragment shader pass on the GPU. The steps provided with self-referencing arrows show the steps, which are calculated with an adjustable amount of iterations. Here, a trade-off arises between accuracy and calculation time. Image from Saalfeld et al. [228] © Springer International Publishing Switzerland 2016.

This equation was determined experimentally by combining three Gaussian functions with varying heights and widths. The first and the third negative terms are responsible for the negative swings. The second positive term is responsible for the steep positive curve. In Figure 5.10, the difference between a constant and a pulsating force is illustrated.

The second render pass calculates the self-advection of the fluid. This is realized with semi-Lagrangian advection [254]. The term "semi-Lagrangian" originates from the mixture of Eulerian and Lagrangian approaches: the calculation places a theoretical particle on the position of a grid cell. Now, the movement of this particle is calculated with methods from particle-based approaches. Here, the most common method for the integration is the Runge-Kutta method [36], which is less error-prone than the simpler and faster Euler method. Interestingly, the differences between both methods are almost not noticeable in the presented prototype (see Figure 5.11)). This is due to the small integration step size used in the prototype. Therefore, the fast Euler method is used to decrease the calculation time.

For the calculation of the diffusion term, the solution of a Poisson equation is necessary. There exist several iterative methods to achieve a numerical solution for this [138]. Here, the Jacobi approach is used, because it can be easily mapped to the GPU [91]. Other methods, such as the Gauß-Seidel method, could be applied as well, but are more difficult to be implemented on the GPU. A general disadvantage of diffusion is the resulting smoothing effect on the applied vector field, which causes loss of details. Therefore, the choice whether diffusion is applied is left to the user.

As stated, the pressure calculation ensures the incompressibility of the velocity vector field. Similar to diffusion, a Poisson equation has to be solved, which is approximated again with the Jacobi iteration method.
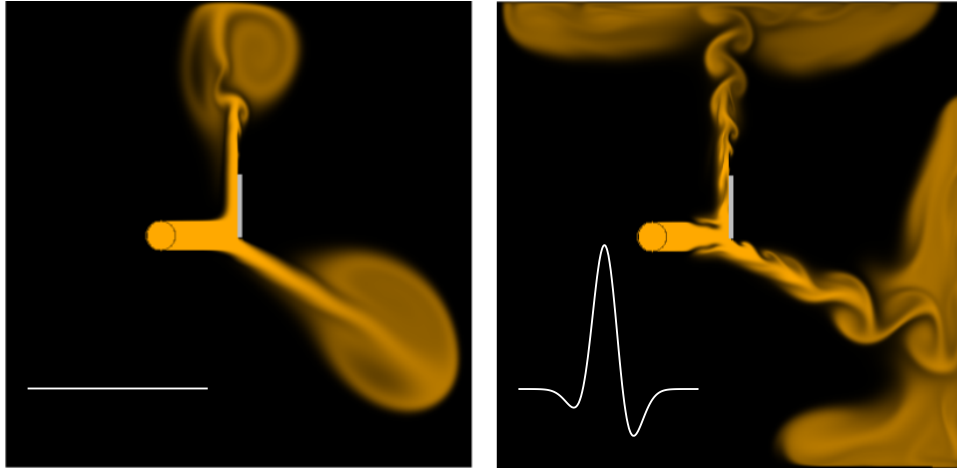
Figure 5.10: In (a) a constant force is applied to the vector field. In (b) a heartbeat-
like function is applied as a factor which mimics a more realistic behavior.
The corresponding functions are plotted at the left bottom. Images from
Saalfeld et al. [228] © Springer International Publishing Switzerland 2016.

Finally, boundary conditions have to be used to simulate the behavior of the
fluid at the vessel wall and the boundary of the sketching canvas. These condi-
tions are necessary for the *velocity* vector field and for the scalar field, describing
the *pressure*. For the velocity vector field, a Dirichlet boundary condition is used,
which states that the velocity *drops to zero* at boundaries. For the scalar field,
a Neumann condition is used, which states that the *derivatives* at boundaries
are zero. To calculate the derivative, it is necessary to have the normal direc-
tion of the boundary. For the borders of the simulation grid, these normals
are obvious, i.e. the normals of the top, right, bottom, and left boundaries are
$(0, -1), (-1, 0), (0, 1)$, and $(1, 0)$, respectively. For determining the normals of
arbitrary boundaries, the neighborhood of the obstacle is used. That means that
for each grid cell, which is marked as an obstacle, eight neighbor cells are an-
alyzed. Depending on the state of these neighbors (marked as obstacle or no
obstacle) the normal is approximated to one of eight possible directions. This
approach is described in more detail by Wu et al. [283].

5.4.2   *Manipulate & Visualize Blood Flow*

As stated, the flow can be manipulated with a force term, which is represented
as a 2D vector field (recall Section 5.2). To allow the user to influence this field
in a flexible and easy way, the user can sketch arrows to manipulate the flow
direction.

To transfer the sketched arrow to the vector field, a naive approach would
be to change the vectors that directly correspond to the sketch. This, however,
leads to a very small area of manipulated flow. Instead, the force is applied in

(a)	(b)
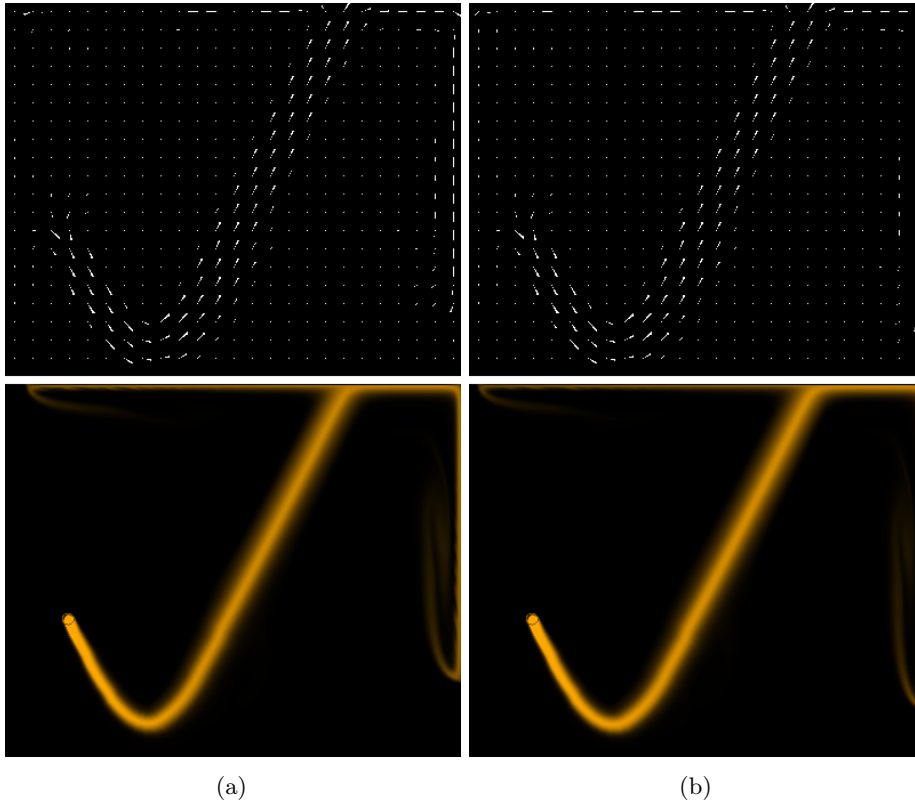
Figure 5.11: Comparison of the Euler (a) and Runge-Kutta 4 (b) integration methods with a step size of 0.3. Both methods are depicted with a modified arrow plot visualization (top) and a scalar field visualization (bottom), which looks similar to a streakline visualization through the continuous placement of ink during the simulation. Since the differences between both methods are almost not noticeable, the faster Euler method is used. Images from Saalfeld et al. [228] © Springer International Publishing Switzerland 2016.

a *region* around the sketched arrow. The size of this region is adjustable and is initially set to the width of a vessel. To achieve a natural effect, the force is decreased in the direction of the border, resulting in a strong force in the center and a weak force at the border.

The blood flow visualization is implemented to yield the positive effects of being easy to understand and to show the behavior of blood in areas such as aneurysms and stenoses in a descriptive way. It is inspired by the idea to place *colored ink* in the vector field (also known as *dye injection*). This allows the physician to emphasize specific areas, which supports the patient's understanding. The width of the ink area is set to the vessel width allowing the physician to quickly fill a vessel with ink. By diffusion and advection, this ink is transported through the vector field. The amount of ink is color-coded with a black-to-hue scale with different colors. This allows using multiple colors, e.g. to show how blood mixes in an aneurysm before and after a treatment, see Figure 5.12. The
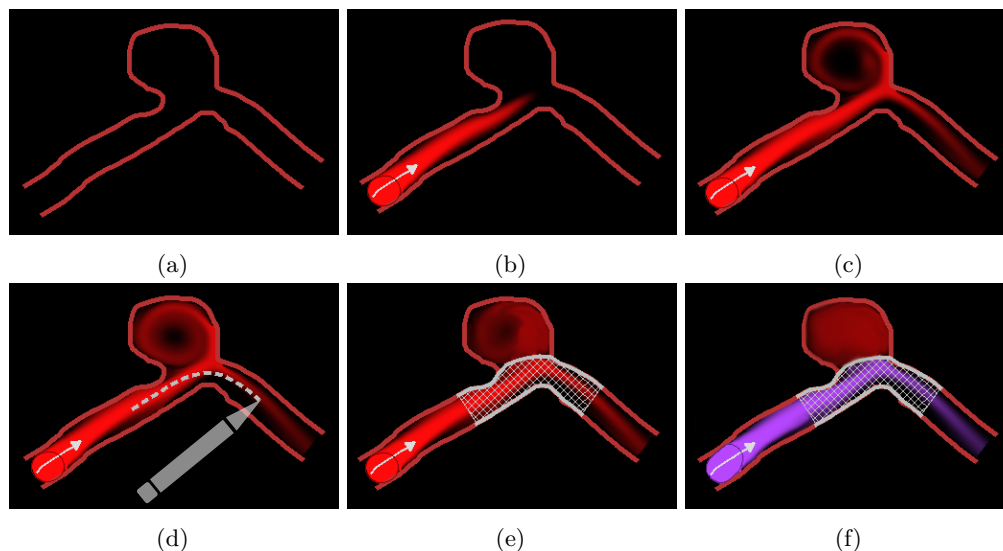
Figure 5.12: Illustration of blood flow before and after a stent is sketched. The physician sketches a vessel with an aneurysm (a). Afterwards, the blood flow is manipulated and visualized (b-c). The stent is sketched (d) and automatically expanded (e). Its influence is illustrated by using a different color for the blood flow (f). Images from Saalfeld et al. [228] © Springer International Publishing Switzerland 2016.

colors are taken from the *CIELAB* color space, which allows choosing colors that are roughly perceptually linearized regarding hue and brightness.

5.5 SKETCHING TREATMENT OPTIONS

The possibility to sketch the most common treatment methods (coiling, clipping and stenting) is implemented. For **coil** sketching, a semi-automatic approach is used. The user sketches roughly around the aneurysm. Then, the neighborhood of every sample point of the rough sketch is analyzed to find the nearest vessel wall. This is done by sending out eight rays in a circular manner from every sample point. This number was determined empirically. Less rays resulted in an inaccurate vessel wall detection and more rays did not improve the result. If one or more rays hit a vessel wall, the sample point is placed on the shortest hit point. If no collision occurs, the point keeps its position. After that, the sketched area is filled with a coil texture. The underlying grid cells are treated as obstacles to prevent blood from entering it. This algorithm is illustrated in Figure 5.13.

Clips can be sketched similar to the line drawing approach from *Sketchpad* [258]. The point where the user starts drawing represents the first point of the clip. As long as the user draws with the pen, the current pen position represents the end point of the clip. These two points are connected with a dashed line to give the user a preview of the clipping result. After the user finishes
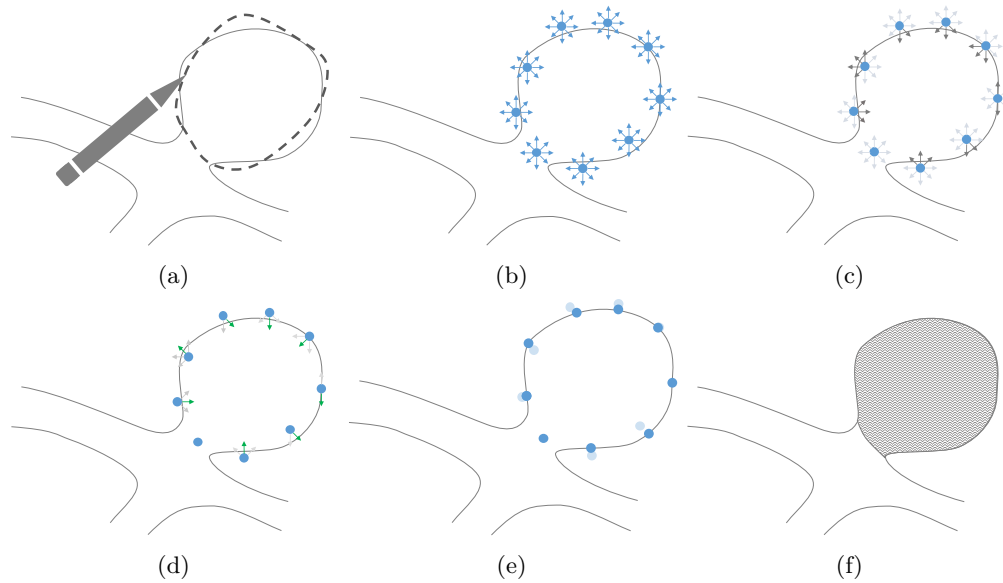
Figure 5.13: Illustrations (a) - (f) show the algorithm to determine the coil area. In (a) the user imprecisely sketches over the vessel wall of the aneurysm. (b) shows the captured sample points as well as the rays, which are sent in a circular manner from each sample point. In (c) all rays that collide with the vessel wall are highlighted, from which those with the shortest distance are used (d). The sample points are moved to the intersection point or remain on their position if no intersection occurred (e). The adjusted sample points build the new area for the coil contour, which lies precisely on the vessel wall. Images from Saalfeld et al. [228] © Springer International Publishing Switzerland 2016.

drawing and raises the pen, the clip is placed and the blood flow simulation is affected by it.

The **stent placement** is also semi-automatic and inspired by the real treatment. The user draws a line in the center of the vessel, which represents the position of the catheter. After the user finishes sketching, the prototype calculates the dilation of the stent. The stent should be dilated in the relevant vessel, but not enter the aneurysm. Since structures are not differentiated semantically (i.e. into types such as vessel and aneurysm), the described behavior must be achieved in a different way. Thus, the surrounding region of the sketched stent is analyzed similar to the coiling approach. The algorithm is illustrated in Figure 5.14. The best results regarding visual aspects are achieved by drawing a line along the center of the vessel. Inaccurate lines may lead to an entering of the stent inside the aneurysm. A disadvantage of the described method is that it depends on four control points obtained through the start and the end point. If not all control points could be determined, e.g. if the vessel is too wide, not all normals are calculated and the stent is not placed. Similar to the coiling
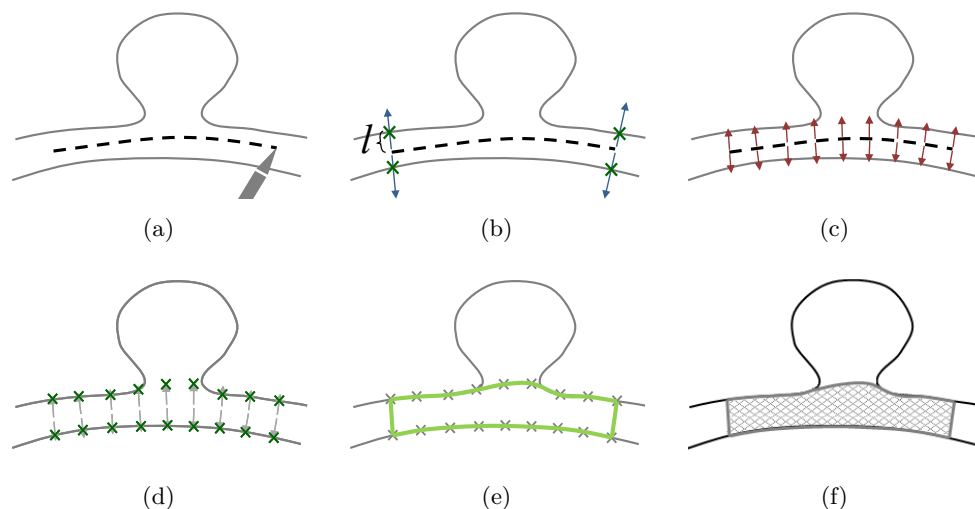
Figure 5.14: Illustrations (a) - (f) present the stent dilation. (a) The user input is illustrated as a sketched line. (b) After the user finishes the line, the normals of the start and end point are determined. The normals have the length of the vessel width. All four normals are tested if they intersect the vessel wall. If not, the stent is discarded. Otherwise, the distance l is determined, which is the longest length of the normal start point (the sketched center line) to its intersection point. (c) Now, for every sampled point of the sketched line, the normals with length l are determined. (d) These normals are tested for intersections with the vessel wall. If they intersect, they are shortened to the intersection point, otherwise they keep the length l. (e) The achieved end points of the normals are connected and form the border of the stent, which is illustrated in (f). Images from Saalfeld et al. [228] © Springer International Publishing Switzerland 2016.

and clipping method, the grid cells under the stent are marked as occupied and influence the fluid simulation immediately.

5.6   DELETE & COPY OBJECTS

The possibility to edit and delete, e.g. stents and coils, is an important aspect regarding the controllability of the prototype. This can be realized by allowing the selection of already created objects. Since a requirement of the prototype is to control it with a pen without any further buttons, the user has to *press and hold* on an object to delete it.

To provide the physician with an easy and fast way to illustrate different treatment options and their influence on the blood flow, a copy feature is added. This can help to understand why a specific treatment is chosen or why another one is not possible. For copying, the user sketches around the objects that should be copied. The created copy follows the pen position until the user raises the pen.
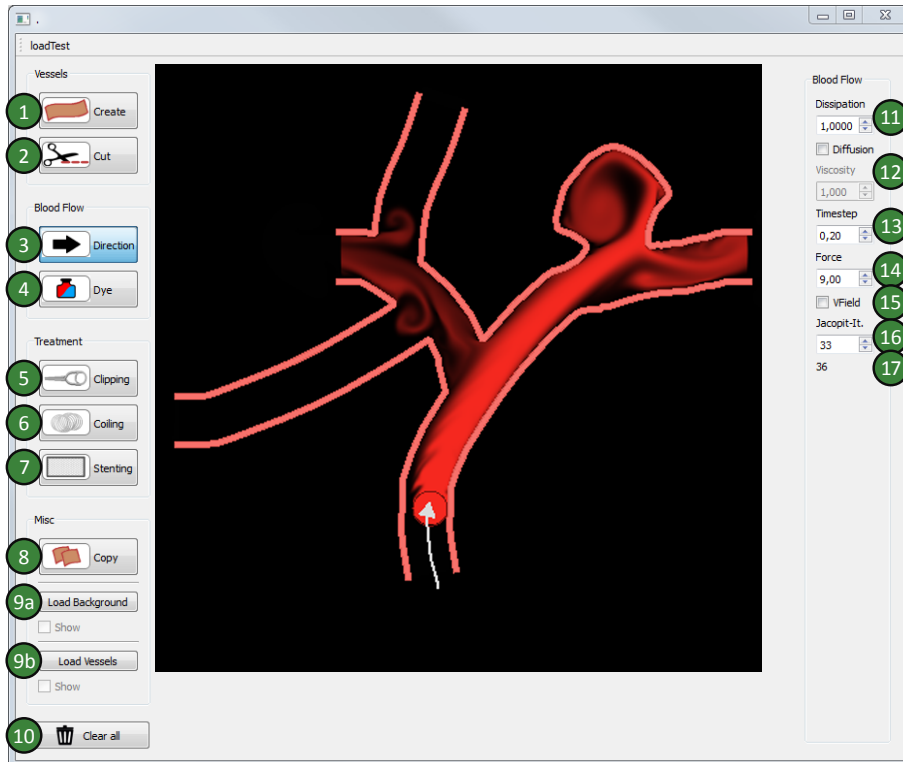
Figure 5.15: The image shows the GUI and the functions of the prototype: (1-2) – create and edit vessels, (3-4) – manipulate and visualize blood flow, (5-7) – sketch treatment options, (8) – copy function, (9a-9b) – load background image to assist the sketching or to load vessel structures out of a monochrome image, and (10) – reset the canvas. The buttons on the right side (11-17) are used to influence the fluid simulation in different ways, e.g. to enable diffusion or change the viscosity. Image from Saalfeld et al. [228] © Springer International Publishing Switzerland 2016.

5.7 GRAPHICAL USER INTERFACE

In Figure 5.15, the GUI of the prototype is shown. The structure of the GUI results from the consideration that the canvas of the grid used for the fluid simulation is quadratic. Therefore, the canvas, in which the user sketches, is also quadratic. Due to the horizontal format of current displays, this yields potential free space on the sides of the canvas. This space is used for the menus. In detail, the space is divided in a left and a right region and used for a semantic differentiation of the functions. On the left side, menus and buttons are placed, which are used to create and manipulate vessels, to sketch treatment options, and to visualize and control blood flow. On the right side, there are menus to control simulation parameters such as the number of iterations for solving or to activate the diffusion process.

5.8   EVALUATION

The evaluation is divided into two parts: first, the usability of the prototype is assessed and second, an unstructured interview with a physician was conducted.

5.8.1   *User Study*

In the following, the user study and its results are presented.

5.8.1.1   *Goals*

The goal of the evaluation was to assess the usability of the 2D sketching approach. For this purpose, the usability questionnaire from Prümper was used again [211] (recall Section 6.8.1.1), which contains questions with a 7-point Likert scale $(---,--,-,\circ,+,++,+++)$. Additionally, the participants were encouraged to comment their activities (think aloud method [124]).

5.8.1.2   *Tasks*

The participants had to sketch common vascular configurations and their treatment, which were shown as 2D sketches on a sheet of paper. Overall, five tasks were stated:

1. Create a stenotic artery by a combined usage of the creating and cutting functions.

2. Sketch a vessel harboring a saccular aneurysm and place a clip at the aneurysm neck.

3a. Create a vessel with a bifurcation. Add an aneurysm at the bifurcation and use the blood flow tools to illustrate blood entering the aneurysm.

3b. Use the coiling function to simulate an aneurysm coiling.

3c. Place a stent in the branching vessel.

For example, they should draw a vessel with a trifurcation. Then, they should use the cutting function to change the vessel into a bifurcation. Furthermore, they were asked to draw an aneurysm and sketch a treatment with the clipping, coiling, and stenting tool. Finally, they should create and visualize the blood flow in a specific direction.

5.8.1.3   *Participants*

The evaluation was conducted with 14 researchers with medical visualization knowledge. Three of the participants were female and eleven male. Their age ranged from 25 to 44 with an average age of 31 years. The participants are

experienced computer users ($\overline{x} = 20$ years, $min = 14$, $max = 30$). Ten of the participants had experience with pen interaction.

5.8.1.4 *Procedure*

The evaluation started with an introduction of all functions of the prototype on a SMARTBoard ($70''$ screen) that allows pen interaction. After that, the participants were asked to perform the exercise and real tasks stated on the given sheet of paper. Afterwards, the participants were asked to fill out the questionnaire.

5.8.1.5 *Results – Observations & Think Aloud*

Mostly, the participants were satisfied with the prototype, e.g. one stated that "it is possible to create vessels and aneurysms according to my own ideas". In general, they stated that the prototype allows a fast and easy generation of vessels with simulated blood flow. Regarding the different tools, the majority of the participants had no problems using them. For example, it was stated that the cutting function "is more precise than conventional eraser tools". Unfortunately, the cutting function lead to misunderstandings during the first use. This was caused by different expectations of its principle functionality, e.g. some participants thought that it can be used similar to a conventional eraser. After some practice, the function was understood and all participants rated this tool as positive. Some participants highlighted that the semi-automatic approach of placing coils and stents is very useful, as these results in a visually more pleasing sketch.

5.8.1.6 *Results – Usability Questionnaire*

In summary, the ratings of all categories were positive and the participants were satisfied with the functional range. The category *error tolerance* had the lowest ratings ($md = 2$). Here, the users were asked if the effort to correct an inadvertently drawn error is significantly high. While the prototype allows correction by deleting objects, such as stents and clips, it is not possible to edit them. Presumably, this was a reason why this category had a relative low rating. All other usability criteria had the highest median rating of $md = 3$. The results of the usability questionnaire are summarized in Figure 5.16

5.8.2 *Unstructured Interview*

An unstructured interview was performed with a physician with 12 years of experience in the field of vascular diseases and patient education. First, the physician was asked to explain the typical patient education procedure of a patient with a vascular pathology. During the process, the patient receives textual and image-based templates with respect to the disease. Additionally, the intervention is
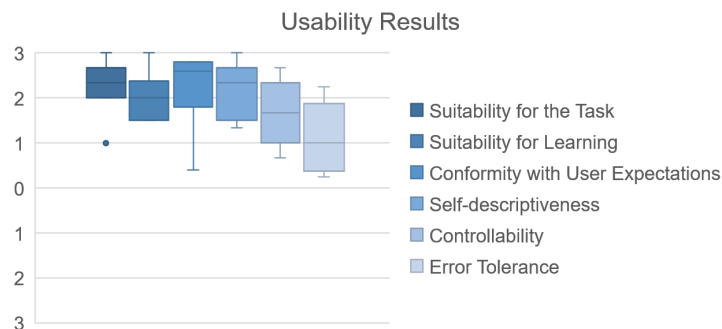
Figure 5.16: Boxplots for each category of the adapted usability questionnaire [211]. The whiskers show the data points that are closest to the limit of 1.5 times the interquartile range. The dot in the category *Suitability for the Task* represented an outlier (rating < 1.5 times the interquartile range).

(a)   (b)
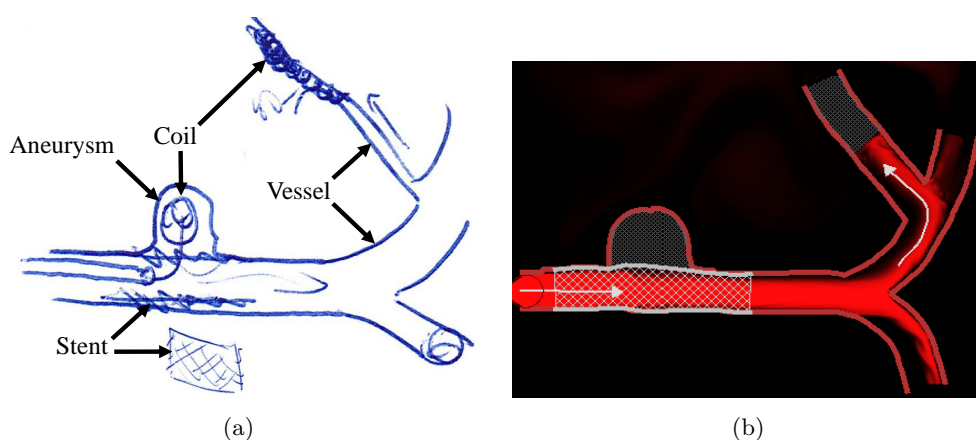
Figure 5.17: On the left side is the hand-drawn sketch of a physician with additional labels. On the right side are the same structures made with the prototype, which the physician rated as clearer and more understandable. Images from Saalfeld et al. [228] © Springer International Publishing Switzerland 2016.

explained verbally and enriched with hand-drawn sketches. The physician was asked to create the same vascular configuration and treatment via a hand-drawn sketch and with the prototype, respectively (see Figure 5.17). The description of the physician revealed the following disadvantages of the *hand-drawn* sketches:

- To correct errors, the physician draws over the existing sketches, which results in a cluttered image.

- The blood flow and the implications of a treatment are usually not drawn, because it is hard to illustrate these and could lead to a confusing image.

- The physician only uses one color to draw all structures, which makes it difficult to distinguish between different elements such as vessels and a clip.

- Some patients have problems to understand the sketch, because they find it difficult to imagine diseases and treatment options.

The physician highlighted several benefits of the prototype compared to the hand-drawn sketch. By using different colors and a consistent representation of structures (e.g. for the vessels or stents), the result is more clear, descriptive and plastic than the hand-drawn sketches, which supports the perception. Due to the illustration of blood flow, the effects of different treatment methods and possible complications are better to understand and to imagine. The final image is easier to understand. Furthermore, the physician stated additional advantages of the prototype, e.g. due to the clearer resulting images, other persons, who were not involved in the sketching process, are able to understand it. This is difficult with hand-drawn sketches, because of their cluttering nature. The physician rated the tool as easy to learn and use, which matches the results of the usability evaluation.

5.9 CONCLUSIONS & DISCUSSION

This section presented methods for 2D sketching of vessels, vascular diseases and treatment options. Furthermore, a real-time blood flow simulation can be manipulated to illustrate the effect of different treatment options. The positive feedback of the user study indicates that the proposed methods are suitable for sketching vascular structures and treatment options. The *structured interview* with the physician revealed further benefits compared to hand-drawn sketches and confirmed the idea to improve patient education and their intelligibility by integrating animated blood flow. The prototype can be improved by a differentiation between healthy vessels, stenoses, and aneurysms. This would allow an easier placement of treatment options or to recreate effects such as the inflation of a stenosis with a stent.

5.9

6

SKETCHING 3D VESSELS & BLOOD FLOW FOR MEDCIAL EDUCATION
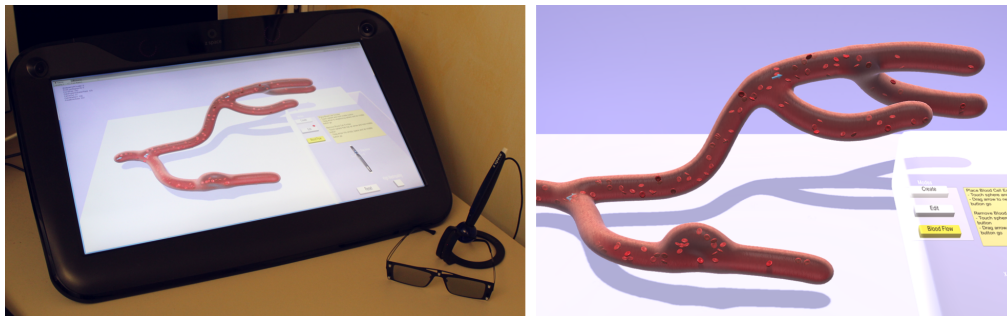
Figure 6.1: The zSpace can be used to sketch vascular structures in real-time for medical education. Images from Saalfeld et al. [238].

THE anatomy and pathology curriculum of the vascular system is a key part in the education of medical students. This raises a likewise challenge for students and educators [201]. Students need to know the spatial relationships, shapes, and names of vessels, and educators need appropriate tools to convey this information. Sketching is used as such a tool: anatomy teachers are used to draw and refine illustrations with further objects and explain how they relate to the overall system or organ (recall Figure 6.2). The successive adding to a more complex structure has a didactic purpose. The students should learn the function of small parts towards a broader understanding of the whole system. In parallel, they are educated to reproduce these sketches.

There exist several limitations with the usage of blackboard drawings:

- It is challenging to represent 3D shapes and spatial relationships on a 2D blackboard.

- The results highly depend on artistic talent. This means that if educators are not able to produce these sketches, they will probably use other approaches.

- The sketched image only conveys one viewing direction and may hide important structures. This is solved to a limited extent by artificially altering

the path of vessels or folding away tissue on the blackboard, but this does not depict the true anatomy.

- Blackboard drawings are difficult to change and correct with a moderate effort.

To solve these limitations, methods are presented to sketch a wide variety of vascular configurations in different body areas and to illustrate common vascular diseases. The challenge of sketching into depth is solved by using the *zSpace*. The dependence on artistic talent is reduced by simplifying the sketching approach: the educator only has to sketch the center line, the 3D surface is generated in real-time around it. This is realized with implicit surfaces. By adding tools to add, edit, and remove vessel branches, the educator has a flexible tool to create a wide variety of complex vascular structures with smooth transitions at branchings. Similar to the prototype of the previous Chapter 5, the sketched vascular system can be enriched with an illustrative blood flow visualization that is realized with a particle system. This addition allows the prototype to directly illustrate the impact of morphological changes to the blood flow, which is not possible with blackboard sketches. The plausible blood flow adapts dynamically to topological changes by interpreting the vascular system as a graph.

The prototype was evaluated with a mixed design evaluation as stated in Chapter 3. First, non-expert users sketched predefined vascular configurations. During sketching, they were interviewed and asked to think aloud. After this, a questionnaire regarding usability aspects was filled out. Furthermore, an anatomy lecturer was interviewed.

The zSpace running the prototype is shown in Figure 6.1. It was developed with the game engine Unity.

In the following, background information on medical education are presented. For information on the cardiovascular system, the reader if referred to the previous Section 5.1. After that, implicit surfaces are explained and how they are used to create vascular structures. Then, the developed prototype is explained comprising details on the sketching and visualization of vascular structures as well as how blood flow can be added. Then, the evaluation is described, including a user study and the interview with the domain expert. The chapter concludes with a discussion of the presented results.

This chapter is based on the publications:

- **Saalfeld**, **P.**, Stojnic, A., Preim, B. & Oeltze-Jafra, S. *Semi-Immersive 3D Sketching of Vascular Structures for Medical Education* in *Proc. of Eurographics Workshop on Visual Computing in Biology and Medicine (VCBM)* (2016), 123–132 [238], and

- **Saalfeld**, **P.**, Oeltze-Jafra, S., Saalfeld, S., Preim, U., Beuing, O. & Preim, B. *Sketching and Annotating Vascular Structures to Support Med-*

ical Teaching, Treatment Planning and Patient Education in *Dirk Bartz Prize for Visual Computing in Medicine* (2017), 5–8 [236].

6.1 BACKGROUND ON TRADITIONAL & COMPUTER-AIDED ANATOMY EDUCATION

Medical students' education starts with anatomy education, where a thorough understanding of the whole healthy human body is imparted. Students should be able to locate anatomical structures, which is an essential prerequisite for surgical interventions. They should be aware of the variability of morphology and location, e.g. of branching patterns of vascular structures. This is realized with approaches considering biological systems, e.g. the circulatory system (systemic anatomy) as well as focusing only on specific parts (regional anatomy). The knowledge is imparted to the students with a variety of courses and media along their academic studies. In lectures and seminars, educators present vascular systems through sketches on blackboards, images, and videos (see Figure 6.2). In parallel, students acquire medical knowledge with anatomic atlases and textbooks.

6.1.1 *Gross Anatomy*

An example of a specific course is the gross anatomy lecture (macroscopic anatomy), where the foundation about general physiology of all body parts is imparted. The cardiovascular system is explained from its central part, the heart, to the peripheral capillaries of the body. Clinical reference is demonstrated by describing possible diseases, patients and examination methods. This reference, however, is mainly added to motivate the students and give them an idea of clinical practice. In the later years, dedicated courses are offered with topics on medical conditions, their reasons, and diagnosis.

6.1.2 *Cadaver Dissection*

Besides lectures and seminars, where knowledge is taught mainly theoretically, preparation courses supplement the curriculum. Here, the student's task is to uncover tissue, vessels and organs of cadavers. During this process, educators explain general anatomic knowledge together with peculiarities, diseases and their cause of the body donor (see Figure 6.3). Cadaver dissection plays an essential role for various reasons, e.g. the training of manual dexterity and communication skills [32]. The color and texture of structures, however, differ strongly from living patients. Other disadvantages of cadaver dissection are the high cost, the difficulty of supply and the short time they can be used [59, 210].

(a)

(b)

(c)
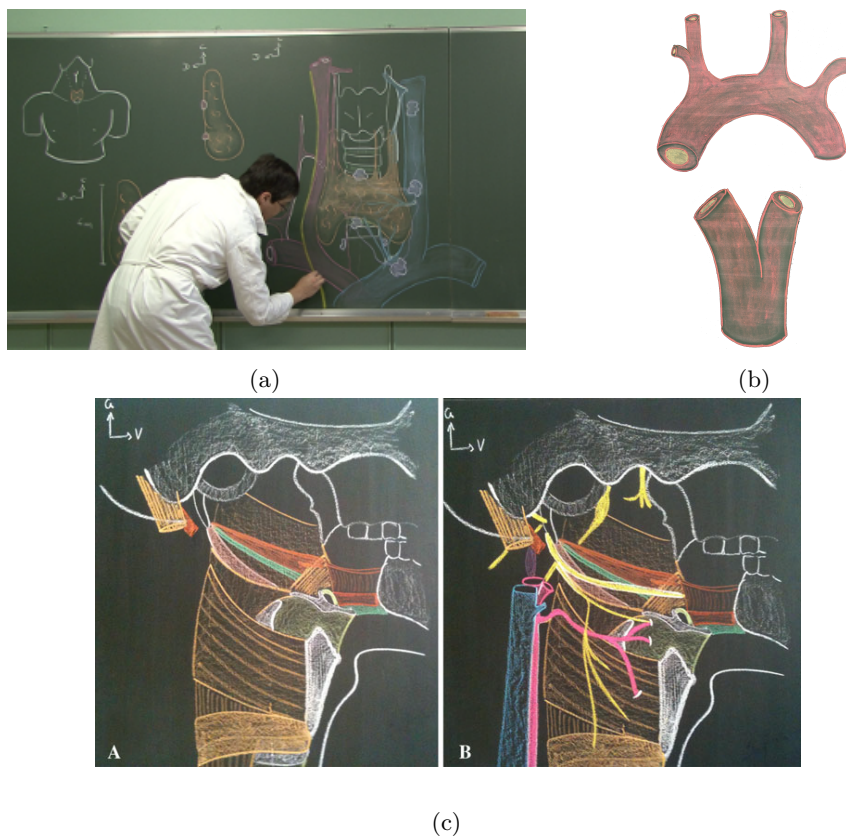
Figure 6.2: Blackboard drawings of the anatomy lecture. In (a), the educator sketches the vascular system of the thyroid from different viewpoints. In (b), two types of sketched vessels are shown [201]. In (c), a dissection of the neck was sketched. The left side shows bones and muscles and on the right side, vascular structures and nerves are added [28]. Images (a) and (b) from Pihuit et al. [201], reprinted with permission. Image (c) from Borelli et al. [28] made available under the Creative Commons Attribution Non-Commercial License.

6.1.3   *Computer Assistance*

Computer assistance in teaching is one approach to overcome disadvantages from "traditional" learning strategies, such as flash card-based learning. Biasutto et al. [22] investigated if the dissection course can be substituted completely with diverse technological resources and tested three groups:

- **Group 1** learned in a traditional way, including cadaver material to observe all the regions and structures,

- **Group 2** used many technological resources but no cadaver dissections, and

Figure 6.3: The educator explains the correlation between structures of a cadaver and radiological image data in a gross anatomy course [196].

- **Group 3** followed the course with both traditional and technological resources.

The study showed that **Group 1** obtained better results than the technologically supported group **Group 2**. **Group 3** performed best, indicating that the traditional dissection course should not be substituted, but instead complemented.

Such complementation of the traditional curriculum with computer assistance was described as early as 1967 from Starkweather to help students explore clinical problems at their own pace [255]. In a literature study, Letterie [150] compared articles from 1988 to 2000 dealing with computer-assisted learning in a wide variety of medical fields. Overall, 96 % of the analyzed articles describe a positive impact of computer-assisted instructions. The used media comprise online technologies, multimedia workstations and VR. However, important to note is that the high percentage of positive impact is presumably distorted by a publication bias (mainly positive results are published). The conducted study led by Kohrmann [133] that was co-authored by the author of this thesis could not show a beneficial impact of computer-assisted learning. They scanned body donors and let students learn with interactive volumetric representations of these scans. The control group learned atlas-based. After that, both groups identified structures on a real body donor and solved a medical puzzle by assembling pieces of the learned regions. In theory, assembling the 3D puzzle requires a spatial understanding and the computer-assisted group should have an advan-

tage. However, no significant differences could be found regarding error rates or required time. Overall, the conducted studies reflect only a short usage of time with a computer-assisted system. A permanent integration into the curriculum is harder to achieve and evaluate, but necessary to assess if it is beneficial or not.

The type of computer assistance can take different forms. They are classified as *very structured* (e.g. digital flash card systems), to *open exploratory* approaches. Consequentially, the strategy has an impact on the type of knowledge that should be imparted with it. A structured approach is beneficial for teaching facts but does not allow students to detour from planned learning paths. Exploratory systems, such as medical 3D puzzles [220] or tools to elaborate vessel variations [249], encourage an independent free exploration, but could result in unproductive learning sessions [51]. Therefore, consideration of students, educators and their needs is important. One example and pioneering work in this direction that evolved from a leading research result to a commercial product is VOXEL-MAN (Hamburg, Germany) [103]. Different versions exist that support either students as a digital anatomical learning atlas [77] or physicians as a surgery trainer [265]. However, even the high effort on research and development of the VOXEL-MAN did not lead to a permanent integration into the curriculum.

6.1.4 *Semi-immersive Systems*

A large proportion of articles in medical journals contains the description "VR-based", but this mostly describes a 2D desktop setting with an interactive 3D model [210]. Since immersive systems can be more motivating than traditional 2D interfaces [214], there is a huge potential for learning. A natural and intuitive interaction allows users to fully focus on the learning scenario, rather than on semantics of the interface [102, 212]. As a result, the cognitive effort can be reduced compared to non-immersive environments. A further advantage is the possibility to illustrate 3D structures in a realistic way, which benefits the learning of *spatial anatomy knowledge* [224]. Besides the misuse of the term "VR-based", the recent survey from Hackett et al. [86] lists 38 VA systems that actually use stereoscopic and autostereoscopic displays. The self-report of learners showed advantages regarding the understanding of spatial structures, but also stated problems related to perception conflicts and artifacts. An interesting setup to teach anatomy was presented by Fellner et al. [64]. They combined stereoscopic *Cinematic Rendering* [63] with a large 8K 3D projection system that can accommodate an audience of 150 people (see Figure 6.4). Cinematic Rendering allows the direct rendering of CT or MRI datasets in a photorealistic way. However, the direct usage of medical image data has a shortcoming: structures that are too close to each other or too small cannot be recorded properly by the image modality. For example the two chest muscles *pectoralis major* and *pectorialis minor*

Figure 6.4: The "dissection theatre of the future" shows a whole body data set with stereoscopic Cinematic Rendering [64]. Image from Fellner et al. [64] made available under the Creative Commons Attribution 4.0 International License.

lie over each other and are not clearly distinguishable even with a 0.5 mm image resolution. Here, manually modeled 3D surfaces are advantageous. Vascular structures, especially complex ones, are among the structures where the benefit of stereoscopic perception is large [1]. According to Luursema [156], students with low spatial ability benefit stronger from stereoscopy.

Some commercial applications and medical schools use the zSpace to support anatomy education, however, without associated scientific publications. For example, the learning platform VISIBLE BODY[1] was ported to the zSpace. The laboratory of the TOBB University of Economics and Technology in Turkey is equipped with several zSpaces. The students and residents can use the zSpace before they participate in cadaveric dissections. One example of published results for neurosurgery training was presented by John et al. [121]. However, to the surprise of the authors, their study could not show advantages induced by stereoscopy.

The zSpace was used for the exploration of vertebras of the cervical spine by the author of this thesis [226]. Since this work does not fit in the scope of sketching, it is briefly mentioned here. Medical students were enabled to inspect the

---

1 https://www.visiblebody.com/de/, last accessed: 11.06.2018
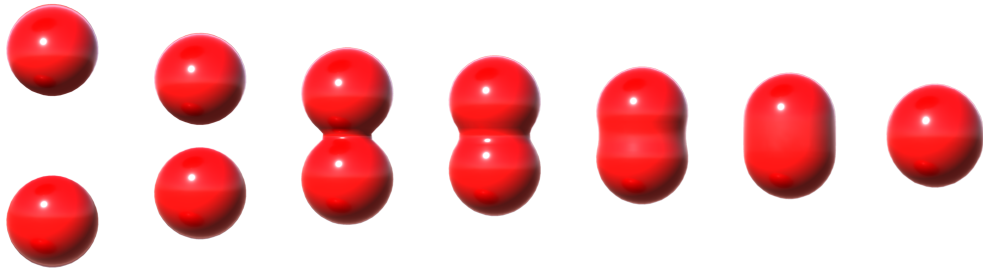
Figure 6.5: As the scalar fields of the two Metaballs overlap, they start to blend together, yielding a smooth, organic shape.

whole cervical spine and single vertebras with a focus and context visualization. Eventually, the spatial representation supports the understating of anatomical relations

A recent comprehensive survey article was written by Preim and Saalfeld [210] (co-authored from the author of this thesis). It presents an extensive overview on virtual anatomy education systems realized as desktop, web-based, and immersive systems. For these systems, the visualization and interaction techniques are discussed.

6.2   BACKGROUND ON IMPLICIT SURFACES & VASCULAR MODELING

In the following, the mathematical background of implicit surfaces is described and their usage to create vascular structures is explained.

6.2.1   *Mathematical Background*

An implicit surface is defined in Euclidean space as the zero set of the implicit equation $F(x, y, z) = 0$. For instance, all points $p(x, y, z)$ satisfying the equation $x^2 + y^2 + z^2 - r^2 = 0$ are on the surface of a sphere with radius r. Implicit surfaces were introduced to computer graphics as *Blobby Molecules* in 1982 to visualize electron density fields of hydrogen atoms [24]. Each atom ("blob") is associated with a *scalar field function*, i.e. a three-dimensional Gaussian function that models the electron density. This function has its peak at the atom's center and falls down in its surroundings.

The implicit surface is then constructed by choosing an *isovalue* that represents the density of interest. An interesting property of implicit surfaces is observable when multiple scalar fields overlap: the constructed surface yields a smooth, organic looking *blending* of the atoms' individual surfaces (see Figure 6.5). This makes implicit surfaces very suitable to model vascular structures.

Since the consideration of the infinitively defined Gaussian function requires the inspection of each point in space, bounded field functions were introduced under the concept of *Metaballs* [182] in 1985 and *Soft Objects* [285] in 1986, respectively. Here, each Metaball represents an atom. This results in different functions to calculate the density based on the distance from a point p in space to the Metaball's center. The field function $F(p)$ for Metaballs is defined as:

$$F(p) = \begin{cases} w\left(1 - 3\left(\frac{d}{r}\right)^2\right) & : 0 \leq d \leq \frac{r}{3} \\ \frac{3w}{2}\left(1 - \frac{d}{r}\right)^2 & : \frac{r}{3} \leq d \leq r \\ 0 & : r \leq d. \end{cases} \tag{6.1}$$

Here, d is the distance from p to the center of the Metaball, w is the weight of the Metaball, and r is its radius of influence. In the described prototype, all Metaballs equally contribute with $w = 1$. The contribution of multiple Metaballs M at p is computed as the sum of their individual function values $F_i(p)$. The implicit surface is then defined based on an isovalue Iso as the zero set of:

$$\sum_{m_i \in M} F_i(p) - Iso = 0 \tag{6.2}$$

The definition of scalar field functions was later extended by J. Bloomenthal and K. Shoemaker from points to more complex structures such as line segments, planar curves, and polygons [25]. This extension allows to model more complex surfaces and is referred to as *Convolution Surfaces*. The general approach of Convolution Surfaces is the same as for Metaballs. However, instead of calculating the distance d between p and the Metaball's center, the distance to other structures such as lines or polygons is calculated.

6.2.2 *Vascular Modeling*

While the interactive 3D sketching of vascular surfaces is new, general vascular modeling techniques have been surveyed and classified before. A general subdivision can be made into *explicit* and *implicit* approaches [104]. Explicit modeling requires a careful, case-specific connection of sets of polygons or parametric patches to ensure smooth surface transitions at branchings. These often lead to self-intersections on the inside of the vessel. In scenarios where the intravascular structure is important, e.g. virtual angioscopy, these artifacts may be problematic. As described, implicit modeling achieves smoothness and an organic look without specific constructional effort. Additionally, no intravascular artifacts occur, benefiting a semi-transparent display and virtual angioscopy applications [105].

Oeltze et al. [187, 188] used Convolution Surfaces [25] for vascular modeling, considering the vessel center line and associated circular cross-sections. Emphasis

was put on faithfully representing the local radius information to prevent blending artifacts. Schumann et al. [240] employed multi-level partition unity (MPU) implicits [189] for reconstructing from a segmentation mask, which facilitates arbitrarily-shaped cross-sections. This is important in scenarios where the correct representation of the original medical data set is mandatory, e.g. treatment planning. For the scenario of anatomical education, circular cross-sections are sufficient. In follow-up work, Schumann et al. [239] presented a post-processing step to enhance the triangle quality of the surface mesh and reduce the number of triangles. Wu et al. [284] avoided such post-processing by a curvature-dependent, quality-aware reconstruction of the vascular surface yielding less triangles in straight regions. Similar to Schumann et al. [240], they generated the surface based on the boundary voxels of an additional segmentation mask. Kretschmer et al. [135] proposed the connection of interpolating free-form contours along the center line and the combination of surface branches by means of Boolean operations. Later, Kretschmer et al. [136] presented a surface reconstruction technique facilitating a modification of incorrect vessel segmentations at interactive frame rates. This method is topologically reliable meaning that even the smallest branches are correctly displayed. The high performance is achieved with a curvature-sensitive sampling strategy that restricts a high sampling rate to vessels with low radius.

The approach of Yureidini et al. [288] is closest to the one used in this thesis, since they distribute Blobby Molecules along a given vessel skeleton. Each Blob is locally adapted to points on the boundary of a segmentation mask. In contrast to Yureidini et al., the approach presented in this thesis lets the user sketch a vessel skeleton with the simplifying assumption of circular cross-sections and provides an on the fly reconstruction of the vessel surface during sketching.

6.3 SKETCHING VASCULAR SYSTEMS

The following section describes the process to create vascular systems and pathologies. The creation is based on sketched center lines.

6.3.1 *Center Line Creation & Editing*

For the creation of lines, the zSpace's stylus is virtually extended with a rod. On the tip of this rod, the 3D positions are sampled and represent the basis to sketch the center lines. Several aspects lead to irregularly sampled data and noise:

- the sampling rate,

- interferences with the optical tracking, e.g. through ambient light,

- the conversion from the analog to a digital signal (quantization), and
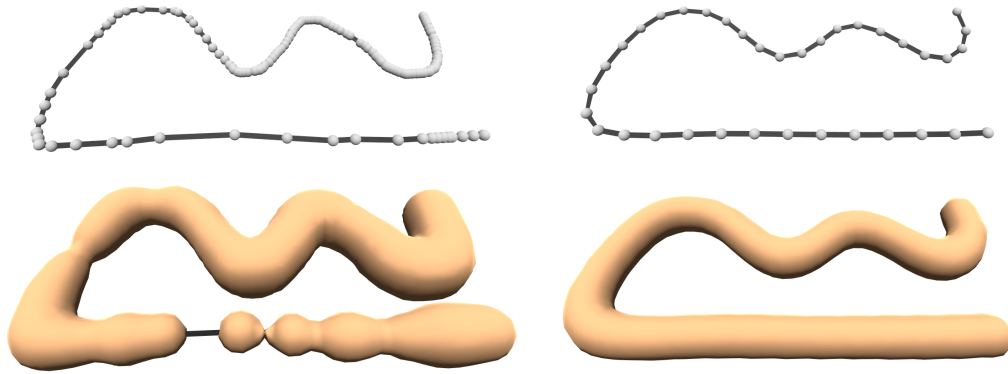
Figure 6.6: A center line based on the raw input data from zSpace's stylus yields the surface shown on the left. By resampling these points with equal distance and smoothing them with a Gaussian 5-neighborhood kernel, the resulting surface is not interrupted anymore and looks more homogeneous (right). Images from Saalfeld et al. [238].

- hand tremble.

However, the Metaballs' surface reconstruction requires points with equal distance. Therefore, the points are resampled and smoothed by a Gaussian kernel [262] (see Figure 6.6). A disadvantage of smoothing is the resulting loss of corners and, thus, complicates the sketching of sharp edges. This can be neglected, because vascular structures have a round and smooth shape. Figure 6.7 gives an overview of the interaction techniques to create and modify vessels. In the following, the techniques are described in more detail.

6.3.1.1 *Create*

The center line is sketched directly and a uniform vessel surface is created around it on the fly. The creation of a center line starts by pressing a button on the stylus. While pressing the button, the user sketches the line by moving the stylus in 3D space (see Figure 6.7a). Each sampled point is stored as a control point and visualized by a sphere.

6.3.1.2 *Edit*

A created center line can be edited with *oversketching* and *erasing*, both triggered with dedicated buttons on the stylus. To oversketch an existing line, the user has to start and finish drawing at a control point.

After releasing the button, the old line is replaced with the new one (see Figure 6.7b). Single control points and branches of the vessel can be deleted with an eraser metaphor. On the tip of the rod, a semi-transparent sphere is created and every control point that touches this sphere is removed (see Figure 6.7e). To
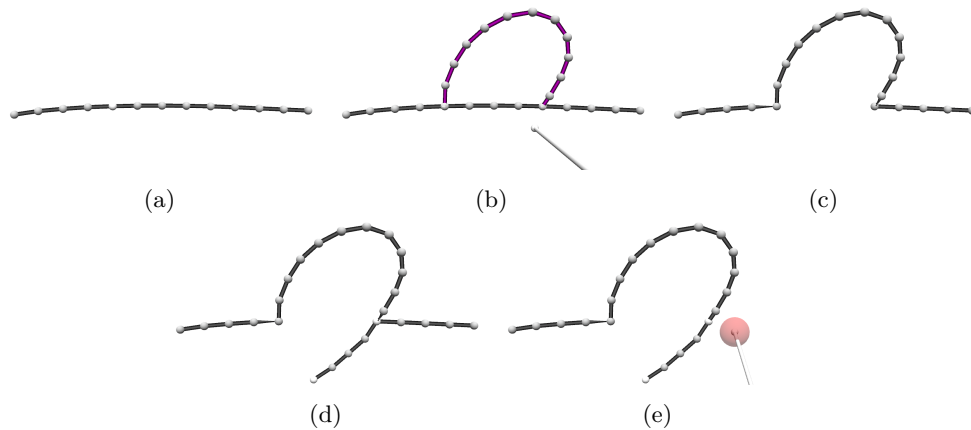
Figure 6.7: The prototype allows the user to create and edit a center line in a flexible way. In (a), a center line is sketched. (b-c) shows the *oversketching* function to correct existing lines. (d) depicts a created branch on the existing line. In (e), the deletion of a branch is illustrated. The user erases existing center lines by sketching over them. Images from Saalfeld et al. [238].

allow the precise deletion of single control points, the diameter of the sphere is smaller than the distance between two control points.

6.3.1.3   *Branches*

A prerequisite to create complex vascular structures is the ability to create n-way branches. This is realized by simply creating new center lines in close distance to control points. The user starts sketching on an existing control point and is supported by snapping (see Figure 6.7d). Here, not only hierarchic structures can be created, but also cycles, which is important for anatomical systems such as the CoW.

6.3.2   *Surface Creation with Metaballs & Marching Cubes*

While sketching the center line, the vessel surface is created around it in real-time. A continuous surface with smooth, organic transitions on branches is created with Metaballs.

The implicit surface is created out of a list of Metaballs, where each Metaball can be defined by a 3D position and its radius of influence r. Metaballs are created for every control point of the center line. Initially, the radius of it is fixed but can be adapted later. By creating control points in close proximity, tubular structures, i.e. vessels are generated. The necessary distance between control points was empirically determined such that a smooth surface without gaps, dents, and bulges is generated (see Figure 6.8).

The surface is reconstructed by:
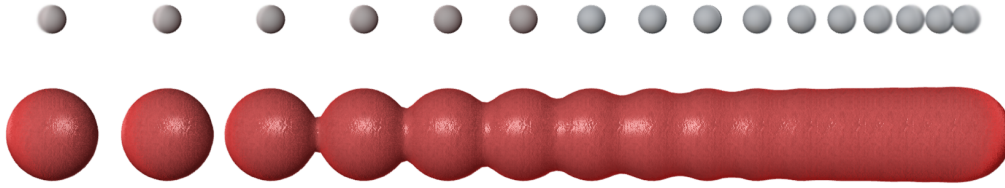
Figure 6.8: If Metaballs are positioned in proximity, the resulting surface recreates a vessel shape.

1. discretizing the 3D space with a specific grid size,

2. calculating a scalar value for each grid cell based on the Metaball formula (see Section 6.2), and

3. applying the Marching Cubes algorithm to polygonize the scalar field and obtain a triangular surface.

For the Metaball and Marching Cubes implementation, the *Skinned Metaballs*[2] asset from the Unity Asset Store was extended.

The quality of the resulting mesh and the computational complexity highly depend on the grid size. A high resolution grid leads to smooth transitions at branchings at the cost of long computation times. However, if the user wants to sketch large vascular structures, the high resolution grid does not allow real-time calculations. Figure 6.9 shows different quality settings that were identified, including the associated grid size, the resulting calculation time and the triangle count. During sketching, the reconstruction of the vessel uses a medium quality setting to allow the user to see the results immediately. After the user finishes sketching (i.e. releases the button), a background thread is started with the high quality setting. After the new surface is calculated, it replaces the medium quality surface. Using a background thread is especially important for semi-immersive environments. If the calculation would be realized in the main application thread, the head tracking would be stopped as well. This is noticeable and disturbing even with light head movements.

6.3.3 *Creating Stenoses & Aneurysms*

The illustration of pathologies is important in medical education. It allows the students to understand the changes in vessel morphology, blood flow and possible risks for a patient. An educator can sketch vascular system parts, which are commonly affected by diseases, and point out differences in their appearance. As described in detail in the previous Section 5.1, the most important vascular diseases are stenoses and aneurysms. Therefore, possibilities to create these pathologies were implemented.

---

2 Skinned Metaballs from Junk Games, http://nkdtr.hatenablog.com/entry/2015/06/05/125027, last accessed: 11.06.2018
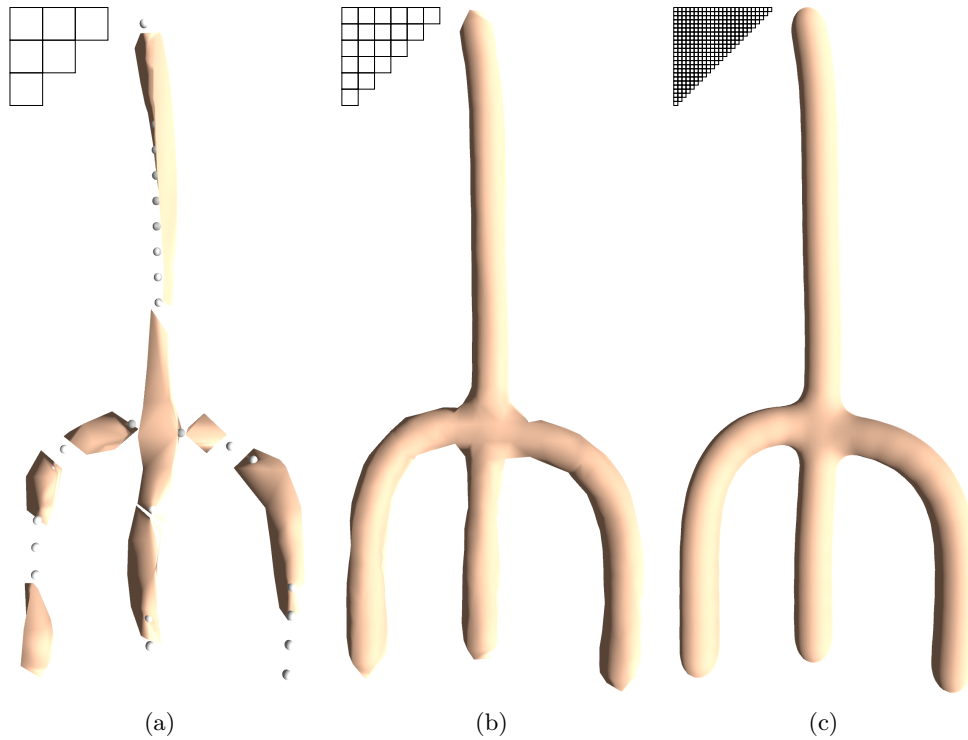
	Grid Cell Size	Calculation Time	#Triangles
(a) low	1	2 ms	852
(b) medium	1/2	15 ms	3,948
(c) high	1/8	768 ms	66,276

Figure 6.9: Different grid cell sizes used to discretize the 3D space are illustrated as well as the resulting vessels. The table shows calculation time and triangle count. During sketching, the medium quality setting was used. After the user finishes, a background thread calculates the surface with the highest quality setting (note: the grid cell size is normalized to illustrate the relative differences between them – therefore, no unit is stated). Images from Saalfeld et al. [238].

The initially sketched vessels have a constant diameter due to the fixed radius of each Metaball. Therefore, decreasing the radius of one or several neighboring Metaballs creates a stenosis. This is achieved by first selecting control points similar to the eraser metaphor. The user draws over control points, which are then selected and highlighted. By pushing the stylus forward, the user decreases the radius of the selected control points and creates a stenosis. Vice versa, by pulling the stylus, the radius is increased resulting in a fusiform aneurysm (see Figure 6.10).
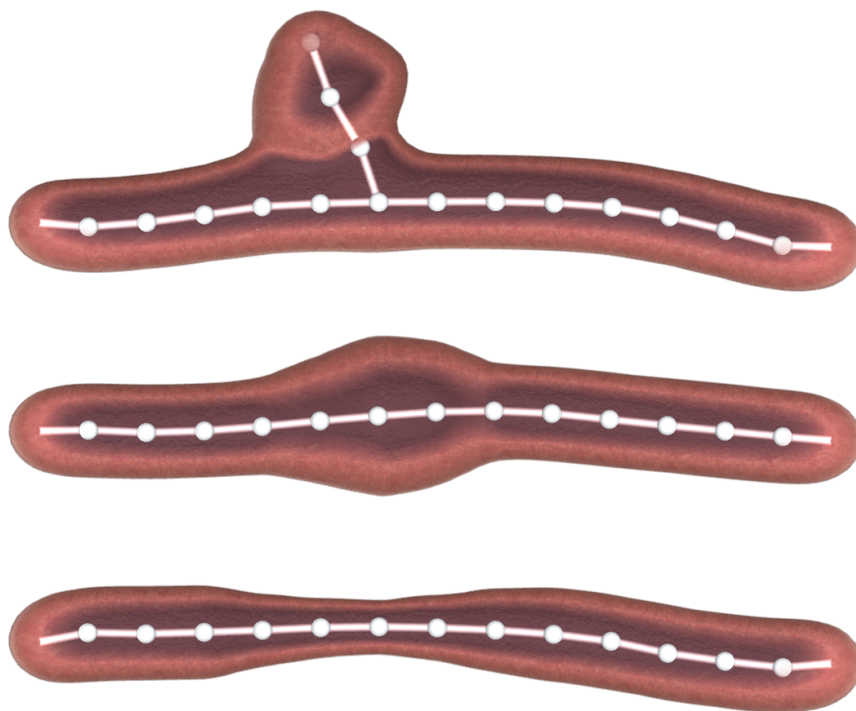
Figure 6.10: Different vascular pathologies can be created with the presented prototype. The top shows a saccular aneurysm, in the center, a fusiform aneurysm is shown and the bottom depicts a stenosis.

However, many aneurysms have a saccular shape and are only bulged to one side. To recreate these, a small branch can be sketched first. By adjusting its diameter (smaller on the aneurysm neck, wider at the dome point), a saccular aneurysm can be created (see Figure 6.10).

6.4 VISUALIZATION OF VASCULAR STRUCTURES

Pihuit et al. [201] render the blood vessels in an illustrative way to recreate blackboard sketches: dark red is used for the contours, light red to fill the surface and white to indicate cross-sections (i.e. holes). In contrast to their work, this thesis aims at a more realistic vascular surface representation, which would not be possible to realize on a blackboard in a reasonable amount of time. Rendering a realistic surface supports the perception of depth and size, as could be shown by Lindeman and Ropinski for volumetric data [153]. Eventually, this leads to an improved perception and understanding of spatial relationships [206].

Therefore, the vessels are not rendered with an illustrative approach, but instead with physically-based shading [195]. This technique simulates the behavior of light more realistically. Here, the energy conservation of light is used, e.g. less light is reflected than received, a high specular amount minimizes the diffuse
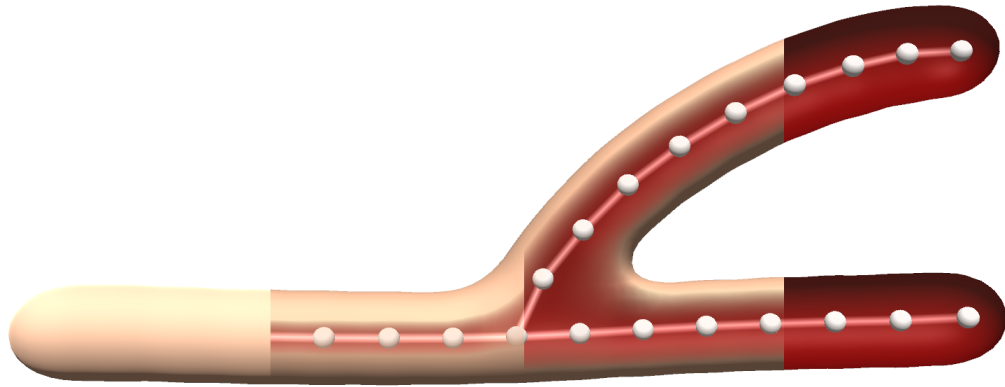
Figure 6.11: In the two-pass rendering, the back faces and front faces are rendered separately. The opacity of the front vessel wall can be adjusted from total occlusion (left), over intermediate steps (center left and center right) to full exposure (right). Images from Saalfeld et al. [238].

proportion, and the surface becomes more reflective at grazing angles (Fresnel effect) [195]. To allow the user to see inside the vessel, a two-pass shader is used, which gives the appearance of an inner and outer vessel wall. In the *first render pass*, only the back faces are rendered. Since they point away from the user, they are flipped first. In the *second render pass*, the remaining front faces are rendered with an addition. The dot product between the normals and the viewing direction is calculated. The result represents how much the face normal is pointing to the user. With a higher value, the transparency is increased. The strength of this effect can be adjusted, i.e. the extent to which the outer vessel wall exposes the inner vessel wall and blood flow (see Figure 6.11).

To further improve the realism of the vascular visualization, textures are used. Since the structure is created in real-time, no precomputed texture coordinates are available. Therefore, an automatic approach from procedural terrain modeling is used, i.e. tri-planar texture mapping [179]. Here, the normal of each vertex is mapped to a texture on the x-, y-, and z-plane. The resulting color is a weighted combination of the three texture colors. This weight depends on the amount the normal is facing in one of the directions. For example, if the normal is facing exactly to the z-direction, only the color of the x-y-plane would be taken into account. The same technique is used for a normal map to give the impression of depth on the vascular surface. To reduce the appearance of repetition artifacts (i.e. tiling), two additional techniques are used:

- Multi-UV mixing – the same texture is used twice and blended with different scaling. Since the same texture is used, no additional resources are necessary (except for the computational effort).
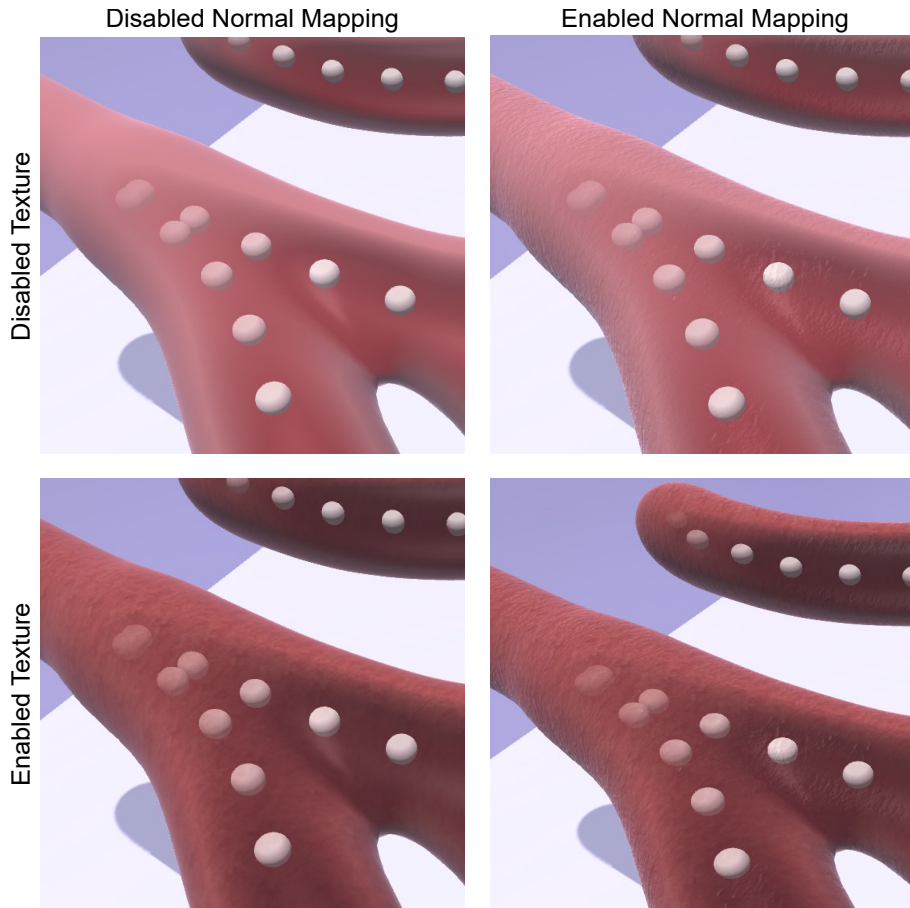
Figure 6.12: The two-pass rendering of the inner and outer vessel wall is improved with tri-planar texture mapping. The results are illustrated with the disabled/enabled texture/normal maps.

- Coherent noise – by using a smooth noise function (small changes in input result in small changes in output), a naturally looking form of noise can be generated and blended into the texture.

In Figure 6.12, a comparison of the vessel visualization with and without texture and normal maps is depicted. This approach is sufficient for vascular structure, since the orientation of the texture does not convey information regarding biological processes. However, it would be inadequate for many other anatomical structures, e.g. almost all muscles. Here, muscle fibers are oriented in the same direction, showing a line from the origin to its insertion. A texture has to convey this information. If the orientation has to be conveyed, other methods should be used, for example a curvature-based approach from Gasteiger et al. [76]. They use a combination of the principle curvature direction of a mesh, its skeleton direction and a preferential direction defined by the user to apply hatches along the fiber direction.

(a)   (b)
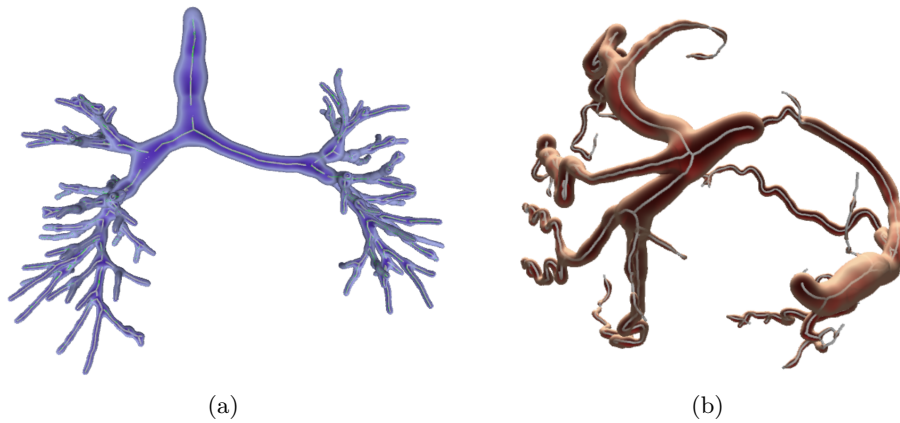
Figure 6.13: Real patient data visualized with Metaballs. For every point of the imported center line, a Metaball is created. The associated diameter is mapped to the Metaball's radius. (a) shows a bronchial tree and (c) the coronary arteries. While (a) is sufficient for education purposes, the diameter of the coronary arteries is too large. However, a reduction would result in gaps on the vessel. Images from Saalfeld et al. [238].

6.5   LIMITATIONS & SOLUTIONS FOR THE IMPORT OF REAL PATIENT DATA

A function to import center lines extracted from real patient data allows students to inspect rare conditions and is faster compared to manually sketch complex vessel trees.

Therefore, the prototype is extended to import center lines in several formats, e.g. the skeleton format of MeVisLab (a cross-platform application framework for medical image processing and scientific visualization, MeVis Medical Solutions AG, Bremen, Germany). In MeVisLab, segmentation masks of volumetric patient data can be generated with diverse image-processing techniques. These masks can be *skeletonized*, yielding a center line with associated diameter information [242].

A simple and direct approach is to create a Metaball for every vertex of the center line and mapping the diameter information on the Metaball's radius. This yields partly sufficient results (see Figure 6.13). However, if control points of the imported center line are too far apart from each other or the diameter is too small, gaps along the vessel occur (see Figure 6.14a). Another problem are blending artifacts that arise if two center lines run too close to each other (see Figure 6.14b).

These problems can be partially solved by using Convolution Surfaces that allow the usage of additional primitives such as line segments, whereas Metaballs only use points. Traversing complex vascular trees results in multiple line segments. These can be used by the Convolution Surface approach, yielding surfaces with detailed vessel branchings and without gaps (see Figure 6.15). These
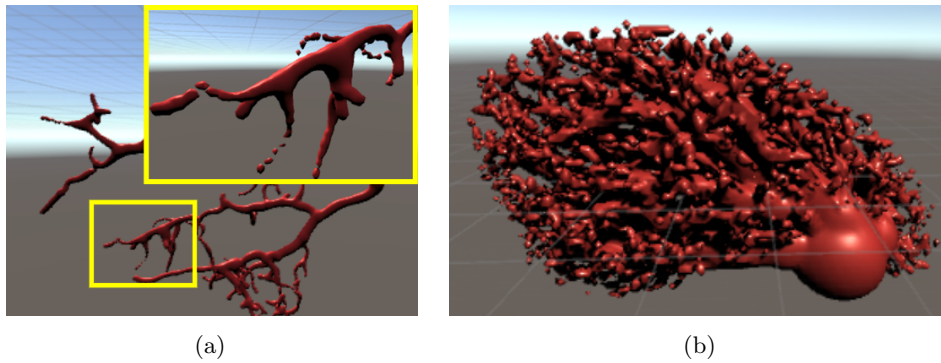
Figure 6.14: Artifacts can arise by using Metaballs for real patient data. In (a), gaps on the intrahepatic vessel occur due to Metaballs placed too wide apart. (b) shows blending artifacts due to the close spatial course of center lines.

benefits, however, are accompanied by a higher computational effort. Interactive frame rates can still be achieved by removing vertices of the center line with a line simplification method. Here, different strategies can be pursued. The results for *skipping vertices in close proximity* and using the *Douglas-Peucker algorithm* [56] (see Section 2.2.3) are illustrated in Figure 6.16.

6.6 ADDING PLAUSIBLE BLOOD FLOW

An illustration of dynamically changing blood flow can support students to understand consequences of pathological vessel changes. This is difficult to realize on blackboard drawings and often only indicated with arrows on top of the 2D drawings. With computer assistance, there are several possibilities to create a blood flow behavior that adapts in real-time to changes on the sketch. Since the goal of the presented prototype is to illustrate blood flow in a plausible and informative way, a physically correct simulation is not necessary.

As discussed in the previous Section 5.4.1, the state of the fluid can be characterized with differing accuracy as well as particle-based or grid-based. Unity already supports particle systems, thus, the particle-based approach is used. However, if a more realistic behavior would be required, e.g. to simulate shear force or rupture of a vessel, an elaborate new implementation would be necessary. Such examples can be found by Müller et al. [173] and Qin et al. [213]. They present a realistic vessel surface and particle interaction for virtual surgery.

From an interactive point of view, the user places particle emitters on control points. By pressing and holding a dedicated stylus button, the emitter is created. While dragging, the user specifies the direction of the blood flow to one of the neighboring control points (see Figure 6.17). Existing particle emitters can be removed by dragging the direction into empty space. The flow rate can be increased by simply placing multiple particle emitters on one control point.

6.6
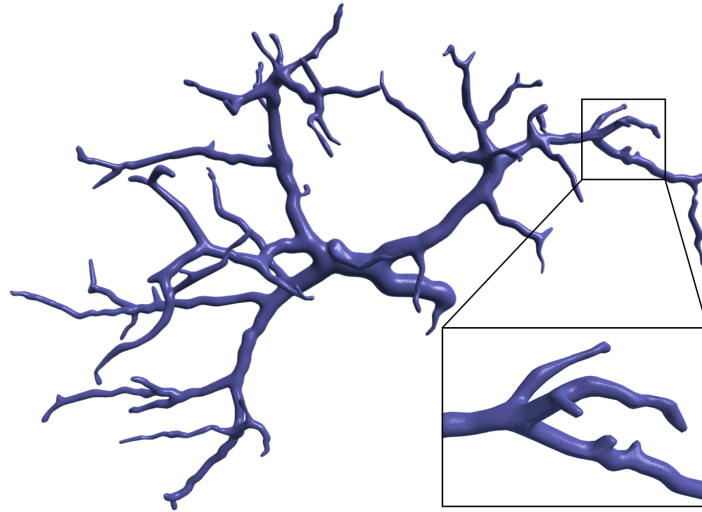
Figure 6.15: The vessel of the liver constructed with Convolution Surfaces. In contrast to Metaballs, detailed vessel branchings are possible and no gaps occur. Image from Preim and Saalfeld [210].

The emitted particles are represented realistically with 3D models of erythrocytes (red blood cells). Their realism is enhanced by the usage of textures and normal maps. By using 3D geometry instead of view-aligned sprites (also called billboards), shadows can be thrown on the inner vessel and enhance the spatial impression (see Figure 6.18).

Each particle is emitted randomly in the cross-section area of the vessel where the emitter was placed. To guide it along the vessel, the sketched center line is employed. Additionally, the vessel surface is used in combination with a collision detection for each particle. If a particle hits the vessel wall, e.g. on a stenosis, it gets repelled and directed closer to the vessel center. Branching vessels are accounted by interpreting the vascular system as a graph similar to the work of Zhu et al. [289]. After traversing the graph in a depth-first search, several paths are obtained. Particles are assigned based on a round-robin strategy, i.e. every new particle is assigned to the next path. If all paths have an assigned particle, the first path is assigned again.

6.7 graphical user interface

An overview of the layout with the control elements is depicted in Figure 6.19. The user can choose one of the three modes *create*, *edit*, and *blood flow*. The modes are activated by pressing virtual buttons with the tip of the virtual rod. For each mode, the assignment of the stylus buttons changes. To aid the user, a textual description of the currently available functions appears permanently. Additionally, an image of the stylus with labeled buttons is shown. This supports

<div align="center">Skip Close Points (SCP)   SCP &
Douglas-Peucker
(medium reduction)   SCP &
Douglas-Peucker
(strong reduction)</div>
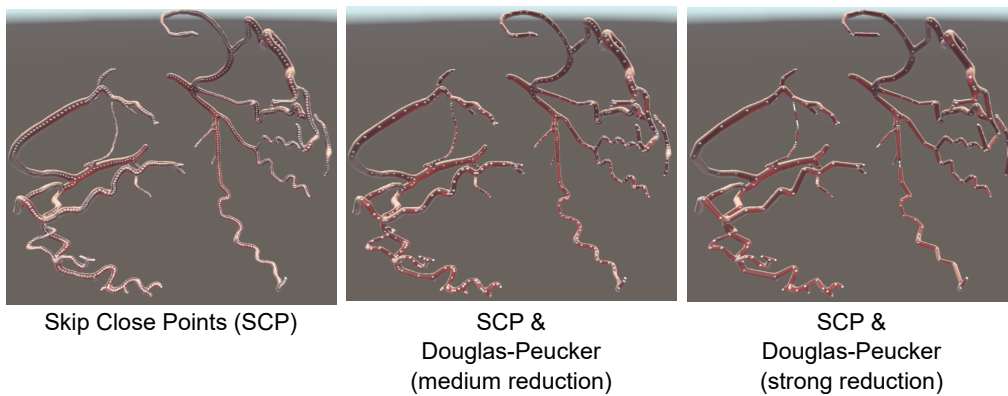
Figure 6.16: The computational effort of Convolution Surfaces can be reduced by simplifying the vertices of the center line by skipping points in close proximity (a) or using methods such as the Douglas-Peucker algorithm [56].

<div align="center">(a)   (b)   (c)</div>
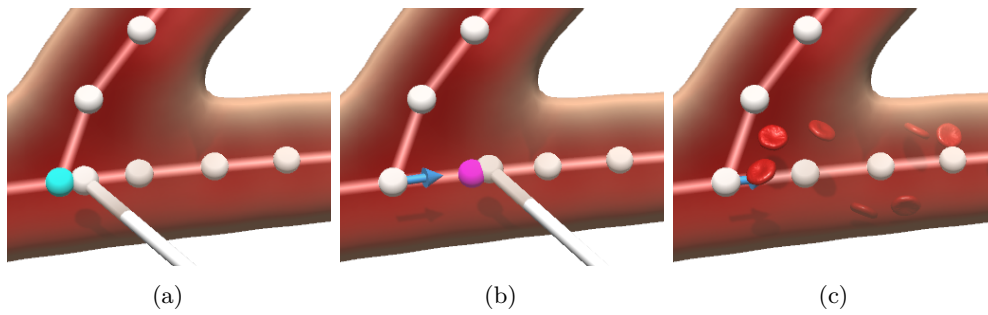
Figure 6.17: Overview of the interaction steps to create blood flow. The user starts dragging on a control point. Now, an arrow gets visible, which points to the direction of the blood flow. The user has to place the arrow on a neighboring control point, and, thus, determine the start position and flow direction of the blood flow. Images from Saalfeld et al. [238].

<div align="center">(a)   (b)</div>
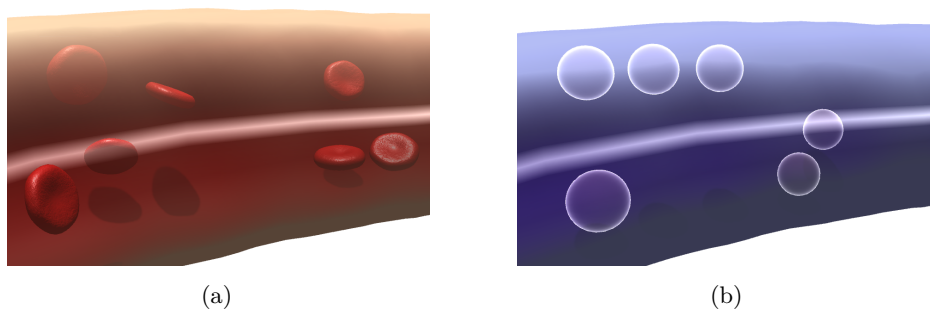
Figure 6.18: Two different possibilities to visualize particles in the prototype are illustrated: (a) depicts the default setting with 3D structures of red blood cells. In (b), an alternative visualization is shown, which can be used to illustrate air flow in bronchial tubes. Images from Saalfeld et al. [238].
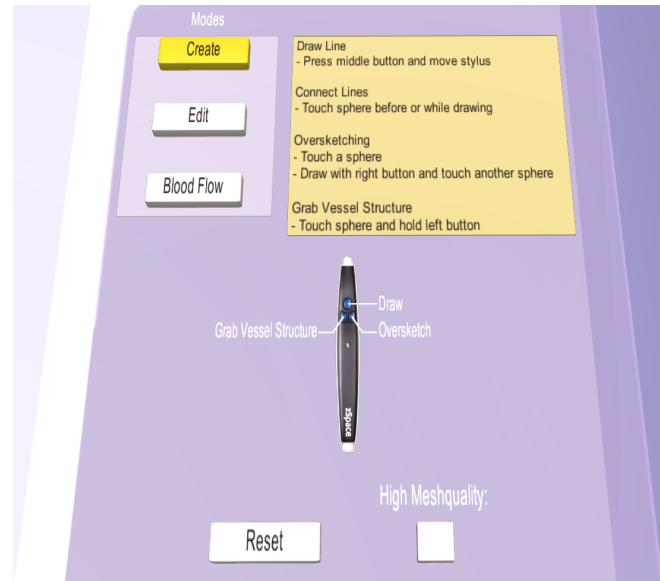
Figure 6.19: The user interface of the presented prototype is part of the virtual world, e.g. buttons are spatial objects. The user can change the sketching modes by pressing buttons with the virtual rod tip. Image from Saalfeld et al. [238].

the self-descriptiveness aspect of usability of the user interface and helps to reduce the learning effort. At the bottom of the user interface, a reset button can be pressed to remove the sketched vascular system and blood flow.

6.8 EVALUATION

This section comprises the evaluation including the user study conducted with novice users and the unstructured interview conducted with an anatomy lecturer.

6.8.1 *User Study*

In the following, the user study and its results are presented.

6.8.1.1 *Goals*

The goal of the evaluation is to assess the usability and usefulness of the semi-immersive sketching approach. This serves as the first step towards an integration into the medical curriculum. Therefore, aspects such as *suitability for the tasks*, *error tolerance* etc. are assessed using a questionnaire from Prümper [211] based on the usability norm ISO 9241-11. The single questions were categorized in the different aspects and were stated with a 7-point Likert scale $(---, --, -, \circ, +, ++, +++)$. However, questions regarding *customizability* were neglected, since the prototype does not support it.

The functions to integrate blood flow and load patient-specific data were suggested during the evaluation and implemented afterwards. Thus, they were not evaluated.

6.8.1.2 *Tasks*

The participants had to reproduce vascular configurations, which were shown as 2D sketches on a sheet of paper. Four tasks were designed, where the participants had to sketch the most common vascular system parts and pathologies. The tasks build up on each other to reproduce the scenario of sketching a more complex vascular system.

First, participants were asked to sketch a trifurcation. Here, at least one branch should be created into depth to make the participants aware of the spatial input and output. After that, the result should be inspected by changing the head position and get familiar with the motion parallax. The second task was to activate the edit mode and delete one branch. On the remaining two branches, a fusiform aneurysm and stenosis should be created. As third task, a new vessel should be sketched and corrected with oversketching. As the fourth and most complex task, a saccular aneurysm should be created. This task involves the creation of at least two branches (the second forming the saccular aneurysm), the deflation of the region around the aneurysm neck and the inflation of the aneurysm itself.

6.8.1.3 *Participants*

The user study was conducted with nine participants (4 female, 5 male). Their age ranged from 18 to 34 ($\bar{x} = 24.6$). All of them are computer scientists. Three participants had experience with ray-based interaction similar or equal to the interaction technique used in the presented prototype. No one had a medical condition leading to problems perceiving stereoscopic content. As discussed in Chapter 3, conducting the user study with computer scientists limits the possibility for generalization, i.e. if the results can be transferred to medical students and educators. However, a similar experience with 3DUIs can be expected for computer scientists and medical students or educators. To attenuate the bias due to a missing medical background, every participant was given a short introduction into the field of vascular systems and their pathologies. Furthermore, the tasks were described very general, e.g. the description of the task to sketch a trifurcation was illustrated with an image and explained without using medical terms.

6.8.1.4 *Procedure*

Starting with an introduction to the medical background, every function of the prototype was described and shown. It was ensured that every participant un-

derstood the medical background and different sketching functions. Then, the task sheet was given. During solving the tasks, participants were encouraged to comment on their actions (think aloud method [124]). This is helpful to obtain insights into the misunderstandings of the participants as well as to understand how the participants predict the behavior of the prototype. After finishing the tasks, the usability questionnaire was handed out.

6.8.1.5 *Results – Observations & Think Aloud*

The semi-immersive 3D sketching was understood by all participants after first drawing trials. Interestingly, participants differed in drawing speed and careful- ness, especially at vessel branchings. All participants were able to reproduce the general shape of the required vessel configurations. Additionally, the par- ticipants were able to sketch into depth and could take advantage of the 3DUI components. Overall, they described the spatial impression as very helpful to get an understanding where the stylus rod is positioned in virtual space.

If participants made errors, they rarely used the oversketching or erasing func- tion. More commonly, the entire sketch was reset. Changing the vessel diameter with the pulling and pushing technique was appreciated by all participants. One participant stated that a possibility to abort the current sketching would be helpful or alternatively, an undo/redo function.

Multiple participants stated that the process of sketching can be supported by the possibility to load pre-defined standard configurations. For example, a trifurcation can be loaded and an aneurysm can be added manually. Another interesting suggestion was the possibility to illustrate the blood flow as well as how it is altered due to vessel changes. Thus, this function was implemented after the evaluation.

6.8.1.6 *Results – Usability Questionnaire*

All of the usability questions were positively rated. The questions regarding the *Error Tolerance* had the lowest rating with $\bar{x} = 1.7$. This matches the results of the observations, since participants often deleted the whole vascular system instead of correcting parts. All other usability aspects had average ratings of $\bar{x} \geq 2.3$, implicating that the interaction techniques are appropriate to sketch vascular structures with the semi-immersive approach. The results of the usability aspects are summarized in Figure 6.20.

6.8.2 *Unstructured Interview*

The unstructured interview was performed with an anatomy lecturer with 12 years of experience as an educator in gross anatomy. This includes giving lectures, seminars and supervise cadaver dissection courses. The setup was similar to the
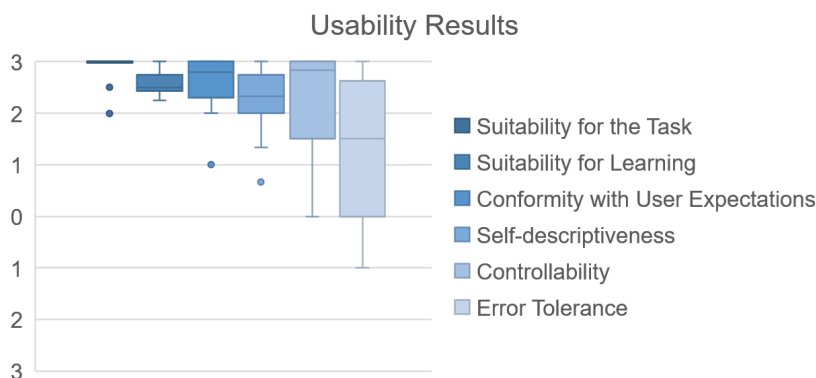
Figure 6.20: Boxplots for each category of the adapted usability questionnaire [211]. Note that the category *Suitability for the Task* was rated predominantly with 3. Therefore, the boxplot is almost not visible. The whiskers show the data points that are closest to the limit of 1.5 times the interquartile range. Outliers are depicted as dots and represent ratings that differ more than 1.5 times the interquartile range.

one of the user study, i.e. the functions of the prototype were shown and the anatomist was asked to sketch common vascular structures.

The anatomist highlighted several benefits of the 3D sketching prototype and compared it with classical approaches. For example, some lecturers illustrate complex structures by using several layers of foils projected with an overhead projector. These foils are used to add complexity to the structure layer by layer and to illustrate spatial depth. This extra step during the creation of the illustrations is not necessary with the 3D sketching prototype. The anatomist further highlighted the spatial impression that is generated by the zSpace and stated that it improves the understanding of anatomical structures, which is helpful for learning. Furthermore, the coupling of 3D input and instant 3D generation of vessels facilitates the creation of complex structures. This is especially helpful for areas where individual differences among persons exist. As an example, the anatomist referenced the renal arteries, which supply the kidneys, as they differ strongly in branching configurations. The illustration of a subset of common configurations would be helpful for students.

Interestingly, the anatomist stated that the usage of the prototype needs a special form of practice. Normally, anatomists recognize and understand 3D representations of anatomical regions, but they do not need the skill to *reproduce* them in 3D. During sketching, the anatomist had problems to recall the spatial track of complex vascular systems, and, thus, could not reproduce them exactly. However, according to the anatomist, this problem can be solved with sufficient preparation.

As a suggestion, it was stated to use the prototype for other anatomical structures. As an example, the anatomist suggested the possibility to sketch the gastrointestinal tract. Here, an additional animation of peristaltic waves (con-

6.9

traction and relaxation of muscles to propagate food) would support students' understanding of the intestine operating principle.

6.9   CONCLUSION & DISCUSSION

The presented prototype contributes to the field of medical education by combining methods from SBM and 3DUIs to create 3D vascular systems and its pathologies in a semi-immersive environment. The vascular surface is reconstructed on the fly with implicit surfaces, yielding a smooth, continuous surface mesh. Here, shortcomings of Metaballs are discussed and how the usage of Convolution Surfaces can overcome them. By enabling the exploration of real patient data and the enrichment with a plausible blood flow simulation, the prototype can be used to convey different vascular phenomena and support medical education.

The applicability of the interaction methods was shown with a usability study. Furthermore, the study revealed several limitations that have to be solved before the prototype can be tested in the medical anatomy curriculum. The usage of flexible interaction techniques allows to create a wide variety of vascular systems but can also result in unnatural and physiologically impossible vessel configurations. This is preventable with plausibility testing. However, trying to prevent these impossible configurations leads to a reduction of flexibility, which in turn might be necessary to illustrate rare conditions or pathologies. For example, in an earlier version of the prototype, it was prevented to sketch *cycles*, since arterial structures are usually organized as hierarchical structures. One exception of this is the *Circle of Willis* that is arranged as a cycle to backup blocked vessels. Another limitation of the prototype is the restriction to vessels with circular cross-sections. A possibility to deform the cross-section could show vessels and pathologies more realistically. More specific problems revealed by the study are related to the editing of sketches and the selection of computer scientists as participants. As described in Section 6.8.1.5, the oversketching feature was rarely used, but instead the whole sketch was reset if errors were made. This may be due to the mode switch that is required for editing and creating. However, a global undo/redo feature would presumably be most useful. The overall positive rating of the usability questionnaire must be carefully interpreted given the fact that only computer scientists participated. It can be assumed that they have a higher affinity for the semi-immersive technology compared to medical students and educators. Therefore, an evaluation with medical participants is necessary.

Future steps are necessary to integrate the prototype into the medical curriculum and dedicated functions can be tailored to the end user. For example, the educator can use it as an authoring system to present lectures and create learning content. To establish the prototype in a lecture environment, the educator and students need to have access to their own zSpace. These need to be synchronized to visualize the same vascular structures on the educator's and students'

<div align="center">(a)   (b)   (c)</div>
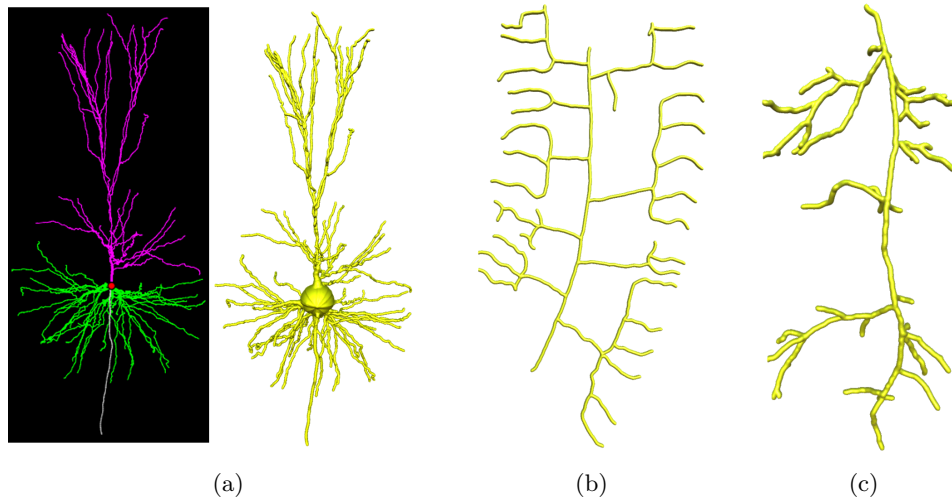
Figure 6.21: Different neurons from the Neuromorpho archive [9] reconstructed to a 3D surface with the presented approach. Neurons shown: (a) human [61], (b) nematode [52], (c) locust [82].

devices. The head tracking, however, has to be decoupled, which allows students to analyze and explore vascular systems from their own perspective.

From a broader perspective, the prototype can be used in patient education to explain different morphologies, pathologies and the impact of a treatment. The techniques used to reconstruct center lines into 3D surfaces can be used for more than vascular data. For example, the website Neuromorpho[3] [9] curates digitally reconstructed neurons, accessible in a center line based format. Figure 6.21 compares images from the website against the 3D models generated with the presented prototype. In contrast to the website's images, the presented approach allows for a better size and shape perception.

---

3 http://neuromorpho.org/, last accessed: 11.06.2018

7

ANNOTATE VASCULAR STRUCTURES FOR TREATMENT PLANNING
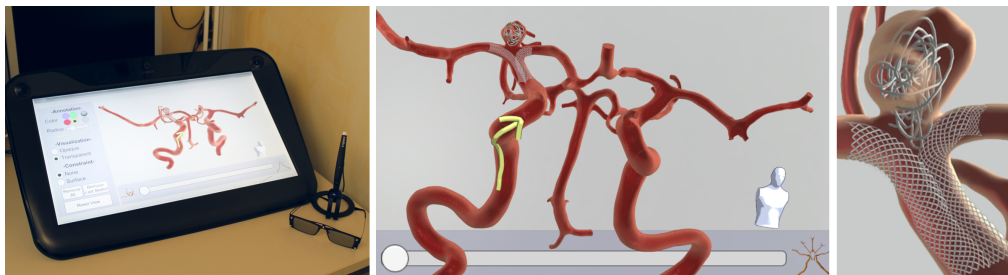
Figure 7.1: The zSpace is used to annotate vascular structures to support treatment planning. Images from Saalfeld et al. [230].

For clinical treatment planning, physicians need to obtain a spatial understanding of the patient's anatomy and pathologies. The shape, volume and spatial relationships of structures have to be considered [225]. Software assistants support the physician in medical practice to reliably and efficiently carry out special tasks [132]. Such tasks comprise access planning, resection and implant planning. The assisting software may provide the possibility to annotate pathologic variations and visualize treatment options [137, 203]. These annotations are usually drawn on print outs and brought into the operation setting [218]. As described in Section 2.2.3, such annotations support the communication [123]. Thus, they are sufficient to elaborate complex treatment strategies.

However, annotations on 3D image data are usually drawn image-based [216], which causes problems when physicians change the view and annotations do not adapt accordingly. A common solution is recalculating the position in the image domain [93], which introduces difficulties during the relocation of annotations due to disturbing non-continuous motions [159] (see Section 2.2.2). In contrast to automatic approaches that were used for annotation positioning, the FAUST (**F**ree-form **A**nnotations on **U**nfolding **S**tructures for **T**reatment Planning) prototype allows to interactively and directly create annotations in object space as 3D sketches. Furthermore, a possibility to *pin* them onto the 3D model is presented. This enables the annotations to still convey their meta-information on

121

dynamic medical data, such as time-varying or unfolding data. 3D sketches are usually applied in product design [69, 115, 194]. The user typically is a stylist with 3D drawing skills acquired through training over time [69]. This may be different for physicians. The annotation of medical structures in 3D with complex treatment options can be laborious and challenging. Therefore, the FAUST prototype assists the physician in different ways:

- the physician can create generic annotations as well as the most common treatment options by sketching and combining center lines only,

- an optional geometric constraint allows sketching directly on the 3D surface,

- the zSpace supports depth perception and 3D sketching with the stereoscopic display and stylus.

As an example of a spatially complex vascular structure, the CoW was chosen that comprises a circular combination of arteries (recall Section 5.1 and Figure 5.4). Fish tank environments such as the zSpace (see Section 2.3.2) are in particular suitable in scenarios where the user manipulates the virtual world from *outside in* and the size of the virtual object is smaller than the user's body [50]. Both applies for the CoW.

Besides the clinical importance, the CoW is well suited for the approach for two reasons. First, it includes many different sub-structures, which results in a variety of access paths and treatment options. The possibility to freely annotate supports the visualization of different treatment plans. Second, the CoW is represented either in its real, self-occluding 3D anatomical state or as a simplified 2D illustration. To maintain a mental representation of both states including annotations, an interactive and seamless transition is useful for the physician.

A user study was conducted according to the guidelines presented in Chapter 3 with novice users to reveal usability problems and to quantify the sense of *presence* (recall Section 2.3.2.2). Additionally, the prototype was tested with a neuroradiologist in an intensive demonstration and testing session, combined with an unstructured interview. Finally, the performance of the prototype was assessed comprising the calculation time to attach annotations to the CoW and the frame rate during interaction and unfolding.

The zSpace running the FAUST prototype is shown in Figure 7.1. The prototype was developed with the game engine Unity.

In the following, background information on the unfolding and animation of 3D surfaces are given. For information on the cardiovascular system and advanced treatment strategies, the reader if referred to the Section 5.1. After that, the developed prototype is explained comprising details on the sketching of annotations, visualization of vascular structures, and interaction techniques to manipulate the 3D surface. Furthermore, a possible procedure of an advanced Y-stenting intervention planned with the prototype is presented. Then, the

evaluation is described, including a user study and the interview with the domain expert. The chapter concludes with a description of the possible integration of the FAUST prototype into clinical practice and a discussion of the presented results.

This chapter is based on the publications:

- **Saalfeld**, **P.**, Glaßer, S. & Preim, B. *3D User Interfaces for Interactive Annotation of Vascular Structures* in *Proc. of Mensch & Computer* (2015), 255–258 [231],

- **Saalfeld**, **P.**, Glaßer, S., Beuing, O., Grundmann, M. & Preim, B. *3D Sketching on Interactively Unfolded Vascular Structures for Treatment Planning* in *Proc. of IEEE 3D User Interfaces (3DUI)* (2016), 267–268 [229],

- **Saalfeld**, **P.**, Glaßer, S., Beuing, O. & Preim, B. The FAUST Framework: Free-Form Annotations on Unfolding Vascular Structures for Treatment Planning. *Computers & Graphics* **65,** 12–21 (2017) [230], and

- **Saalfeld**, **P.**, Oeltze-Jafra, S., Saalfeld, S., Preim, U., Beuing, O. & Preim, B. *Sketching and Annotating Vascular Structures to Support Medical Teaching, Treatment Planning and Patient Education* in *Dirk Bartz Prize for Visual Computing in Medicine* (2017), 5–8 [236].

7.1 BACKGROUND ON UNFOLDING MEDICAL DATA & ANIMATION

This section comprises related work of how curved structures from medical image data are unfolded. Additionally, animations are discussed for a seamless blending of structures from their original, curved shape to a flattened one. The unfolding of medical data sets is of high interest in medicine for tubular shapes such as blood vessels, bronchi or the colon [203]. The tomographic image data that is acquired from these structures rarely present the necessary information in a single image plane. This motivates the unfolding of these structures. An established technique to realize this is Curved Planar Reformation (CPR) [125]. Here, the center line of the tubular structure is derived and flattened. The flattened structure is then mapped into a new, single image providing its longitudinal view. This allows the physician to investigate vascular pathologies in a simplified view. There exist several adaptations of the CPR, which focus on specific structures. For example, Williams et al. [279] introduced an extension that is suitable for large, hollow structures such as the trachea or the colon. To investigate the whole tubular structure with these two methods, the visualization has to be rotated around the central axis. An approach to aggregate these rotated images in one image was suggested by Mistelbauer et al. [169]. All these techniques allow a depiction of the unfolded structures in an additional 2D view. However, the task

7.1

to mentally transfer the distorted unfolded image to the 3D volume is left to the physician, who must alternately investigate the 2D and the 3D view. Neugebauer et al. [177] solved this by embedding a 2D projection of a cerebral aneurysm surface as contextual information around the 3D visualization. Another approach is used by Vilanova et al. [271]. They integrate the unfolding directly into the 3D volume rendering by using the center line of a colon to flatten it for virtual endoscopy. The presented solution in this thesis is based on this idea. However, instead of visualizing only the unfolded structure, the FAUST prototype allows the physician to seamlessly blend between the original and unfolded 3D representation in an animated, interactive manner.

In general, there are two possibilities to represent the animation of 3D meshes: keyframe and skeletal animations [154]. In **keyframe animations**, several sequences of the same but deformed mesh are stored. For the animation, the sequences are played consecutively. This approach is memory-intensive, since each mesh has to be loaded during animation. Furthermore, the final result depends on the amount of keyframes, which have to be hand-crafted in a time-consuming process. In **skeletal animation**, the original surface representation is provided with a skeleton represented by a set of interconnected bones. As a skeleton, the center line can be employed. Here, each line segment of the center line becomes a bone of the skeleton. In contrast to keyframe animation, the vertices of the surface are not animated directly. Instead, in a process called *skinning*, every vertex is assigned to one or multiple bones with a specific weight. The weight determines how strongly each bone influences a specific vertex. Now, the bones are animated and the vertices are transformed accordingly.

Previous research also investigated how the pre-processing steps for skeletal animation can be automated. For example, Au et al. [11] describe a method to automatically obtain the skeleton of a given surface with mesh contraction and Wade et al. [274] compute the skeleton with a preprocessing step of voxelization. Baran and Popović automatize the next step, i.e. the rigging of a skeleton and surface mesh to simplify the animation [19]. The intersection artifacts due to the commonly used *linear blending skinning* [151] can be minimized by transforming the mesh into an implicit representation [268] (see Section 6.2). Further approaches and a comparison of different linear blending methods were presented by Chaudhry et al. [43] and Jacka et al. [116].

7.2 MATERIAL

This section describes the transformation of the 3D medical image data of the CoW into a surface model. Afterwards, the workflow to create the animated unfolding vessel is described. The whole process is illustrated in Figure 7.2.

| MRI Dataset from Healthy Circle of Willis | Segmentation & Surface Mesh Extraction | Smoothing & Cutting Off Unnecessary Outlets | Artifically Modeling Aneurysm and Stenosis | Generating a Skeleton for Skeletal Animation | Unfolding with Forward and Inverse Kinematics |
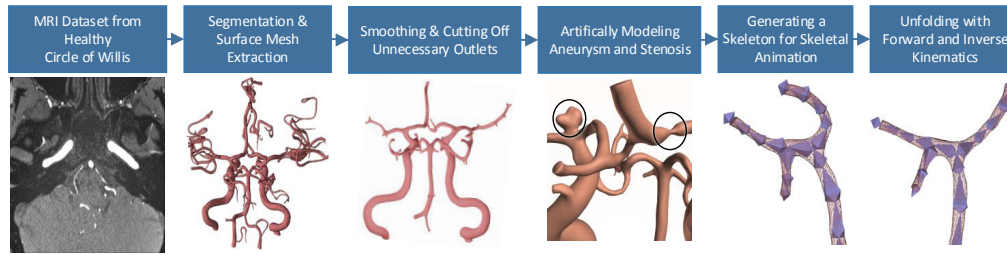
Figure 7.2: Workflow to create the unfolding Circle of Willis from Magnetic Resonance Imaging. Image from Saalfeld et al. [230].

7.2.1 *Reconstruction of the CoW's 3D Surface*

The CoW was extracted from a healthy patient's MRI data set, which was acquired for clinical education using the MAGNETOM Skyra 3T (Siemens Healthcare GmbH, Erlangen, Germany) with a 20-channel head/neck coil and a voxel resolution of $0.26\,\text{mm} \times 0.26\,\text{mm} \times 0.5\,\text{mm}$. For the 3D surface mesh extraction, the procedure described by Glaßer et al. [79] was used. The mesh was extracted with MeVisLab by applying a threshold-based segmentation and using the Marching Cubes algorithm. Subsequently, the extracted triangular surface mesh was smoothed with Sculptris (Pixologic, Los Angeles, USA). Unnecessary outlets were cut off with Blender (Blender foundation, Amsterdam, the Netherlands). After that, an aneurysm and a stenosis based on real clinical patient data was artificially modeled onto the surface. The generated pathologies were approved by an interventional neuroradiologist.

7.2.2 *Unfolding the Surface*

The unfolding of the CoW is realized with skeletal animation. As discussed in Section 7.1, this is less memory-intensive compared to keyframe animations and not restricted to the amount of keyframes. Normally, the skeleton consists of a hierarchical set of connected bones. However, the reconstructed CoW is a closed surface with a genus of one, i.e. it has a hole. Therefore, an automatic procedure to create a center line would result in a cyclic graph instead of a hierarchy. Instead, the skeleton was created manually inside the modeling and animation application 3ds Max (Autodesk, Inc., California, USA). The usage of 3ds Max has shown to be beneficial, since it offers capabilities to deform the skeleton together with the surface and generate an animation that can be imported by Unity. First, multiple skeletons (consisting of bones) are created and attached to the reconstructed CoW (see Figure 7.2). After skinning to assign the CoW's vertices to the skeleton, the skeleton was unfolded with a combination of forward and inverse kinematics. Now, two surface states are obtained: (1) the "folded state" that represents the original and anatomically correct state and the (2) un-
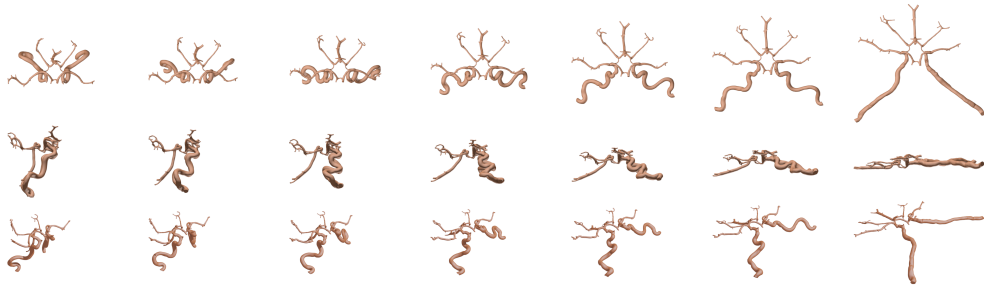
Figure 7.3: Overview of the animated unfolding from orthographic top (1st row), ortho-graphic left (2nd row) and perspective 3D (3rd row). Images from Saalfeld et al. [230].

folded state that shows the complex vascular structure of the CoW in a simplified, flattened form. By interpolating between these states, a seamless and smooth animation is created (see Figure 7.3). In character animation, the limbs of the initial mesh are normally spread apart, which eases the rigging and skinning process but can lead to deformations and overlapping artifacts during animations. This is different for the CoW due to its initial folded state. During the unfolding, no overlapping artifacts but slight deformations occurred. Yet, the introduced deformations are acceptable even for medical treatment planning. This is because the unfolded CoW is an abstract representation of the anatomically correct CoW. Occurring artifacts in this state might be visually unpleasing, but do not influence treatment decisions. For the original, folded structure, anatomical correctness is required. But since this state remained unaffected from the unfolding procedure, the correctness is ensured.

7.3   ANNOTATION OF UNFOLDING VASCULAR STRUCTURES

This section comprises details about the free-form annotation, including technical realization aspects, different types of annotations and their visualization. Additionally, the animated unfolding of the CoW and the annotations is described.

7.3.1   *Creating & Attaching Annotations*

The free-form annotations are sampled from the zSpace's stylus as described in the previous Section 6.3.1. These points are *linked* to the 3D surface. Thus, they adapt their position and shape during the unfolding of the CoW. The linking is realized by connecting each annotation point A_i to its closest surface vertex S_{A_i}.

7.3.1.1   *K-D Trees for Efficient Attachment*

Since the closest surface vertex S_{A_i} is searched during run-time, a fast retrieval is necessary. The naive approach of testing all surface vertices against an an-

(a)   (b)
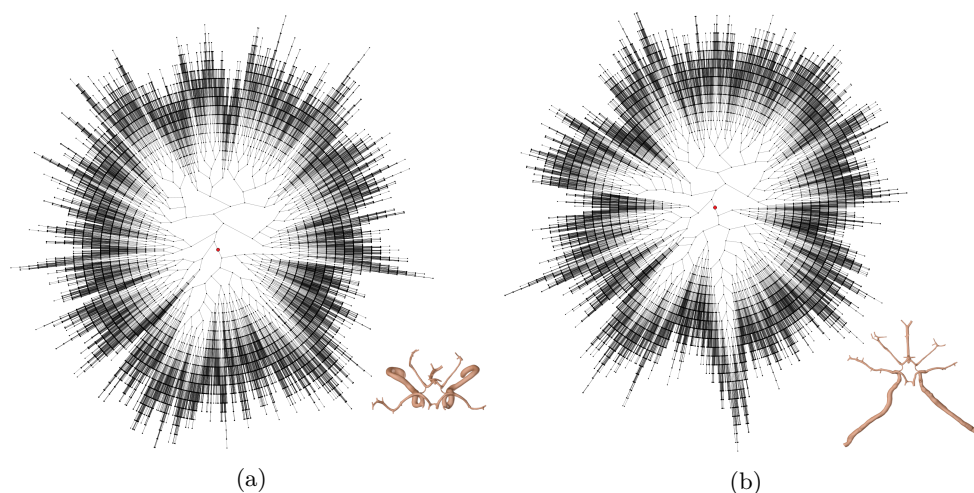
Figure 7.4: Depiction of the resulting k-d trees of the (a) folded and (b) unfolded Circle of Willis surface. Both trees contain 33,653 nodes and have differing maximum depths of (a) 28 and (b) 26, respectively. The images are created with the graph visualization software *Graphviz* using a radial layout presented by Graham Wills [280].

notation point A_i is too slow. This was evaluated by generating 1,000 random points inside the bounding box of the CoW surface with 33,653 vertices.[1] Finding the closest vertex for all points took 2,728 ms, i.e. 2.7 ms per comparison. A more efficient approach is to store all vertices of the surface in a k-d tree. K-d trees are k-dimensional space-partitioning data structures. Every non-leaf node implicitly splits the space in two half-spaces. Here, a common approach is to cycle to each of the three dimensions, e.g. the root splits all nodes at the x-axis, the root's children split at the y-axis, the root's grand children on the z-axis, and the root's grand grand children at the x-axis again etc. Splitting each axis at the median of all vertices results in a balanced tree, but also in long build-up times. Instead, the FAUST prototype uses a simple *median of three* heuristic to find a reasonable split position, resulting in slightly unbalanced trees, faster build-up times and fast enough query times. The time to build-up a k-d tree with 33,653 vertices took about 48.2 ms. Searching for the same 1,000 points as with the naive approach took about 148 ms (theoretically >0.2 ms per query), resulting in one order of magnitude faster look-up times.

Important to note is that the interactive unfolding changes the position of the surface's vertices. Therefore, one k-d tree only represents a specific unfolding state. Hence, an adjustable amount of k-d trees in different unfolding states is generated and stored in a list. The k-d trees for the folded and unfolded state are depicted in Figure 7.4.

---

1 Hardware specifications for the test: Intel(R) Core(TM) i7-7700HQ CPU @ 2.80 GHz, 16 GB RAM, NVIDIA GeForce GTX 1050 Ti

(a)   (b)
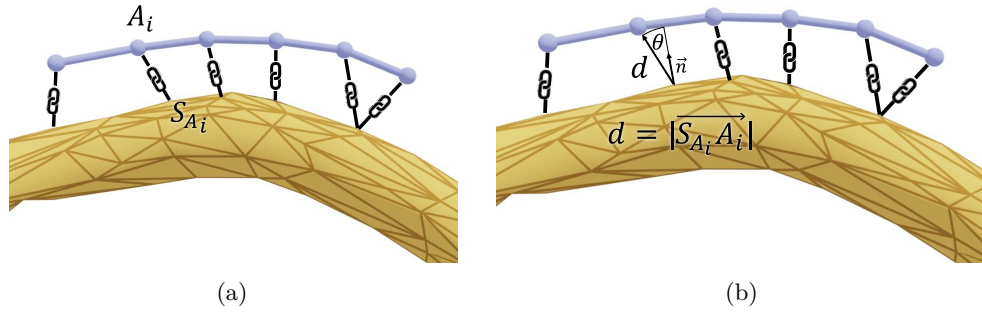
Figure 7.5: For each annotation point A_i the closest surface vertex S_{A_i} is determined by searching in a k-d tree in order to link the annotation to the surface (a). Then, the relative position consisting of a rotation angle θ and the distance d is stored. The annotation point A_i maintains these two properties during unfolding of the Circle of Willis. Images from Saalfeld et al. [230].

If the user starts annotating, the current unfolding state is compared with states in the list. The most similar state together with its k-d tree is selected. Now, a relative description between A_i and S_{A_i} is necessary. First, the distance $d = |\overrightarrow{S_{A_i}A_i}|$ is calculated. Then, the angle between the normal $\vec{n}$ from S_{A_i} and the vector $\vec{v} = \overrightarrow{S_{A_i}A_i}$ is calculated as $\theta = \angle(\vec{n}, \vec{v})$ and stored as a quaternion. During unfolding, it is ensured that this relative description, i.e. the distance d and θ, is maintained. This process is illustrated in Figure 7.5.

7.3.1.2   *Line Simplification and Smoothing*

Since the relative position and rotation of every annotation point has to be updated during unfolding, a low amount of annotation points ensures a high frame rate. To reduce the amount of points, the Douglas-Peucker algorithm [56] from Section 6.5 cannot be used, since the animated unfolding induces non-rigid changes to the annotation shape. Unequally sampled points would result in distorted annotations. Therefore, the points were equidistantly resampled instead. This is realized by discarding all points which exhibit a distance to their neighbors that falls below a certain threshold. If the user moves the stylus very fast, this threshold is exceeded. In this case, additional points are generated between the last and most recent point. This fast and simple resampling method is only problematic if:

1. the threshold is too large and no detailed annotations can be sketched or

2. if the sampling rate is too low during fast sketching.

The threshold was determined empirically by sketching coils, which are the thinnest structures and require the most details. Since the FAUST prototype allows real-time sketching with this threshold, the first problem is addressed. To solve the second problem, a relationship between the sketching speed and the

(a)

(b)
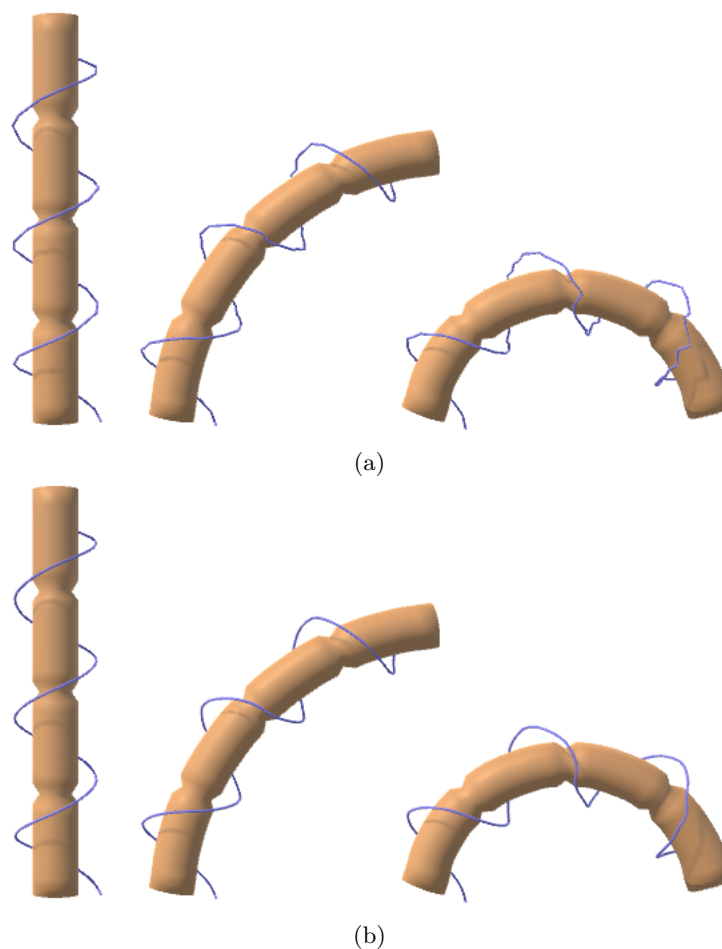
Figure 7.6: The illustration shows a bended tubular shape surrounded by a spiral free-form annotation. The distortion of the annotation during bending is shown for (a) no smoothing and (b) 5-neighborhood Gaussian smoothing. Images from Saalfeld et al. [230].

sample rate has to be found. This was realized by filming fast sketching of several annotations. Here, a covered distance of approximately 19 cm/s was measured. The stylus is tracked with 100 Hz, i.e. a sampling point is created every 1.9 mm. This distance is sufficient, since a physician only draws annotations with low curvature with fast speed such as stents and access paths. For annotations with higher curvature, the physician usually pays particular attention to details and, therefore, sketches with slower speed.

During the unfolding, undesired effects could hamper the visualization of the sketches, i.e. a sketched straight line in the unfolded state could result in a zig-zag line in the folded state. To weaken this effect, visual representation of the annotation points is smoothed with 5-neighborhood Gaussian smoothing (see Figure 7.6).

7.3
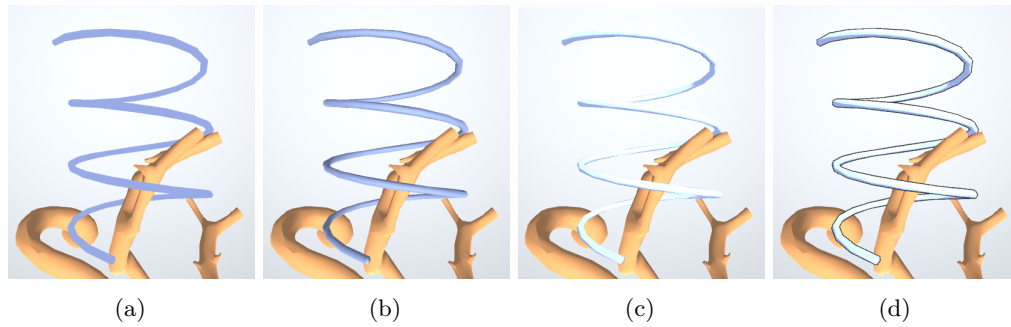
Figure 7.7: An overview of the different improvements to the sketch rendering techniques implemented in the FAUST prototype: (a) shows a monochrome rendering, (b) a Phong Shading, (c) a cel-shading and (d) a cel-shading with a silhouette. Images from Saalfeld et al. [230].

7.3.2 *Types & Visualization of Annotations*

The user can create three different types of annotations that are illustrated in Figure 7.8:

- generic annotations,

- stents, and

- coils.

This differentiation is chosen based on typical tasks in treatment planning. For heterogeneous tasks, such as highlighting important regions and illustrating access paths, the generic annotations are a flexible tool to sketch different configurations. Stenting and stent-assisted coiling are the most common treatment options.

For all types, a procedurally generated cylindrical surface is created along the sketched line in real-time. The surface allows to support depth perception by applying shading techniques. Furthermore, the radius of the cylindrical surface can be adjusted. Thus, the user can sketch stents with varying diameters for different vessels or thin coils inside an aneurysm. An optional aiding function is implemented that constrains annotations to lay on the planning model's surface. This helps to, e.g. illustrate an access path along a vessel. For the *generic annotations*, the user can choose between four colors. Different rendering techniques were tested (see Figure 7.7). Here, an illustrative cel-shading [161] was chosen, as it supports the visual differentiation between the CoW and annotations but simultaneously conveys shading information. A silhouette further improves the contrast between the vessel structure and background.

To annotate the vascular structure with *stents*, a grid texture is applied to the cylindrical surface. By using the alpha channel of the texture, the user is able to look through the struts, which results in a realistic stent illustration. Here, x
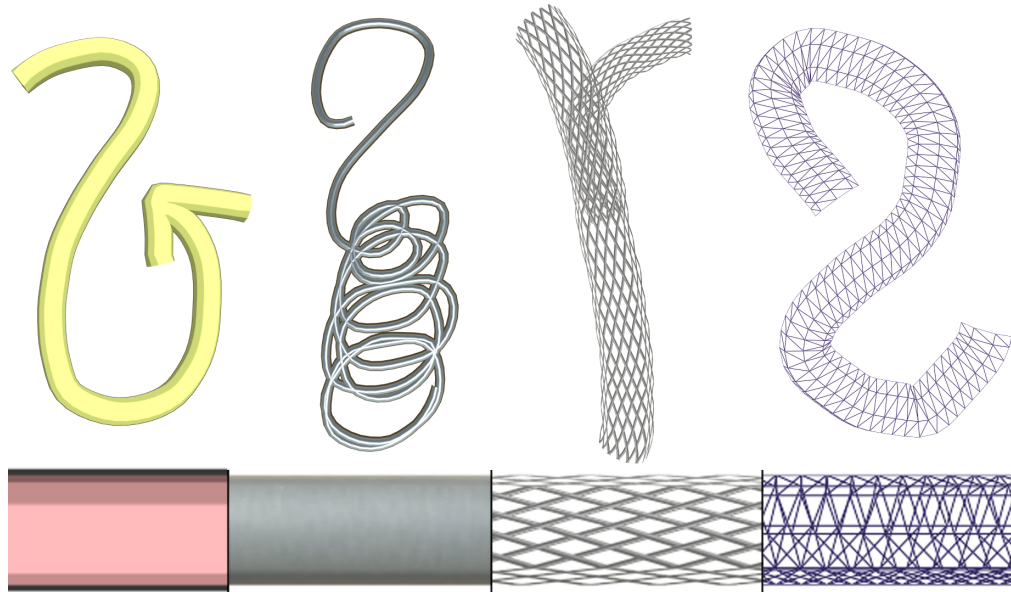
Figure 7.8: An overview of different annotation types from left to right: generic yellow annotation, coil, stent. The last image shows the wireframe of the procedurally generated cylinder. Images from Saalfeld et al. [230].

and y texture coordinates are required to apply a texture to the procedurally generated surface. These are calculated during sketching by increasing the x-coordinate along the sketched path. The y-coordinate is mapped around the 360 degrees of the cylinder. For *coils*, a brushed metal texture is applied with the same approach. Additionally, metal shading properties are used in the shader.

7.3.3 *Animated Unfolding*

For the animation of the unfolding CoW, a slider widget is used (see Figure 7.9). The value of the slider is mapped to 0 and 1, representing the two states (0: original and folded, 1: unfolded, recall Section 7.2.2). If the slider value is changed, the position and orientation of every skeleton's bone is interpolated to this value, resulting in a transforming CoW. Simultaneously, the annotations are transformed accordingly. The value is continuously approached over time to guarantee a smooth transition without abrupt changes of the unfolding state.

7.4 VISUALIZATION OF THE VASCULAR STRUCTURES

The CoW is visualized equally to the approach described in the previous Section 6.4. Thus, it is rendered with physically-based rendering and provided texture and normal maps. To allow the users to sketch inside the CoW, they can choose between two visualizations: a fully opaque one and a shading technique,

7.4
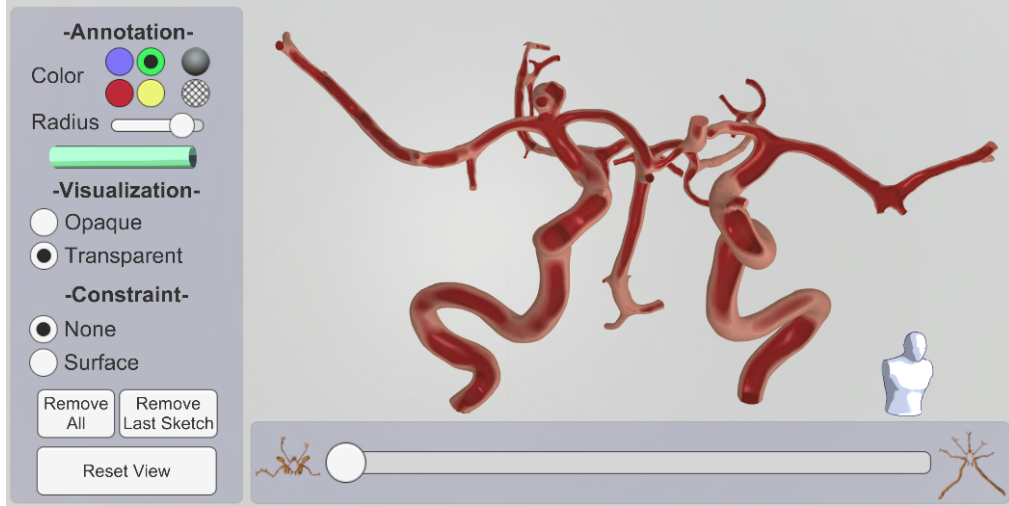
Figure 7.9: The image depicts the GUI of the FAUST prototype. On the left, the physician can choose between different annotation and visualization types, constrain the sketches to the surface and reset the view. The interactive unfolding is realized with the slider widget at the bottom. The torso at the right bottom illustrates the current orientation of the Circle of Willis. Images from Saalfeld et al. [230].

which reveals the inside of the vessel. In Figure 7.10, the two visualization techniques with and without texture and normal mapping are depicted.

7.5 TRANSLATION & ROTATION

Since precise manipulation is important to add annotations in a meaningful way, translation and rotation are separated in the FAUST prototype (see Section 2.1.2.3). Either action is activated by pressing a dedicated stylus button (see Figure 7.11). Translation is realized with a direct approach, where the position of the rod tip T is used to calculate the stylus' movement with $\vec{m} = \overrightarrow{T_{start}T_{end}}$. The CoW is then translated by $\vec{m}$ (see Figure 7.12a). For rotation, the Arcball-3D technique is used, because it was preferred by almost all participants in the study of Katzakis et al. [126] and it is suitable for small, thin objects, such as the vessels of the CoW (see Section 2.1.2.2). Here, the structure is surrounded by an invisible sphere. The intersection point P_i of the ray and the sphere surface is used to calculate the rotation angle α. If the rotation button is pressed, the vector $\vec{v_1}$ is determined with the sphere center S_c as $\vec{v_1} = \overrightarrow{S_c P_i}$. During movement of the stylus, the new vector $\vec{v_2} = \overrightarrow{S_c P_{iNew}}$ is calculated. The rotation axis $\vec{R}$ is extracted as $\vec{v_1} \times \vec{v_2}$ and the rotation angle α is defined as $\alpha = \angle \vec{v_1} \vec{v_2}$ (see Figure 7.12b).
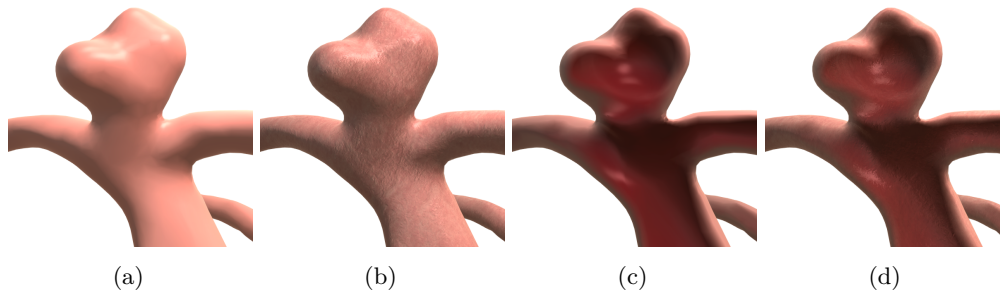
Figure 7.10: The physician can choose between an opaque (a, b) and a semi-transparent (c, d) visualization of the vascular structure. To improve the visualization, a texture and normal map is applied to the surface via tri-planar texture mapping (b, d). Images from Saalfeld et al. [230].
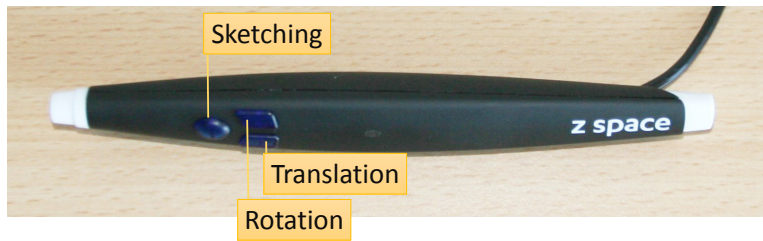
Figure 7.11: The zSpace's stylus with the assigned functions to the different buttons. Image from Saalfeld et al. [230].
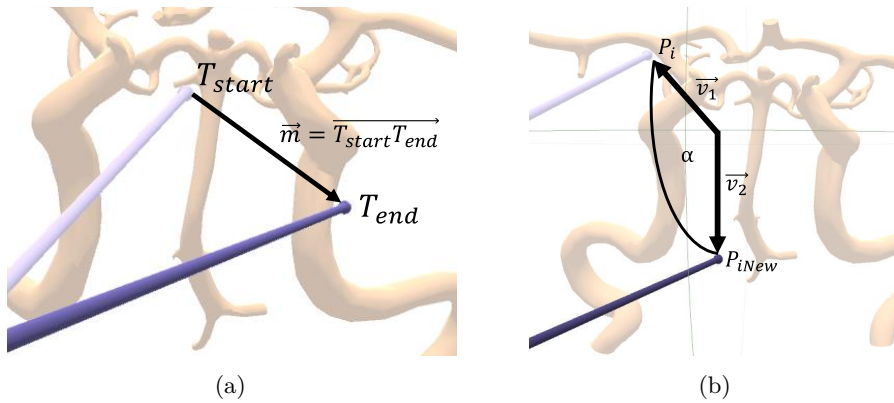
Figure 7.12: The translation is realized by moving the 3D object about the movement $\vec{m}$ of the ray tip (a). For rotation, the Arcball 3D technique [126] is used, where the rotation is derived from the ray intersection with an invisible bounding sphere (b). Images from Saalfeld et al. [230].

7.6 GRAPHICAL USER INTERFACE

The GUI of the FAUST prototype is depicted in Figure 7.9. The user can choose one of six different annotation visualizations and is able to adjust its diameter with a slider. Furthermore, the visualization of the CoW can be changed. Beneath, the possibility to constrain the sketch to lie on the surface can be activated. Additionally, the user can delete the last sketch and all sketches, respectively. At the bottom of the prototype there is a slider widget that allows unfolding the CoW.

To support the physician maintaining an overview of the CoW's orientation, a torso with synchronized orientation is visualized in the right bottom corner. Additionally, the physician can reset the view by pressing a button that restores the initial frontal view.

7.7 USING THE FAUST PROTOTYPE FOR A Y-STENTING PROCEDURE

A possible sequence to plan the Y-stenting procedure with the FAUST prototype is illustrated in Figure 7.13. The physician starts by investigating the vascular structures and highlighting pathologies with generic annotations (see Figure 7.13a). Then, the access paths have to be defined. Here, a completely unfolded CoW allows an easier 3D sketching. Additionally, the annotations are constrained to lie on the surface (see Figure 7.13b). Now, the Y-stent is placed to treat the aneurysm with a large neck size. Two stents have to be placed with different diameters (see Figure 7.13c). Finally, the physician plans to reduce the aneurysm inflow by sketching thin coils inside the aneurysm to illustrate stent-assisted coiling (see Figure 7.13d).

7.8 EVALUATION

The user evaluation was realized in two steps:

1. Computer scientists with advanced knowledge on vascular systems used the prototype to sketch different annotations.

2. A demo session and unstructured interview was conducted with an experienced neuroradiologist.

Additionally, the performance was evaluated by measuring the calculation time to attach annotations as well as the frame rate drop caused by adding annotations.

7.8.1 *User Study*

In the following, the user study and its results are presented.

(a)

(b)

(c)

(d)
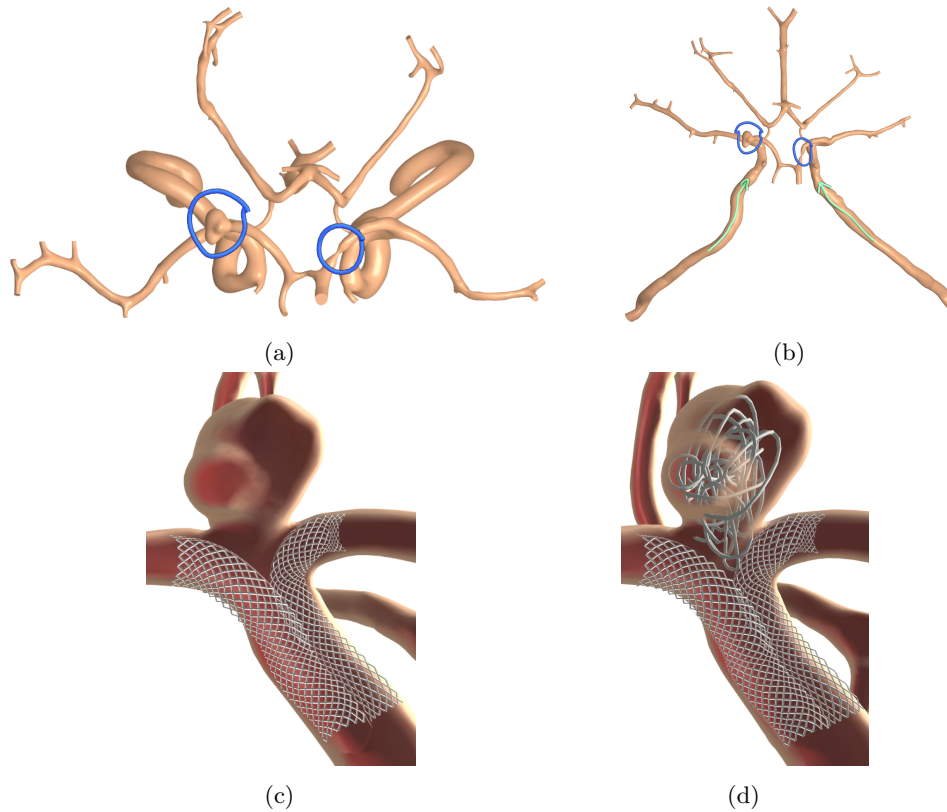
Figure 7.13: The images illustrate a possible treatment planning of the Y-stenting procedure. In (a) pathologies (an aneurysm and stenosis) of the Circle of Willis are highlighted with generic annotations. The unfolded Circle of Willis is depicted in (b). Two possible access paths are sketched on the vascular surface. In (c), the transparent visualization is used to allow the physician to sketch inside. A Y-stent is sketched in the bifurcating arteries under the aneurysm. The final step of treatment planning, i.e. placing the coil inside the aneurysm, is shown in (d). Images from Saalfeld et al. [230].

7.8.1.1 *Goals*

The goal of the evaluation was to assess the usability and user comfort in using the 3D annotation sketching. For this purpose, general questions were stated. Furthermore, the benefit in using the immersive zSpace should be quantified. Therefore, the *presence* questionnaire from Witmer and Singer [281] was used, which quantifies aspects such as realism and the quality of the interface. Some questions did not match the prototype, e.g. regarding sound or haptic feedback. These were left out. Both questionnaires used a 7-point Likert scale $(---,--,-,\circ,+,++,+++)$.

Table 7.1: Years of participants' experience in domains related to the prototype ($\bar{x}$ − mean, s − standard deviation).

	min	max	$\bar{x}$	s
Exp. with Medical Applications	1	12	3.9	3.5
Exp. with Scientific Visualization	0	12	4.0	3.6
Exp. with 3DUI	0	3	1.2	1.0

7.8.1.2 *Tasks*

The participants' tasks were used to simulate the treatment planning for different pathologies. First, they were asked to treat the stenosis by defining an access path and sketch a stent with appropriate size along the stenosis. After that, the more advanced treatment planning for Y-stenting of the aneurysm of the CoW should be performed. This was divided in several sub-tasks:

- unfold the CoW,

- sketch an access path along the internal carotid artery,

- fold the CoW back to its original shape,

- sketch two stents that touch each other into the supporting vessels of the aneurysm, and

- sketch a coil inside the aneurysm to fill it.

7.8.1.3 *Participants*

Nine participants took part in the study (one female, eight males) with an age between 26 and 38 ($\bar{x} = 28.8$). No one had a medical condition leading to problems perceiving stereoscopic content. All participants were computer scientists with a background in medical visualization. Therefore, they had basic medical knowledge on the human vascular system, most common pathologies (aneurysms and stenoses) and treatment options (coiling, clipping and stenting). However, they were unfamiliar with the advanced Y-stenting procedure and the particularities of the CoW (see Section 5.1). The experience of the participants in different domains is represented in Table 7.1.

7.8.1.4 *Procedure*

After assuring that each participant was familiar with basics regarding the human vascular system, the dataset was explained in more detail by:

- explaining the particularities of the CoW,

- highlighting the stenosis and aneurysm on the CoW model, and

- describing the Y-stenting procedure to treat cerebral aneurysms.

After this, each participant was introduced to the FAUST prototype, including a training of interaction techniques to translate, rotate and unfold the CoW followed by an explanation of the 3D sketching. After the training session, the participants were asked to solve the tasks, i.e. use the prototype to plan different treatment options. During the training and treatment planning, the participants were asked to comment their actions (think aloud method [124]). After the demo session, a questionnaire was handed out.

7.8.1.5 *Results – Observations & Think Aloud*

During the training session, most participants stated that it is unfamiliar to sketch in 3D space. The reason for this is presumably that there is no comparable real world metaphor for 3D sketching. Five participants commented positively on the representation of the sketches. They stated that the shading supports shape perception and is visually pleasing. Further positive aspects mentioned by the participants are the realistic appearance of the CoW due to shading and fish tank VR as well as the intuitive control of the slider widget.

Two participants suggested to show a projection of the shadow of the virtual stylus rod. This could help avoid the problems of the first misplaced annotations. Another proposition by one participant was the addition of templates for frequently sketched objects. For example a stent template can be used, where the user sets two points inside the vessel and the stent is created automatically.

7.8.1.6 *Results – Presence Questionnaire*

Although the participants had very little experience with 3DUIs ($\bar{x} = 1.2$ years) compared to medical applications ($\bar{x} = 3.9$ years), the rating of the interaction techniques was overall positive. This is in particular relevant since a similar experience ratio can be expected by physicians. The simplicity and plausibility of the unfolding was rated with $md = 3$. The question "how naturally the sketching is" was rated with $md = 2$. This result is promising, since 3D sketching bears the risk to be complicated due to the introduced third dimension. For the presence questionnaire, the questions are combined into the pre-defined categories:

- PA – Possibility to Act,

- R – Realism,

- PE – Possibility to Examine,

- QI – Quality of Interface, and

- SE – Self-evaluation of Performance.
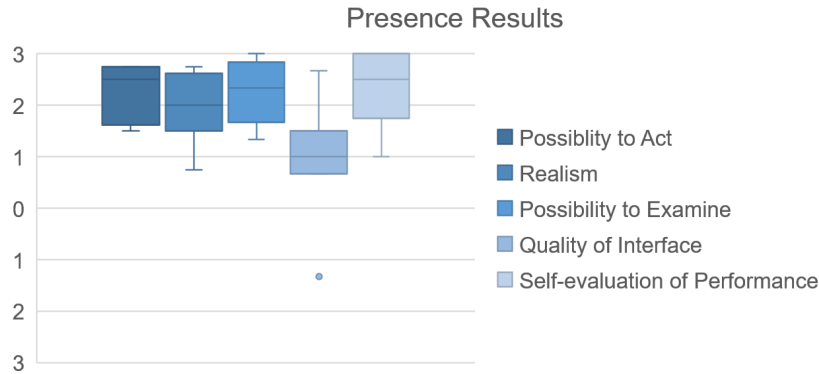
Figure 7.14: The boxplots summarize the results for different categories of the adapted presence questionnaire [281]. All categories were positively rated by the majority of the participants. The whiskers show the data points that are closest to the limit of 1.5 times the interquartile range. The dot in the category *Quality of Interface* represents an outlier (rating < 1.5 times the interquartile range).

All categories were positively rated, which supports the intention to use the zS-pace to make the representation of the CoW more realistic and tangible. The lowest result was achieved in the category QI ($md = 1$). The participants had difficulties to locate the virtual rod tip during the first annotations, which resulted in misplaced annotations. The highest rating was achieved in the category SE ($md = 2.5$), i.e. the participants had the impression that their performance was good. All results are summarized in Figure 7.14.

7.8.2 *Unstructured Interview*

The unstructured interview was performed with a neuroradiologist with more than 20 years of professional experience. The setup of the demo session and interview is similar to the user study, except that the medical introduction was left out.

The physician highlighted several benefits:

- The sketching works well to describe access paths. The unfolded view supports this even more, because the paths could be sketched more easily.

- The unfolded state gives a spatial overview of the vascular structure and transitions, which is more difficult to comprehend in 2D displays.

- The prototype allows for an improved understanding of anatomical structures, e.g. the size of the aneurysm neck or the location of small branching vessels. This helps during interventions, where the angiographic 2D images lead to occlusion.

- For Y-stenting, it is necessary that both stents end at the same position. Here, the original folded structure could be used to mark this position. The following unfolding supports the estimation of the necessary length of the stents.

Furthermore, the neuroradiologist suggested additional features to improve the prototype and pointed out drawbacks. For example, a tool to allow the measurement of vessel diameters would be helpful. The combination of several sketches to realize complex spatial structures is difficult to achieve. The neuroradiologist suggested a feature which allows to snap on old sketches or merge points that are close to each other.

7.8.3 *Performance*

For the performance evaluation, the same desktop computer was used as in the evaluation. It is equipped with an Intel Core i7-2600K 3.7 GHz 16 GB RAM and an Nvidia Quadro 4000. The most calculation-intensive steps in the FAUST prototype are the attachment of annotations to the CoW and their non-rigid transformations during unfolding. Each annotation consists of a sequence of connected control points. The number of these points is essential for the performance. However, statements regarding their quantity without considering the resulting annotations would be meaningless. Therefore, several annotations were sketched and the resulting control points were counted. For sketched stents, generic annotations and coils, in average 30, 40 and 250 control points are necessary. Thus, for one annotation approximately $(30 + 40 + 250)/3 = 107$ control points are used.

To quantify the performance, the time was logged that is necessary to attach 107 control points on the CoW planning model with 33,653 vertices and 65,514 triangles. This took on average 151 ms. Since the attachment is performed after the physician finishes sketching, this time is almost unnoticeable. Additionally, the frame rate was analyzed during user interaction and CoW unfolding. Initially, the FAUST prototype runs with 30 FPS (per eye). The frame rate was measured after adding control points in steps of 500. The performance drop was around 1 FPS every 500 control points, i.e. at 2,000 added control points, 25 FPS and with 4,500 control points, 20 FPS were achieved.

The prototype is impractical to use below 15 FPS, which happens if more than 7,000 control points are added. Using the approximated control point number of an annotation, this means $7,000/107 = 65$ annotations could be added until the prototype is unusable. The interview and session with the neuroradiologist showed that not even one third of 65 annotations are used for one treatment planning session. Thus, the FAUST prototype runs at usable frame rates.

7.9 INTEGRATION INTO CLINICAL PRACTICE

To introduce the FAUST prototype into clinical practice, several aspects have to be considered. The most important ones are:

1. the acquisition costs,

2. available space,

3. familiarization to the 3D display, glasses and ray-based interaction techniques as well as

4. the time pressure in clinical routine.

These issues were discussed with a neuroradiologist. The acquisition costs of the zSpace are moderate compared to other hardware in interventional radiology. If available space is problematic, the zSpace is usable as a normal 2D display and, thus, can replace the existing one used for treatment planning. The polarized glasses are the most invasive component, since they darken the view of the physician. This would be problematic during interventions; for planning alone, it is acceptable. Regarding the familiarization aspect, innovations in interventional radiology are common. Therefore, neuroradiologists are used to invest learning time for new technologies. The fundamental precondition for this is that the introduced technology is highly beneficial for the patient, e.g. regarding risk minimization during interventions. The same argument applies for the time pressure during clinical routine. According to the physician, patient safety is more important than short planning times.

Considering the general possibility to fit in additional planning, this is possible for either elected or critical cases. For elective cases, where sufficient planning time is available, the treatment usually starts with medication for several days before an intervention. In this period, the FAUST prototype can be used for treatment planning. Even for critical cases, where an aneurysm is ruptured, it is not unusual to observe the patient overnight and start with treatment the next day. Even in this period, the usage of the prototype is possible.

7.10 CONCLUSION & DISCUSSION

Complex structures, such as patient-individual vessel trees with pathologies, require an excellent knowledge of the spatial variations and the 3D extent. At the example of the CoW with two pathologies, ways to support physicians in treatment planning were investigated. The FAUST prototype allows to freely create 3D sketches and enables physicians to annotate structures with a wide variety of treatment options. With the interactive unfolding, the whole CoW can be investigated at once and occlusions can be resolved. Additionally, vessel thickness variations, which often occur in the cerebral vessel system, can be analyzed more

easily. Conventional imaging cannot depict the same information, e.g. digital angiography yields a projection image with superimpositions, and tomographic image data is not sufficient for assessing bended vessel structures.

The assessment of the interaction techniques, usability and presence of the prototype yield positive results. The interview with the neuroradiologist indicates that the FAUST prototype improves the spatial overview of vascular structures and supports the understanding of anatomical structures compared to angiographic 2D images. Regarding the performance evaluation, real-time frame rates are achieved for the attachment of annotations and during interaction with a high number of annotations. A general statement of the interviewed neuroradiologist was that "everything that supports the understanding of the anatomy and pathology is helpful in treatment planning". The user study shows that the prototype can support this understanding. However, the benefit has to be tested in a realistic clinical scenario including its time pressure.

The FAUST prototype was evaluated with cerebral structures and pathologies, but it can be adapted to a wide range of complex anatomical structures, including the treatment of vascular diseases in general or an unfolding colon. Here, other dynamic data can be used, such as time-varying data of a beating heart. For future work, the usage of the prototype in the area of patient documentation should be investigated. The possibility to preserve a wide variety of annotations together with a 3D representation of the structure could greatly improve the documentation.

8

CONCLUSION

THIS thesis presented 3DUIs to support several medical domains, i.e. interventional radiology, patient education, medical teaching and treatment planning. This comprised interaction techniques as well as the usage of input and output devices. Furthermore, comprehensive guidelines were given to quantitatively evaluate interactive medical visualizations targeting computer scientists and engineers. These guidelines comprise a distinction of evaluation approaches and appropriate statistical tests for a variety of collected data.

8.1 FREEHAND GESTURES

For interventional radiology support, freehand gestures were presented. These allow physicians to control radiographic workstation software in a touchless manner, which eventually allows them to inspect patient's radiographic data in a sterile way. Overall, two gesture sets were introduced. The first supports basic tasks by tackling the exploration of 2D and 3D data. On this basis, an improved second gesture set was introduced to solve basic and more complex tasks, such as creating measurements on the medical data. Furthermore, the second developed prototype integrated functions to facilitate executing and memorizing the gestures.

To assess the usefulness and performance of both gesture sets, user studies were conducted in which the freehand gestures were compared to established interaction methods, i.e. touch as well as mouse and keyboard control. Unfortunately, both studies showed that the freehand gestures were inferior. This was shown for task completion time and accuracy as well as for intuitiveness and usability. The first study indicated that for complex spatial tasks freehand gestures can compete with established interaction techniques. However, the second study could not confirm such a correlation.

Although both studies have shown that the used freehand gestures were inferior to established techniques, these results have to be weighted against the strongest advantage of touchless interaction. Ultimately, freehand gesture interaction ensures asepsis and reduces the risk of infection. While this argument can compensate for aspects such as longer task completion times and a reduced

usability, the inferior results for accuracy are not acceptable. Here, the deviations in measurement results can lead to a different treatment strategy with fatal consequences. Even the algorithm support to improve the accuracy could not change this.

A possibility for improvement and an interesting research direction for future work would be using semi-automatic measurements to compensate for the inaccuracies of freehand gestures. During pointing on structures, the area around the pointer position could be analyzed. From there, interesting features can be detected automatically, e.g. via gradient-based approaches. Now, if a structure is found, important measurements can be calculated and visualized automatically, e.g. showing the volume of the structure of interest and calculating the shortest distances to other structures.

8.2 SKETCHING

The sketching chapters presented the benefits of sketching in the medical domains of patient education, teaching, and treatment planning. Here, approaches to create vascular structures and annotations were presented.

8.2.1 *Patient Education*

The visualization of vascular structures, treatment options and blood flow varied depending on the particular medical domain. For patient education, an abstract and simplified visualization was chosen, since the priority is to strengthen the patient's understanding of diseases and treatment options. Thus, an approach to sketch 2D vessels, pathologies, treatment options and blood flow was presented. These sketches can be drawn on graphic tablets and interactive whiteboards. The developed prototype supports physicians to explain different treatment strategies for vascular pathologies to patients. The simplified 2D representation allows the patient to follow explanations more easily.

The user study and interview with a physician showed the usability of the prototype and advantages compared to hand-drawn sketches. The sketching resulted in a clearer image that is easier to understand. Furthermore, the depiction of real-time blood allows to convey the impact of different treatment strategies that cannot be shown with hand-drawn sketches.

8.2.2 *Medical Education*

In medical education the requirements on the visualization are different. In contrast to patient education, an abstract visualization of vascular structures can lead to misconceptions. The spatial properties and courses of vessels are an important aspect in anatomy education and can be better conveyed with a realistic

visualization. Therefore, anatomy and pathology education was supported by allowing the creation of 3D vessels with integrated blood flow. Additionally, the zSpace was used to allow an easier 3D sketching and support the depth perception of the rendered 3D structures. This provides anatomy educators with a novel tool to create and explain complex spatial relationships of interlinked vascular structures and blood flow behavior.

The conducted user study and interview with an anatomist could show the usability and usefulness of the developed prototype. Interestingly, the anatomist was not able to reproduce the spatial course of vascular structures immediately. While reproducing anatomical structures on blackboards is an acquired skill of many anatomists and recognizing the spatial course on a cadaver is also a common task, there is currently no need to replicate 3D structures in 3D. Thus, a special preparation is necessary according to the anatomist. In future investigations, it would be interesting to analyze if this form of special preparation and the aimed investigation of spatial properties of anatomical structures is beneficial for anatomists or physicians.

8.2.3 *Treatment Planning*

For treatment planning, an abstract and a realistic visualization can be useful. Physicians have a profound understanding of the human anatomy, including spatial relationships and courses of vessels. Therefore, they are able to transfer information of an abstract visualization to the real morphology. However, realistic visualizations are able to depict pathologies more accurate and they prevent to loose information due to an introduced abstraction. This helps the physician in mapping previous experience from interventions to the current case and supports to prepare a treatment strategy. Here, particular attention is required due to the amount of uncertainty that was introduced in the process from the reconstruction of image data to the final 3D planning model. A realistic visualization creates the impression of accuracy, which can be critical if the underlying medical image data was, e.g. noisy. Still, the treatment planning was again facilitated with the zSpace to allow physicians explore and analyze 3D vascular structures and sketch free-form annotations on 3D planning models. This enables the physician to illustrate various treatment options. The user study and the interview showed the general applicability of the prototype. The participants were able to create 3D sketches according to their expectations. The physician stated that an introduction of the zSpace in the treatment planning process is possible, even if this leads to longer treatment planning times. However, a verification of the improved treatment planning is necessary before that. The easy manipulation of the 3D planning model and the 3D sketching of arbitrary annotations would also be beneficial for documentation, which is a possible application scenario of the prototype in the future.

8.3

8.3   FREEHAND GESTURES VS. SKETCHING

Inspecting the interaction techniques of freehand gestures and sketching in this thesis allows to draw a conclusion that would not be possible by inspecting just one research area. For example, if this thesis would have focused on sterile input for interventional support alone, an optimistic conclusion would be that the usage of this natural and intuitive interaction technique would be beneficial for other fields such as patient education, medical teaching, and treatment planning as well. Although this might be true to a limited extent, freehand input lacks the reliable and accurate recognition of gestures, which can be frustrating in actual use. This downside is arguably acceptable for interventional support due to the achieved sterility. For the other inspected medical areas, sterility is not necessary. Therefore, an interaction technique based on a reliable spatial input device also allows natural interaction and easy object manipulation. This form of input is possible with the zSpace and 3D sketching, which is a more adequate device for the areas of medical education and treatment planning.

8.4   THE ZSPACE

The usage of the zSpace is beneficial, because it allows to get immersed, supports the spatial understanding due to the additional depth cues and 3D interaction, and is mildly intrusive, since only glasses have to be worn. However, it limits the available space in which vessels and annotations can be created and it is only effectively usable by one person. Therefore, transferring the sketching techniques into a fully immersive environment is an interesting future research topic. This would allow a collaborative solution where, e.g. one educator and several students could simultaneously sketch and annotate medical structures. However, a fully immersive environment would be more intrusive. By using, e.g. a HWD, teachers and physicians would be excluded from their surroundings. Here, it is more difficult for teachers to overview the students or for a physician to evaluate the emotional state of a patient.

BIBLIOGRAPHY

1. Abildgaard, A., Witwit, A. K., Karlsen, J. S., Jacobsen, E. A., Tennøe, B., Ringstad, G. & Due-Tønnessen, P. An autostereoscopic 3D display can improve visualization of 3D models from intracranial MR angiography. *International Journal of Computer Assisted Radiology and Surgery (IJCARS)* **5,** 549–54 (2010).

2. Agrawala, M., Beers, A. C., McDowall, I., Fröhlich, B., Bolas, M. & Hanrahan, P. *The Two-user Responsive Workbench: Support for Collaboration Through Individual Views of a Shared Space* in *Proc. of SIGGRAPH* (1997), 327–332.

3. Alexe, A., Gaildrat, V. & Barthe, L. *Interactive Modelling from Sketches Using Spherical Implicit Functions* in *Proc. of Computer Graphics, Virtual Reality, Visualisation and Interaction in Africa* (2004), 25–34.

4. Ali, K., Hartmann, K. & Strothotte, T. Label Layout for Interactive 3D Illustrations. *Journal of the WSCG* **13,** 1–8 (2005).

5. Andrews, K. *Evaluation Comes in Many Guises* in *Workshop on BEyond time and errors: novel evaLuation methods for Information Visualization* (2008).

6. Aras, R., Shen, Y. & Noor, A. Quantitative assessment of the effectiveness of using display techniques with a haptic device for manipulating 3D objects in virtual environments. *Advances in Engineering Software* **76,** 43–47 (2014).

7. Arora, R., Kazi, R. H., Anderson, F., Grossman, T., Singh, K. & Fitzmaurice, G. *Experimental Evaluation of Sketching on Surfaces in VR* in *Proc. of ACM SIGCHI conference on Human factors in computing systems (CHI)* (2017), 5643–5654.

8. Arthur, K. W., Booth, K. S. & Ware, C. Evaluating 3D Task Performance for Fish Tank Virtual Worlds. *ACM Trans. Inf. Syst.* **11,** 239–265 (1993).

9. Ascoli, G. A., Donohue, D. E. & Halavi, M. NeuroMorpho.Org: a central resource for neuronal morphologies. *J. Neurosci.* **27,** 9247–9251 (2007).

10. Assenmacher, I., Hentschel, B., Ni, C., Kuhlen, T. & Bischof, C. *Interactive Data Annotation in Virtual Environments* in *Proc. of Eurographics Conference on Virtual Environments* (2006), 119–126.

11. Au, O. K.-C., Tai, C.-L., Chu, H.-K., Cohen-Or, D. & Lee, T.-Y. Skeleton Extraction by Mesh Contraction. *ACM Trans. Graph.* **27,** 44:1–44:10 (2008).

12. Bade, R., Ritter, F. & Preim, B. *Usability Comparison of Mouse-Based Interaction Techniques for Predictable 3d Rotation* in *Proc. of Smart Graphics* (2005), 138–150.

13. Baer, A., Gasteiger, R., Cunningham, D. & Preim., B. Perceptual evaluation of ghosted view techniques for the exploration of vascular structures and embedded flow. *Computer Graphics Forum (CGF)* **30,** 811–820 (2011).

14. Baer, A. *Perception Guided Evaluation of 3D Medical Visualizations* PhD thesis (University of Magdeburg, 2015).

15. Baer, A., Hübler, A., **Saalfeld**, **P.**, Cunningham, D. & Preim, B. *A Comparative User Study of a 2D and an Autostereoscopic 3D Display for a Tympanoplastic Surgery* in *Proc. of Eurographics Workshop on Visual Computing in Biology and Medicine (VCBM)* (2014), 181–190.

16. Baer, A., Lawonn, K., **Saalfeld**, **P.** & Preim, B. *Statistical Analysis of a Qualitative Evaluation on Feature Lines* in *Proc. of Workshop Bildverarbeitung für die Medizin* (2015), 71–76.

17. Bangor, A., Kortum, P. & Miller, J. Determining What Individual SUS Scores Mean: Adding an Adjective Rating Scale. *Usability Studies* **4,** 114–123 (2009).

18. Banks, M. & Cohen, E. *Real Time Spline Curves from Interactively Sketched Data* in *Proc. of ACM Symposium on Interactive 3D Graphics* (1990), 99–107.

19. Baran, I. & Popović, J. Automatic Rigging and Animation of 3D Characters. *ACM Trans. Graph.* **26** (2007).

20. Bartz, D., Cunningham, D., Fischer, J. & Wallraven, C. The role of perception for computer graphics. *Eurographics state-of-the-art-reports,* 65–86 (2008).

21. Bederson, J. B., Connolly, E. S., Batjer, H. H., Dacey, R. G., Dion, J. E., Diringer, M. N., Duldner, J. E., Harbaugh, R. E., Patel, A. B. & Rosenwasser, R. H. Guidelines for the Management of Aneurysmal Subarachnoid Hemorrhage: A Statement for Healthcare Professionals From a Special Writing Group of the Stroke Council, American Heart Association. *Stroke* **40,** 994–1025 (2009).

22. Biasutto, S. N., Caussa, L. I. & Criado del Rio, L. E. Teaching anatomy: cadavers vs. computers? *Ann. Anat.* **188,** 187–190 (2006).

23. Bizzotto, N., Costanzo, A., Bizzotto, L., Regis, D., Sandri, A. & Magnan, B. Leap Motion Gesture Control With OsiriX in the Operating Room to Control Imaging. *Surgical Innovation* **21,** 655–656 (2014).

24. Blinn, J. F. A generalization of algebraic surface drawing. *ACM Transactions on Graphics* **1,** 235–256 (1982).

25. Bloomenthal, J. & Shoemake, K. Convolution Surfaces. *Proc. of SIGGRAPH* **25,** 251–256 (1991).

26. Borgelt, C., Yang, X., Nogales-Cadenas, R., Carmona-Saez, P. & Pascual-Montano, A. *Finding Closed Frequent Item Sets by Intersecting Transactions* in *Proc. of International Conference on Extending Database Technology* (2011), 367–376.

27. Borkin, M., Gajos, K., Peters, A., Mitsouras, D., Melchionna, S., Rybicki, F., Feldman, C. & Pfister, H. Evaluation of Artery Visualizations for Heart Disease Diagnosis. *IEEE Transactions of Visualization and Computer Graphics (TVCG)* **17,** 2479–2488 (2011).

28. Borrelli, M., Leung, B., Morgan, M., Saxena, S. & Hunter, A. Should drawing be incorporated into the teaching of anatomy? *Journal of Contemporary Medical Education* **6,** 34–48 (2 2018).

29. Bouzit, M., Burdea, G., Popescu, G. & Boian, R. The Rutgers Master II-new design force-feedback glove. *IEEE/ASME Transactions on Mechatronics* **7,** 256–263 (2002).

30. Bowman, D. A. & Hodges, L. F. *An Evaluation of Techniques for Grabbing and Manipulating Remote Objects in Immersive Virtual Environments* in *Proc. of Interactive 3D Graphics* (1997), 35–ff.

31. Bowman, D. A., Kruijff, E., LaViola, J. J. & Poupyrev, I. *3D User Interfaces: Theory and Practice* (Addison Wesley Longman Publishing Co., Inc., Redwood City, CA, USA, 2004).

32. Brenton, H., Hernandez, J., Bello, F., Strutton, P., Purkayastha, S., Firth, T. & Darzi, A. Using Multimedia and Web3D to Enhance Anatomy Teaching. *Comput. Educ.* **49,** 32–53 (2007).

33. Bridson, R. *Fluid Simulation for Computer Graphics* (A K Peters/CRC Press, 2008).

34. Brooke, J. in *Usability Evaluation in Industry* (Taylor and Francis, 1996).

35. Bruckner, S. & Gröller, E. *VolumeShop: An Interactive System for Direct Volume Illustration* in *Proc. of Visualization* (2005), 671–678.

36. Butcher, J. C. A History of Runge-Kutta Methods. *Appl. Numer. Math.* **20,** 247–260 (1996).

37. Cai, W., Feng, D. & Fulton, R. Web-based digital medical images. *IEEE Computer Graphics and Applications* **21,** 44–47 (2001).

38. Card, S. K., Mackinlay, J. D. & Robertson, G. G. *The Design Space of Input Devices* in *Proc. of SIGCHI Conference on Human Factors in Computing Systems* (1990), 117–124.

39. Carpendale, S. in *Information Visualization: Human-Centered Issues and Perspectives* (eds Kerren, A., Stasko, J. T., Fekete, J.-D. & North, C.) 19–45 (Springer Berlin Heidelberg, Berlin, Heidelberg, 2008).

40. Chang, L. Y., Pollard, N. S., Mitchell, T. M. & Xing, E. P. *Feature selection for grasp recognition from optical markers* in *IEEE/RSJ International Conference on Intelligent Robots and Systems* (2007), 2944–2950.

41. Chattopadhyay, D. & Bolchini, D. *Understanding Visual Feedback in Large-Display Touchless Interactions: An Exploratory Study* tech. rep. (Indiana University, 2014).

42. Chau, Y., Mondot, L., Sachet, M., Gaudart, J., Fontaine, D., Lonjon, M. & Sédat, J. Modification of cerebral vascular anatomy induced by Leo stent placement depending on the site of stenting: A series of 102 cases. *Interventional neuroradiology : journal of peritherapeutic neuroradiology, surgical procedures and related neurosciences* **22,** 666–673 (2016).

43. Chaudhry, E., Bian, S., Ugail, H., Jin, X., You, L. & Zhang, J. J. Dynamic skin deformation using finite difference solutions for character animation. *Computers & Graphics* **46,** 294–305 (2015).

44. Chen, M., Mountford, S. J. & Sellen, A. A Study in Interactive 3-D Rotation Using 2-D Control Devices. *Proc. of SIGGRAPH* **22,** 121–129 (1988).

45. Ciarlet, P., Glowinski, R. & Lions, J. *Numerical Methods for Non-Newtonian Fluids: Special Volume* (Elsevier, 2011).

46. Crabtree, A., Rodden, T., Tolmie, P. & Button, G. *Ethnography Considered Harmful* in *Proc. of ACM SIGCHI conference on Human factors in computing systems (CHI)* (2009), 879–888.

47. Creswell, J. W. *Research Design: Qualitative, Quantitative, and Mixed Methods Approaches* (Sage publications, 2013).

48. Cunningham, D. & Wallraven, C. *Experimental Design: From User Studies to Psychophysics* (A. K. Peters, Ltd., 2011).

49. Cutkosky, M. R. On grasp choice, grasp models, and the design of hands for manufacturing tasks. *IEEE Transactions on Robotics and Automation* **5,** 269–279 (1989).

50. Demiralp, C., Jackson, C. D., Karelitz, D. B., Zhang, S. & Laidlaw, D. H. CAVE and Fishtank Virtual-Reality Displays: A Qualitative and Quantitative Comparison. *IEEE Transactions of Visualization and Computer Graphics (TVCG)* **12,** 323–330 (2006).

51. Dev, P., Hoffer, E. P. & Barnett, G. O. in *Medical informatics* 610–637 (Springer, 2001).

52. Diaz-Balzac, C. A., Rahman, M., Lazaro-Pena, M. I., Martin Hernandez, L. A., Salzberg, Y., Aguirre-Chen, C., Kaprielian, Z. & Bulow, H. E. Muscle- and Skin-Derived Cues Jointly Orchestrate Patterning of Somatosensory Dendrites. *Curr. Biol.* **26,** 2379–2387 (2016).

53. Díaz, J., Ropinski, T., Navazo, I., Gobbetti, E. & Vázquez, P.-P. An experimental study on the effects of shading in 3D perception of volumetric models. *The Visual Computer,* 1–15 (2015).

54. Ding, C. & Liu, L. A Survey of Sketch Based Modeling Systems. *Frontiers of Computer Science* **10,** 985–999 (2016).

55. Dipietro, L., Sabatini, A. M. & Dario, P. A Survey of Glove-Based Systems and Their Applications. *IEEE Transactions on Systems, Man, and Cybernetics, Part C (Applications and Reviews)* **38,** 461–482 (2008).

56. Douglas, D. H. & Peucker, T. K. Algorithms for the Reduction of the Number of Points Required to Represent a Digitized Line or its Caricature. *Cartographica: The International Journal for Geographic Information and Geovisualization* **10,** 112–122 (1973).

57. Ehrsson, H. H., Fagergren, E. & Forssberg, H. Differential fronto-parietal activation depending on force used in a precision grip task: an fMRI study. *J. Neurophysiol.* **85,** 2613–2623 (2001).

58. Eroglu, S., Gebhardt, S., Schmitz, P., Rausch, D. & Kuhlen, T. W. *Fluid Sketching - Immersive Sketching Based on Fluid Flow* in *Proc. of IEEE Virtual Reality (VR)* to appear (2018).

59. Estai, M. & Bunt, S. Best teaching practices in anatomy education: A critical review. *Ann. Anat.* **208,** 151–157 (2016).

60. European Heart Network. *European Cardiovascular Disease Statistics* http://www.ehnheart.org/cvd-statistics.html. last accesses 11.06.2018. 2017.

61. Eyal, G., Verhoog, M. B., Testa-Silva, G., Deitcher, Y., Lodder, J. C., Benavides-Piccione, R., Morales, J., DeFelipe, J., de Kock, C. P., Mansvelder, H. D. & Segev, I. Unique membrane properties and enhanced signal processing in human neocortical neurons. *Elife* **5** (Oct. 2016).

62. Fedorov, A., Beichel, R., Kalpathy-Cramer, J., Finet, J., Fillion-Robin, J. C., Pujol, S., Bauer, C., Jennings, D., Fennessy, F., Sonka, M., Buatti, J., Aylward, S., Miller, J. V., Pieper, S. & Kikinis, R. 3D Slicer as an image computing platform for the Quantitative Imaging Network. *Magn. Reson. Imaging* **30,** 1323–1341 (2012).

63. Fellner, F. A. Introducing Cinematic Rendering: A Novel Technique for Post-Processing Medical Imaging Data. *Journal of Biomedical Science and Engineering* **09,** 170–175 (2016).

64. Fellner, F. A., Engel, K. & Kremer, C. Virtual Anatomy: The Dissecting Theatre of the Future—Implementation of Cinematic Rendering in a Large 8 K High-Resolution Projection Environment. *Journal of Biomedical Science and Engineering* **10,** 367–375 (2017).

65. Ferziger, J. H. & Perić, M. in *Proc. of Computational Methods for Fluid Dynamics* 309–328 (Springer Berlin Heidelberg, 2002).

66. Field, A. *Discovering statistics using SPSS* (Sage publications, 2009).

67. Fikkert, W., van der Vet, P. & Nijholt, A. in *Multimedia Interaction and Intelligent User Interfaces: Principles, Methods and Applications* 215–242 (Springer London, 2010).

68. Fitts, P. M. The information capacity of the human motor system in controlling the amplitude of movement. *J Exp Psychol* **47,** 381–391 (1954).

69. Fleisch, T., Brunetti, G., Santos, P. & Stork, A. *Stroke-Input Methods for Immersive Styling Environments* in *Proc. of Shape Modeling and Applications* (2004), 275–283.

70. Fröhlich, B., Hochstrate, J., Skuk, V. & Huckauf, A. *The GlobeFish and the GlobeMouse: Two New Six Degree of Freedom Input Devices for Graphics Applications* in *Proc. of ACM SIGCHI conference on Human factors in computing systems (CHI)* (2006), 191–199.

71. Fröhlich, B. & Plate, J. *The Cubic Mouse: A New Device for Three-dimensional Input* in *Proc. of ACM SIGCHI conference on Human factors in computing systems (CHI)* (2000), 526–531.

72. Gallo, L. & Pietro, G. D. in *Multimedia Techniques for Device and Ambient Intelligence* (eds Jeong, J. & Damiani, E.) 115–134 (Springer, Boston, MA, Boston, MA, 2009).

73. Gao, B., Baharoglu, M. I., Cohen, A. D. & Malek, A. M. Stent-assisted coiling of intracranial bifurcation aneurysms leads to immediate and delayed intracranial vascular angle remodeling. *AJNR Am J Neuroradiol* **33,** 649–654 (2012).

74. Gasteiger, R., Neugebauer, M., Kubisch, C. & Preim, B. *Visualization of Cerebral Aneurysms with Embedded Blood Flow Information* in *Proc. of Eurographics Workshop on Visual Computing in Biology and Medicine (VCBM)* (2010), 25–32.

75. Gasteiger, R. *Visual Exploration of Cardiovascular Hemodynamics* PhD thesis (Otto-von-Guericke University Magdeburg, 2014).

76. Gasteiger, R., Tietjen, C., Baer, A. & Preim, B. *Curvature- and Model-Based Surface Hatching of Anatomical Structures Derived from Clinical Volume Datasets* in *Smart Graphics* (Springer Berlin Heidelberg, 2008), 255–262.

77. Gehrmann, S., Hohne, K. H., Linhart, W., Pflesser, B., Pommert, A., Riemer, M., Tiede, U., Windolf, J., Schumacher, U. & Rueger, J. M. A Novel Interactive Anatomic Atlas of the Hand. *Clin Anat* **19,** 258–266 (2006).

78. Gescheider, G. A. *Psychophysics: the Fundamentals* (Psychology Press, 2013).

79. Glaßer, S., Hoffmann, T., Voß, S., Klink, F. & Preim, B. *Extraction of Patient-Specific 3D Cerebral Artery and Wall Thickness Models from 2D OCT and Structured-Light 3D Scanner Data* in *Proc. of German Society of Computer- and Robot-Assisted Surgery (CURAC)* (2016), 197–202.

80. Glaßer, S., Hirsch, J., Berg, P., **Saalfeld**, **P.**, Beuing, O., Janiga, G. & Preim, B. *Evaluation of Time-Dependent Wall Shear Stress Visualizations for Cerebral Aneurysms* in *Proc. of Workshop Bildverarbeitung für die Medizin* (Springer Verlag, 2016), 236–241.

81. Glaßer, S., **Saalfeld**, **P.**, Berg, P., Merten, N. & Preim, B. *How to Evaluate Medical Visualizations on the Example of 3D Aneurysm Surfaces* in *Proc. of Eurographics Workshop on Visual Computing in Biology and Medicine (VCBM)* (2016), 153–162.

82. Gonzalez-Bellido, P. T., Peng, H., Yang, J., Georgopoulos, A. P. & Olberg, R. M. Eight pairs of descending visual neurons in the dragonfly give wing motor centers accurate population vector of prey direction. *Proc. Natl. Acad. Sci. U.S.A.* **110,** 696–701 (2013).

83. Götzelmann, T., Ali, K., Hartmann, K. & Strothotte, T. *Form Follows Function: Aesthetic Interactive Labels* in *Proc. of Computational Aesthetics in Graphics, Visualization and Imaging* (2005), 193–200.

84. Gray, H. & Lewis, W. H. *Anatomy of the Human Body* (Philadelphia, Lea & Febiger, 1918).

85. Guna, J., Jakus, G., Pogacnik, M., Tomazic, S. & Sodnik, J. An analysis of the precision and reliability of the leap motion sensor and its suitability for static and dynamic tracking. *Sensors (Basel)* **14,** 3702–3720 (2014).

86. Hackett, M. & Proctor, M. Three-dimensional display technologies for anatomical education: a literature Review. *J Sci Educ Technol* **25,** 641–54 (2016).

87. Hagedorn, B. & Döllner, J. *Sketch-Based Navigation in 3D Virtual Environments* in *Proc. of International Symposium on Smart Graphics* (Springer Berlin Heidelberg, Berlin, Heidelberg, 2008), 239–246.

88. Hagedorn, J. G., Dunkers, J. P., Satterfield, S. G., Peskin, A. P., Kelso, J. T. & Terrill, J. E. Measurement Tools for the Immersive Visualization Environment: Steps Toward the Virtual Laboratory. *Journal of Research of the National Institute of Standards and Technology* **112,** 257–270 (2007).

89. Hand, C. A Survey of 3D Interaction Techniques. *Computer Graphics Forum (CGF)* **16,** 269–281 (1997).

90. Hanna, G. B., Shimi, S. M. & Cuschieri, A. Task Performance in Endoscopic Surgery is Influenced by Location of the Iage Display. *Ann. Surg.* **227,** 481–484 (1998).

91. Harris, M. J. *GPU Gems Chapter 38, Fast Fluid Dynamics Simulation on the GPU* (Pearson Higher Education, 2004).

92. Hartmann, K., Ali, K. & Strothotte, T. *Floating Labels: Applying Dynamic Potential Fields for Label Layout* in *Proc. of International Symposium on Smart Graphics* (2004), 101–13.

93. Hartmann, K., Götzelmann, T., Ali, K. & Strothotte, T. *Metrics for Functional and Aesthetic Label Layouts* in *Proc. of Smart Graphics* (Springer-Verlag, 2005), 115–126.

94. He, L., Guayaquil-Sosa, A. & McGraw, T. *Medical Image Atlas Interaction in Virtual Reality* in *Workshop on Immersive Analytics: Exploring Future Interaction and Visualization Technologies for Data Analytics* (2017).

95. Heckel, F., Moltz, J. H., Tietjen, C. & Hahn, H. K. Sketch-Based Editing Tools for Tumour Segmentation in 3D Medical Images. *Computer Graphics Forum (CGF)* **32,** 144–157 (2013).

96. Herold, J. & Stahovich, T. F. *The 1$^¢$; Recognizer: A Fast, Accurate, and Easy-to-implement Handwritten Gesture Recognition Technique* in *Proc. of Sketch-Based Interfaces and Modeling Symposium (SBIM)* (Eurographics Association, 2012), 39–46.

97. Hettig, J., Mewes, A., Riabikin, O., Skalej, M., Preim, B. & Hansen, C. *Exploration of 3D Medical Image Data for Interventional Radiology using Myoelectric Gesture Control* in *Proc. of Eurographics Workshop on Visual Computing in Biology and Medicine (VCBM)* (2015), 177–185.

98. Hettig, J., **Saalfeld**, **P.**, Luz, M., Becker, M., Skalej, M. & Hansen, C. Comparison of Gesture and Conventional Interaction Techniques for Interventional Neuroradiology. *International Journal of Computer Assisted Radiology and Surgery (IJCARS),* 1–11 (2017).

99. Hettig, J., **Saalfeld**, **P.**, Luz, M., Skalej, M. & Hansen, C. *Evaluation of Human-Computer Interaction Techniques in Interventional Radiology* in *Proc. of Computer Assisted Radiology and Surgery* (Springer, 2016), 185–186.

100. Hinckley, K., Pausch, R., Proffitt, D. & Kassell, N. F. Two-handed Virtual Manipulation. *ACM Trans. Comput.-Hum. Interact.* **5,** 260–302 (1998).

101. Hochman, J. B., Unger, B., Kraut, J., Pisa, J. & Hombach-Klonisch, S. Gesture-controlled interactive three dimensional anatomy: a novel teaching tool in head and neck surgery. *Journal of Otolaryngology-Head & Neck Surgery* **43,** P135–P136 (2014).

102. Hoffman, H. & Vu, D. Virtual reality: teaching tool of the twenty-first century? *Acad Med* **72,** 1076–1081 (1997).

103. Höhne, K. H., Petersik, A., Pflesser, B., Pommert, A., Priesmeyer, K., Riemer, M., Schiemann, T., Schubert, R., Tiede, U., Urban, M., Frederking, H., Lowndes, M. & Morris, J. *VOXEL-MAN 3D Navigator: Brain and Skull. Regional, Functional and Radiological Anatomy* (Springer Electronic Media, Heidelberg, 2001).

104. Hong, Q. *A Survey on the Visualization and Reconstruction of Vasculatures* in *Proc. of SPIE, International Conference on Graphic and Image Processing* (2014), 90690F–90690F-5.

105. Hong, Q., Li, Q. & Tian, J. in *Computational Science and Its Applications* 592–603 (Springer, 2011).

106. Hötker, A. M., Pitton, M. B., Mildenberger, P. & Düber, C. Speech and motion control for interventional radiology: requirements and feasibility. *International Journal of Computer Assisted Radiology and Surgery (IJCARS)* **8,** 997–1002 (2013).

107. Huang, H.-M., Rauch, U. & Liaw, S.-S. Investigating Learners' Attitudes Toward Virtual Reality Learning Environments: Based on a Constructivist Approach. *Comput. Educ.* **55,** 1171–1182 (2010).

108. Hübler, A., Hansen, C., Beuing, O., Skalej, M. & Preim, B. *Workflow Analysis for Interventional Neuroradiology using Frequent Pattern Mining* in *Proc. of German Society of Computer- and Robot-Assisted Surgery (CURAC)* (2014), 165–168.

109. Huckauf, A., Fröhlich, B., Kulik, A. & Hochstrate, J. On 3D Input Devices. *IEEE Comput. Graph. Appl. Mag.* **26,** 15–19 (2006).

110. Hurtienne, J. & Naumann, A. QUESI – A questionnaire for measuring the subjective consequences of intuitive use. *Interdisciplinary College* **536** (2010).

111. Igarashi, T., Matsuoka, S., Kawachiya, S. & Tanaka, H. *Interactive Beautification: A Technique for Rapid Geometric Design* in *Proc. of ACM Conference on User Interface Software and Technlogy (UIST)* (1997), 105–114.

112. Igarashi, T., Matsuoka, S. & Tanaka, H. *Teddy: A Sketching Interface for 3D Freeform Design* in *Proc. of SIGGRAPH* (2007).

113. Imhof, E. Positioning Names on Maps. *The American Cartographer* **2,** 128–144 (1975).

114. Isenberg, T., Isenberg, P., Chen, J., Sedlmair, M. & Moller, T. A systematic review on the practice of evaluating visualization. *IEEE Transactions of Visualization and Computer Graphics (TVCG)* **19,** 2818–2827 (2013) (cit. on pp. 2, 39, 48).

115. Israel, J., Wiese, E., Mateescu, M., Zöllner, C. & Stark, R. Investigating three-dimensional sketching for early conceptual design – Results from expert discussions and user studies. *Computers & Graphics* **33,** 462–473 (2009).

116. Jacka, D., Reid, A., Merry, B. & Gain, J. *A Comparison of Linear Skinning Techniques for Character Animation* in *Proc. of International Conference on Computer Graphics, Virtual Reality, Visualisation and Interaction in Africa* (ACM, 2007), 177–186.

117. Jackson, B. & Keefe, D. F. Lift-Off: Using Reference Imagery and Freehand Sketching to Create 3D Models in VR. *IEEE Transactions of Visualization and Computer Graphics (TVCG)* **22,** 1442–1451 (2016).

118. Jacob, R. J., Girouard, A., Hirshfield, L. M., Horn, M. S., Shaer, O., Solovey, E. T. & Zigelbaum, J. *Reality-based Interaction: A Framework for post-WIMP Interfaces* in *Proc. of ACM SIGCHI conference on Human factors in computing systems (CHI)* (ACM, 2008), 201–210.

119.   Jankowski, J. & Hachet, M. Advances in Interaction with 3D Environments. *Computer Graphics Forum (CGF)* **34,** 152–190 (2015) (cit. on pp. 1, 5).

120.   Jankowski, J. & Hachet, M. *A Survey of Interaction Techniques for Interactive 3D Environments* in *Eurographics - State of the Art Reports* (2013).

121.   John, N. W., Phillips, N. I., ap Cenydd, L., Pop, S. R., Coope, D., Kamaly-Asl, I., de Souza, C. & Watt, S. J. The Use of Stereoscopy in a Neurosurgery Training Virtual Environment. *Presence* **25,** 289–298 (2016).

122.   John, N. W., Phillips, N. I., Cenydd, L. a., Pop, S. R., Coope, D., Kamaly-Asl, I., de Souza, C. & Watt, S. J. The Use of Stereoscopy in a Neurosurgery Training Virtual Environment. *Presence: Teleoper. Virtual Environ.* **24,** 289–298 (2016).

123.   Jorge, J. & Samavati, F. *Sketch-based Interfaces and Modeling* (Springer London, 2011).

124.   Jørgensen, A. H. Thinking-aloud in User Interface Design: a Method Promoting Cognitive Ergonomics. *Ergonomics* **33,** 501–507 (1990).

125.   Kanitsar, A., Fleischmann, D., Wegenkittl, R., Felkel, P. & Gröller, E. *CPR: Curved Planar Reformation* in *Proc. of Visualization* (2002), 37–44.

126.   Katzakis, N., Seki, K., Kiyokawa, K. & Takemura, H. *Mesh-Grab and Arcball-3D: Ray-based 6-DOF Object Manipulation* in *Proc. of Asia Pacific Conference on Computer Human Interaction* (2013), 129–136.

127.   Kayembe, K. N., Sasahara, M. & Hazama, F. Cerebral Aneurysms and Variations in the Circle of Willis. *Stroke* **15,** 846–50 (1984).

128.   Keulers, B. *Computer-based Patient Education: Its Potential in General and Plastic Surgery* PhD thesis (University Nijmegen, 2008).

129.   Kim, S.-H., Yi, J. S. & Elmqvist, N. *Oopsy-daisy: Failure Stories in Quantitative Evaluation Studies for Visualizations* in *Proc. of Beyond Time and Errors: Novel Evaluation Methods for Visualization (BELIV)* (2014), 142–146.

130.   Kim, Y. & Bae, S.-H. *Sketchingwithhands: 3d sketching handheld products with first-person hand posture* in *Proc. of ACM Conference on User Interface Software and Technlogy (UIST)* (2016), 797–808.

131.   Kim, Y., Lee, J. H., An, S.-G. & Bae, S.-H. *Agile 3D Sketching with Air Scaffolding* in *Extended Abstracts of the CHI Conference on Human Factors in Computing Systems* (2018), D411:1–D411:1.

132.   Klein, J., Friman, O., Hadwiger, M., Preim, B., Ritter, F., Vilanova, A., Zachmann, G. & Bartz, D. Visual computing for medical diagnosis and treatment. *Computers & Graphics* **33,** 554–565 (2009).

133.   Kohrmann, A., D'Hanis, W., **Saalfeld**, **P.**, Kellermann, K., Roskoden, T., Rathmann, A., Dornheim, L., Pohlenz, P., Preim, B. & Rothkötter, H.-J. *Comparative study in gross anatomy education: Differences in learning spatial anatomy using 3d-models of body-donor-CT-scans or a traditional atlas* in *Proc. of Anatomische Gesellschaft* (2016).

134.   Kosara, R., Healey, C. G., Interrante, V., Laidlaw, D. H. & Ware, C. User studies: why, how, and when? *IEEE Comput. Graph. Appl. Mag.* **23,** 20–25 (2003).

135. Kretschmer, J., Beck, T., Tietjen, C., Preim, B. & Stamminger, M. Reliable Adaptive Modelling of Vascular Structures with Non-Circular Cross-Sections. *Computer Graphics Forum (CGF)* **31,** 1055–1064 (2012).

136. Kretschmer, J., Godenschwager, C., Preim, B. & Stamminger, M. Interactive patient-specific vascular modeling with sweep surfaces. *IEEE Transactions of Visualization and Computer Graphics (TVCG)* **19,** 2828–2837 (2013).

137. Krüger, A., Stampe, K., Irrgang, S., Richter, I., Strauß, G. & Preim, B. *Eingabegeräte und Interaktionstechniken für die virtuelle Endoskopie* in *Proc. of Mensch & Computer* (2008), 237–246.

138. Krüger, J. & Westermann, R. Linear Algebra Operators for GPU Implementation of Numerical Algorithms. *ACM Transactions on Graphics* **22,** 908–916 (2003).

139. Krüger, W., Bohn, C.-A., Fröhlich, B., Schuth, H., Strauss, W. & Wesche, G. The Responsive Workbench: a virtual work environment. *IEEE Computer* **28,** 42–48 (1995).

140. Krüger, W. & Fröhlich, B. The Responsive Workbench. *IEEE Comput. Graph. Appl. Mag.* **14,** 12–15 (1994).

141. Kulik, A., Hochstrate, J., Kunert, A. & Froehlich, B. *Demo: The Globefish: A novel input device for desktop-based 3D interaction* in *Proc. of IEEE 3D User Interfaces (3DUI)* (2009), 159–159.

142. Kutikhin, A., Brusina, E. & Yuzhalin, A. E. in *Viruses and Atherosclerosis* 1–3 (Springer New York, 2013).

143. Lam, H., Bertini, E., Isenberg, P., Plaisant, C. & Carpendale, S. Empirical studies in information visualization: Seven scenarios. *IEEE Transactions of Visualization and Computer Graphics (TVCG)* **18,** 1520–1536 (2012).

144. Lang, H., Radtke, A., Hindennach, M. & et al. Impact of Virtual Tumor Resection and Computer-Assisted Risk Analysis on Operation Planning and Intraoperative Strategy in Major Hepatic Resection. *Archives of Surgery* **140,** 629–638 (2005).

145. LaViola, J. J. 3D Gestural Interaction: The State of the Field. *ISRN Artificial Intelligence,* 1–18 (2013).

146. LaViola, J. J., Kruijff, E., McMahan, R. P., Bowman, D. & Poupyrev, I. P. *3D User Interfaces: Theory and Practice (2nd Edition)* (Addison-Wesley Professional, Redwood City, CA, USA, 2017) (cit. on pp. 1, 5, 24, 30, 37).

147. LaViola, J. J. & Litwiller, T. *Evaluating the Benefits of 3D Stereo in Modern Video Games* in *Proc. of ACM SIGCHI conference on Human factors in computing systems (CHI)* (2011), 2345–2354.

148. Lawonn, K., Baer, A., **Saalfeld**, **P.** & Preim, B. *Comparative Evaluation of Feature Line Techniques for Shape Depiction* in *Proc. of Vision, Modeling, and Visualization (VMV)* (2014), 31–38.

149. Lawonn, K., **Saalfeld**, **P.** & Preim, B. *Illustrative Visualization of Endoscopic Views* in *Proc. of Workshop Bildverarbeitung für die Medizin* (Springer Verlag, 2014), 276–281.

150. Letterie, G. S. Medical Education as a Science: The Quality of Evidence for Computer-assisted Instruction. *Am. J. Obstet. Gynecol.* **188,** 849–853 (2003).

151. Lewis, J. P., Cordner, M. & Fong, N. *Pose Space Deformation: A Unified Approach to Shape Interpolation and Skeleton-driven Deformation* in *Proc. of Annual Conference on Computer Graphics and Interactive Techniques* (2000), 165–172.

152. Lidal, E. M. *Sketch-based Storytelling for Cognitive Problem Solving* PhD thesis (Department of Informatics, University of Bergen, Norway, June 2013).

153. Lindemann, F. & Ropinski, T. About the Influence of Illumination Models on Image Comprehension in Direct Volume Rendering. *IEEE Transactions of Visualization and Computer Graphics (TVCG)* **17,** 1922–1931 (2011).

154. Lobao, A. S., Evangelista, B. P. & Grootjans, R. *Beginning XNA 3.0 Game Programming: From Novice to Professional* (Apress, Berkely, CA, USA, 2009).

155. Lundstrom, C., Rydell, T., Forsell, C., Persson, A. & Ynnerman, A. Multi-Touch Table System for Medical Visualization: Application to Orthopedic Surgery Planning. *IEEE Transactions of Visualization and Computer Graphics (TVCG)* **17,** 1775–1784 (2011).

156. Luursema, J.-M., Verwey, W. B., Kommers, P. A. & Annema, J.-H. The role of stereopsis in virtual anatomical learning. *Interacting with Computers* **20,** 455–60 (2008).

157. Luz, M., Strauss, G. & Manzey, D. Impact of image-guided surgery on surgeons' performance: a literature review. *International Journal of Human Factors and Ergonomics* **4,** 229–263 (2016).

158. Ma, Y., Mao, Z.-H., Jia, W., Li, C., Yang, J. & Sun, M. Magnetic hand tracking for human-computer interface. *IEEE Transactions on Magnetics* **47,** 970–973 (2011).

159. Madsen, J. B., Tatzqern, M., Madsen, C. B., Schmalstieg, D. & Kalkofen, D. Temporal Coherence Strategies for Augmented Reality Labeling. *IEEE Transactions of Visualization and Computer Graphics (TVCG)* **22,** 1415–1423 (2016).

160. Mauser, S. & Burgert, O. Touch-free, gesture-based control of medical devices and software based on the leap motion controller. *Stud Health Technol Inform* **196,** 265–270 (2014).

161. McGuire, M. & Fein, A. *Real-time Rendering of Cartoon Smoke and Clouds* in *Proc. of International Symposium on Non-photorealistic Animation and Rendering* (2006), 21–26.

162. Mendes, D., Caputo, F. M., Giachetti, A., Ferreira, A. & Jorge, J. A Survey on 3D Virtual Object Manipulation: From the Desktop to Immersive Virtual Environments. *Computer Graphics Forum (CGF).* https://onlinelibrary.wiley.com/doi/abs/10.1111/cgf.13390 (2018).

163. Mendes, D., Sousa, M., Lorena, R., Ferreira, A. & Jorge, J. *Using Custom Transformation Axes for Mid-air Manipulation of 3D Virtual Objects* in *Proc. of Virtual Reality Software and Technology* (2017), 27:1–27:8.

164. Mentis, H. M., O'Hara, K., Sellen, A. & Trivedi, R. *Interaction Proxemics and Image Use in Neurosurgery* in *Proc. of ACM SIGCHI conference on Human factors in computing systems (CHI)* (2012), 927–936.

165. Merten, N., Saalfeld, S., Hanses, M., Becker, M., Adler, S. & Preim, B. *A Software Prototype for Treatment Planning and Intervention Support of Robot-Assisted Radiofrequency Ablations of Vertebral Metastases* in *Proc. of German Society of Computer- and Robot-Assisted Surgery (CURAC)* (2017), 89–94.

166. Mewes, A., Hensen, B., Wacker, F. & Hansen, C. Touchless Interaction with Software in Interventional Radiology and Surgery: A Systematic Literature Review. *International Journal of Computer Assisted Radiology and Surgery (IJCARS)* **12,** 291–305 (2 2017).

167. Mewes, A., **Saalfeld, P.**, Riabikin, O., Skalej, M. & Hansen, C. A Gesture-Controlled Projection Display for CT-Guided Interventions. *International Journal of Computer Assisted Radiology and Surgery (IJCARS)* **11,** 157–164 (2016).

168. Mihelj, M., Novak, D. & Begus, S. *Virtual Reality Technology and Applications* (Springer Publishing Company, Incorporated, 2013).

169. Mistelbauer, G., Morar, A., Varchola, A., Schernthaner, R., Baclija, I., Köchl, A., Kanitsar, A., Bruckner, S. & Gröller, E. Vessel Visualization Using Curvicircular Feature Aggregation. *Computer Graphics Forum (CGF)* **32,** 231–240 (2013).

170. Mönch, J., Mühler, K., Hansen, C., Oldhafer, K.-J., Stavrou, G., Hillert, C., Logge, C. & Preim, B. The LiverSurgeryTrainer: training of computer-based planning in liver resection surgery. *International Journal of Computer Assisted Radiology and Surgery (IJCARS)* **8,** 809–818 (5 2013).

171. Mühler, K. & Preim, B. *Automatic Textual Annotation for Surgical Planning* in *Proc. of Vision, Modeling, and Visualization (VMV)* (2009), 277–284.

172. Mühler, K., Tietjen, C., Ritter, F. & Preim, B. The Medical Exploration Toolkit: An Efficient Support for Visual Computing in Surgical Planning and Training. *IEEE Transactions of Visualization and Computer Graphics (TVCG)* **16,** 133–146 (2010).

173. Müller, M., Schirm, S. & Teschner, M. Interactive Blood Simulation for Virtual Surgery Based on Smoothed Particle Hydrodynamics. *Technol. Health Care* **12,** 25–31 (2004).

174. Napier, J. R. The Prehensile Movements of the Human Hand. *Bone & Joint Journal* **38-B,** 902–913 (1956).

175. Naya, F., Contero, M., Aleixos, N. & Company, P. *ParSketch: A Sketch-based Interface for a 2D Parametric Geometry Editor* in *Proc. of the International Conference on Human-computer Interaction: Interaction Platforms and Techniques* (Springer-Verlag, 2007), 115–124.

176. Neugebauer, M., Diehl, V., Skalej, M. & Preim, B. *Geometric Reconstruction of the Ostium of Cerebral Aneurysms* in *Proc. of Vision, Modeling, and Visualization (VMV)* (2010), 307–314.

177. Neugebauer, M., Gasteiger, R., Beuing, O., Diehl, V., Skalej, M. & Preim, B. *Map Displays for the Analysis of Scalar Data on Cerebral Aneurysm Surfaces* in *Computer Graphics Forum (CGF)* **28 (3)** (2009), 895–902.

178. Newman, I. & Benz, C. R. *Qualitative-Quantitative Research Methodology: Exploring the Interactive Continuum* (SIU Press, 1998).

179. Nguyen, H. *Gpu Gems 3* (Addison-Wesley Professional, 2007).

180.   Ni, T., Bowman, D. A., North, C. & McMahan, R. P. Design and Evaluation of Freehand Menu Selection Interfaces Using Tilt and Pinch Gestures. *Int. J. Hum.-Comput. Stud.* **69,** 551–562 (2011).

181.   Niedermann, B., Nöllenburg, M. & Rutter, I. *Radial contour labeling with straight leaders* in *IEEE Pacific Visualization Symposium (PacificVis)* (2017), 295–304.

182.   Nishimura, H., Hirai, M., Kawai, T., Kawata, T., Shirakawa, I. & Omura, K. Object modeling by distribution function and a method of image generation. *The Transactions of the Institute of Electronics and Communication Engineers of Japan* **68,** 718–725 (1985).

183.   Norman, D. *The Design of Everyday Things: Revised and Expanded Edition* (Basic Books, 2013) (cit. on p. 1).

184.   Nowke, C., Schmidt, M., van Albada, S. J., Eppler, J. M., Bakker, R., Diesrnann, M., Hentschel, B. & Kuhlen, T. *VisNEST - Interactive analysis of neural activity data* in *IEEE Symposium on Biological Data Visualization* (2013), 65–72.

185.   O'Hara, K., Gonzalez, G., Sellen, A., Penney, G., Varnavas, A., Mentis, H., Criminisi, A., Corish, R., Rouncefield, M., Dastur, N. & Carrell, T. Touchless Interaction in Surgery. *Communications of the ACM* **57,** 70–77 (2014).

186.   Oeltze-Jafra, S. & Preim, B. *Survey of Labeling Techniques in Medical Visualizations* in *Proc. of Eurographics Workshop on Visual Computing in Biology and Medicine (VCBM)* (2014), 199–208.

187.   Oeltze, S. & Preim, B. *Visualization of Anatomic Tree Structures with Convolution Surfaces* in *Proc. of EuroVis* (Springer, 2004), 311–320.

188.   Oeltze, S. & Preim, B. Visualization of Vascular Structures: Method, Validation and Evaluation. *IEEE Transactions on Medical Imaging (TMI)* **25(4),** 540–549 (2005).

189.   Ohtake, Y., Belyaev, A., Alexa, M., Turk, G. & Seidel, H.-P. *Multi-level partition of unity implicits* in *Proc. of SIGGRAPH* (2005), 463–470.

190.   Olsen, L., Samavati, F. F., Sousa, M. C. & Jorge, J. *A Taxonomy of Modeling Techniques using Sketch-Based Interfaces* in *Proc. of Eurographics - State of the Art Reports (STARs)* (2008), 39–57.

191.   Olsen, L., Samavati, F. F., Sousa, M. C. & Jorge, J. A. Sketch-based modeling: A survey. *Computers & Graphics* **33,** 85–103 (2009) (cit. on pp. 2, 21).

192.   Patel, H., Stefani, O., Sharples, S., Hoffmann, H., Karaseitanidis, I. & Amditis, A. Human Centred Design of 3-D Interaction Devices to Control Virtual Environments. *International Journal of Human-Computer Studies* **64,** 207–220 (2006).

193.   Paulsen, F. & Waschke, J. *Sobotta Atlas of Human Anatomy, Head, Neck and Neuroanatomy* 15th ed. (Urban & Fischer, 2013).

194.   Perkunder, H., Israel, J. H. & Alexa, M. *Shape Modeling with Sketched Feature Lines in Immersive 3D Environments* in *Proc. of Sketch-Based Interfaces and Modeling Symposium (SBIM)* (2010), 127–134.

195.   Pharr, M. & Humphreys, G. *Physically Based Rendering, Second Edition: From Theory To Implementation* (Morgan Kaufmann Publishers Inc., 2010).

196. Phillips, A. W., Smith, S. G., Ross, C. F. & Straus, C. M. Direct correlation of radiologic and cadaveric structures in a gross anatomy course. *Med Teach* **34,** e779–784 (2012).

197. Pick, S., Hentschel, B., Tedjo-Palczynski, I., Wolter, M. & Kuhlen, T. *Automated Positioning of Annotations in Immersive Virtual Environments* in *Proc. of Eurographics Conference on Virtual Environments* (Eurographics Association, 2010), 1–8.

198. Pick, S., Weyers, B., Hentschel, B. & Kuhlen, T. W. Design and Evaluation of Data Annotation Workflows for CAVE-like Virtual Environments. *IEEE Transactions of Visualization and Computer Graphics (TVCG)* **22,** 1452–1461 (2016).

199. Pick, S. & Kuhlen, T. W. *A framework for developing flexible virtual-reality-centered annotation systems* in *IEEE Workshop on Software Engineering and Architectures for Realtime Interactive Systems (SEARIS)* (2015), 10–17.

200. Piegl, L. Interactive Data Interpolation by Rational Bezier Curves. *IEEE Comput. Graph. Appl. Mag.* **7,** 45–58 (1987).

201. Pihuit, A., Cani, M.-P. & Palombi, O. *Sketch-based Modeling of Vascular Systems: A First Step Towards Interactive Teaching of Anatomy* in *Proc. of Sketch-Based Interfaces and Modeling Symposium (SBIM)* (2010), 151–158.

202. Poupyrev, I., Ichikawa, T., Weghorst, S. & Billinghurst, M. Egocentric Object Manipulation in Virtual Environments: Empirical Evaluation of Interaction Techniques. *Computer Graphics Forum* **17,** 41–52. ISSN: 1467-8659 (1998).

203. Preim, B. & Botha, C. *Visual Computing for Medicine* (Morgan Kaufmann Publishers, 2013).

204. Preim, B., Tietjen, C., Spindler, W. & Peitgen, H. O. *Integration of Measurement Tools in Medical 3D Visualizations* in *Proc. of Visualization* (2002), 21–28.

205. Preim, B. & Dachselt, R. *Interaktive Systeme - Band 1: Grundlagen, Graphical User Interfaces, Informationsvisualisierung* (Springer, 2010).

206. Preim, B., Baer, A., Cunningham, D., Isenberg, T. & Ropinski, T. A survey of perceptually motivated 3D visualization of medical image data. *Computer Graphics Forum (CGF)* **35,** 501–525 (2016).

207. Preim, B. & Dachselt, R. *Interaktive Systeme – Band 2: User Interface Engineering, 3D-Interaktion, Natural User Interfaces* (Springer Vieweg, Berlin, 2015) (cit. on pp. 1, 12, 20, 26, 27).

208. Preim, B. & Raab, A. *Annotation von topographisch komplizierten 3D-Modellen* in *Proc. of Simulation and Visualization* (1998), 128–40.

209. Preim, B., Ritter, A., Strothotte, T., Pohle, T., Forsey, D. R. & Bartram, L. *Consistency of Rendered Images and Their Textual Labels* in *Proc. of Edu + CompuGraphics* (1995), 201–210.

210. Preim, B. & **Saalfeld**, **P.** A Survey of Virtual Human Anatomy Education Systems. *Computers & Graphics* **71,** 132–153 (2018).

211. Prümper, J. *Der Benutzungsfragebogen ISONORM 9241/10: Ergebnisse zur Reliabilität und Validität* in *Proc. of Software-Ergonomie: Usability Engineering: Integration von Mensch-Computer-Interaktion und Software-Entwicklung* (1997), 254–262.

212. Psotka, J. Immersive training systems: Virtual reality and education and training. *Instructional Science* **23,** 405–431 (1995).

213. Qin, J., Pang, W.-M., Nguyen, B. P., Ni, D. & Chui, C.-K. *Particle-based Simulation of Blood Flow and Vessel Wall Interactions in Virtual Surgery* in *Proc. of Information and Communication Technology* (2010), 128–133.

214. Regian, J. W., Shebilske, W. L. & Monk, J. M. Virtual Reality: An Instructional Medium for Visual-Spatial Tasks. *Journal of Communication* **42,** 136–149 (1992).

215. Reid, C. & Owen, A. in, 1–20 (Springer Singapore, 2015).

216. Reiner, B. & Siegel, E. Radiology Reporting: Returning to Our Image-Centric Roots. *American Journal of Roentgenology* **187,** 1151–1155 (5 2006).

217. Riduwan, M., Basori, A. H. & Mohamed, F. Finger-based Gestural Interaction for Exploration of 3D Heart Visualization. *Procedia - Social and Behavioral Sciences* **97,** 684–690 (2013).

218. Ritter, F., Hansen, C., Dicken, V., Konrad, O., Preim, B. & o. Peitgen, H. Real-Time Illustration of Vascular Structures. *IEEE Transactions of Visualization and Computer Graphics (TVCG)* **12,** 877–884 (2006).

219. Ritter, F., Berendt, B., Fischer, B., Richter, R. & Preim, B. *Virtual 3D Jigsaw Puzzles: Studying the Effect of Exploring Spatial Relations with Subliminal Guidance* in *Proc. of Mensch & Computer* (2002), 363–372.

220. Ritter, F., Preim, B., Deussen, O. & Strothotte, T. Using a 3d Puzzle as a Metaphor for Learning Spatial Relations. *Proc. of Graphics Interface,* 171–178 (2000).

221. Ropinski, T., Praßni, J., Roters, J. & Hinrichs, K. *Internal Labels as Shape Cues for Medical Illustration* in *Proc. of Vision, Modeling, and Visualization (VMV)* (2007), 203–212.

222. Rosa, G. M. & Elizondo, M. L. Use of a Gesture User Interface as a Touchless Image Navigation System in Dental Surgery: Case Series Report. *Imaging Sci. Dent.* **44,** 155–160 (2014).

223. Rosenberg, L. B. *The effect of interocular distance upon operator performance using stereoscopic displays to perform virtual depth tasks* in *Proc. of IEEE Virtual Reality (VR)* (1993), 27–32.

224. Rosse, C. The potential of computerized representations of anatomy in the training of health care providers. *Acad Med* **70,** 499–505 (1995).

225. Rössling, I., Cyrus, C., Dornheim, L., Boehm, A. & Preim, B. Fast and Flexible Distance Measures for Treatment Planning. *International Journal of Computer Assisted Radiology and Surgery (IJCARS)* **5,** 633–646 (2010).

226. **Saalfeld**, **P.**, Baer, A., Lawonn, K., Preim, U. & Preim, B. *Das 3D User Interface zSpace - Verwendung zur Exploration und Inspektion von Wirbeln der Halswirbelsäule* in *Proc. of Workshop Bildverarbeitung für die Medizin* (2015), 83–88.

227. **Saalfeld**, **P.**, Baer, A., Preim, U., Preim, B. & Lawonn, K. *Sketching 2D Vessels and Vascular Diseases with Integrated Blood Flow* in *Proc. of Computer Graphics Theory and Applications (GRAPP)* (2015), 379–390.

228. **Saalfeld**, **P.**, Baer, A., Preim, U., Preim, B. & Lawonn, K. in *Computer Vision, Imaging and Computer Graphics Theory and Applications, Revised Selected Papers* 19–40 (Springer International Publishing, 2016).

229. **Saalfeld**, **P.**, Glaßer, S., Beuing, O., Grundmann, M. & Preim, B. *3D Sketching on Interactively Unfolded Vascular Structures for Treatment Planning* in *Proc. of IEEE 3D User Interfaces (3DUI)* (2016), 267–268.

230. **Saalfeld**, **P.**, Glaßer, S., Beuing, O. & Preim, B. The FAUST Framework: Free-Form Annotations on Unfolding Vascular Structures for Treatment Planning. *Computers & Graphics* **65,** 12–21 (2017).

231. **Saalfeld**, **P.**, Glaßer, S. & Preim, B. *3D User Interfaces for Interactive Annotation of Vascular Structures* in *Proc. of Mensch & Computer* (2015), 255–258.

232. **Saalfeld**, **P.**, Kasper, D., Preim, B. & Hansen, C. *Touchless Measurement of Medical Image Data for Interventional Support* in *Proc. of Mensch & Computer* (2017), 83–92.

233. **Saalfeld**, **P.**, Luz, M., Berg, P., Preim, B. & Glaßer, S. Guidelines for Quantitative Evaluation of Medical Visualizations on the Example of 3D Aneurysm Surface Comparisons. *Computer Graphics Forum (CGF)* **37,** 226–238 (2017).

234. **Saalfeld**, **P.**, Mewes, A., Hansen, C. & Preim, B. *Gaze-Based Annotations: Labels on Demand* in *Proc. of German Society of Computer- and Robot-Assisted Surgery (CURAC)* (2015), 261–266.

235. **Saalfeld**, **P.**, Mewes, A., Luz, M., Preim, B. & Hansen, C. *Comparative Evaluation of Gesture and Touch Input for Medical Software* in *Proc. of Mensch & Computer* (2015), 143–152.

236. **Saalfeld**, **P.**, Oeltze-Jafra, S., Saalfeld, S., Preim, U., Beuing, O. & Preim, B. *Sketching and Annotating Vascular Structures to Support Medical Teaching, Treatment Planning and Patient Education* in *Dirk Bartz Prize for Visual Computing in Medicine* (2017), 5–8.

237. **Saalfeld**, **P.**, Patzschke, J. & Preim, B. *An Immersive System for Exploring and Measuring Medical Image Data* in *Proc. of Mensch & Computer* (2017), 73–82.

238. **Saalfeld**, **P.**, Stojnic, A., Preim, B. & Oeltze-Jafra, S. *Semi-Immersive 3D Sketching of Vascular Structures for Medical Education* in *Proc. of Eurographics Workshop on Visual Computing in Biology and Medicine (VCBM)* (2016), 123–132.

239. Schumann, C., Neugebauer, M., Bade, R., Preim, B. & Peitgen, H.-O. Implicit vessel surface reconstruction for visualization and CFD simulation. *International Journal of Computer Assisted Radiology and Surgery (IJCARS)* **2,** 275–286 (2008).

240. Schumann, C., Oeltze, S., Bade, R., Preim, B. & Peitgen, H.-O. *Model-free Surface Visualization of Vascular Trees.* in *IEEE Eurographics Symposium on Visualization (EuroVis)* (2007), 283–290.

241. Schwarz, L. A., Bigdelou, A. & Navab, N. *Learning Gestures for Customizable Human-Computer Interaction in the Operating Room* in *Proc. of Medical Image Computing and Computer-Assisted Intervention (MICCAI)* **6891** (Springer, 2011), 129–136.

242. Selle, D., Preim, B., Schenk, A. & Peitgen, H.-O. Analysis of Vasculature for Liver Surgery Planning. *IEEE Transactions on Medical Imaging (TMI)* **21,** 1344–1357 (2002).

243. Shen, J., Luo, Y., Wu, Z., Tian, Y. & Deng, Q. CUDA-based Real-time Hand Gesture Interaction and Visualization for CT Volume Dataset Using Leap Motion. *Visual Computer* **32,** 359–370 (2016).

244. Sherman, W. R. & Craig, A. B. *Understanding Virtual Reality: Interface, Application, and Design* (Morgan Kaufmann Publishers Inc., 2002).

245. Sherwood, L. *Human Physiology: From Cells to Systems* (Cengage Learning, 2012).

246. Shi, W. & Cheung, C. Performance Evaluation of Line Simplification Algorithms for Vector Generalization. *The Cartographic Journal* **43,** 27–44 (2006).

247. Shoemake, K. *ARCBALL: a user interface for specifying three-dimensional orientation using a mouse* in *Graphics Interface* **92** (1992), 151–156.

248. Smit, N., Hofstede, C.-W., Kraima, A., Jansma, D., deRuiter, M., Eisemann, E. & Vilanova, A. *The Online Anatomical Human: Web-based Anatomy Education* in *Eurographics 2016 - Education Papers* (The Eurographics Association, 2016).

249. Smit, N., Kraima, A., Jansma, D., deRuiter, M., Eisemann, E. & Vilanova, A. *VarVis: Visualizing Anatomical Variation in Branching Structures* in *Proc. of Eurographics / IEEE VGTC Conference on Visualization: Short Papers* (2016), 49–53.

250. Song, H., Benko, H., Guimbretiere, F., Izadi, S., Cao, X. & Hinckley, K. *Grips and Gestures on a Multi-touch Pen* in *Proc. of Human Factors in Computing Systems* (2011), 1323–1332.

251. Song, P., Goh, W. B., Hutama, W., Fu, C.-W. & Liu, X. *A Handle Bar Metaphor for Virtual Object Manipulation with Mid-air Interaction* in *Proc. of ACM SIGCHI conference on Human factors in computing systems (CHI)* (2012), 1297–1306.

252. Sousa, M., Mendes, D., Paulo, S., Matela, N., Jorge, J. & Lopes, D. S. *VR-RRRoom: Virtual Reality for Radiologists in the Reading Room* in *Proc. of ACM SIGCHI conference on Human factors in computing systems (CHI)* (2017), 4057–4062.

253. Soutschek, S., Penne, J., Hornegger, J. & Kornhuber, J. 3-D gesture-based scene navigation in medical imaging applications using Time-of-Flight cameras. *IEEE Computer Society Conference on Computer Vision and Pattern Recognition Workshops*, 1–6 (2008).

254. Stam, J. *Stable Fluids* in *Proc. of SIGGRAPH* (1999).

255. Starkweather, J. A. Computer-assisted learning in medical education. *Can Med Assoc J* **97,** 733–738 (1967).

256. Stevenson, D., Gardner, H., Neilson, W., Beenen, E., Gananadha, S., Fergusson, J., Jeans, P., Mews, P. & Bandi, H. Evidence from the surgeons: gesture control of image data displayed during surgery. *Behaviour & Information Technology* **35,** 1063–1079 (2016).

257.   Stoakley, R., Conway, M. J. & Pausch, R. *Virtual Reality on a WIM: Interactive Worlds in Miniature* in *Proc. of ACM SIGCHI conference on Human factors in computing systems (CHI)* (1995), 265–272.

258.   Sutherland, I. E. *Sketchpad, A Man-Machine Graphical Communication System* (Garland Publishing, New York, 1963).

259.   Takala, T. M., Rauhamaa, P. & Takala, T. *Survey of 3DUI applications and development challenges* in *Proc. of IEEE 3D User Interfaces (3DUI)* (2012).

260.   Tani, B. S., Maia, R. S. & v. Wangenheim, A. *A Gesture Interface for Radiological Workstations* in *IEEE International Symposium on Computer-Based Medical Systems (CBMS)* (2007), 27–32.

261.   Tatzgern, M., Kalkofen, D., Grasset, R. & Schmalstieg, D. *Hedgehog Labeling: View Management Techniques for External Labels in 3D Space* in *Proc. of IEEE Virtual Reality (VR)* (2014), 27–32.

262.   Taubin, G. *Curve and Surface Smoothing Without Shrinkage* in *Proc. of Computer Vision* (IEEE Computer Society, 1995), 852–857.

263.   Teather, R. J. & Stuerzlinger, W. *Guidelines for 3D Positioning Techniques* in *Proc. of Future Play* (2007), 61–68.

264.   Teitelbaum, G. P., Higashida, R. T., Halbach, V. V., Larsen, D. W., McDougall, C. G., Dowd, C. F. & Hieshima, G. B. Flow-directed Use of Electrolytically Detachable Platinum Embolization Coils. *Journal of Vascular and Interventional Radiology* **5,** 453–456 (1994).

265.   Tolsdorff, B., Pommert, A., Hohne, K. H., Petersik, A., Pflesser, B., Tiede, U. & Leuwer, R. Virtual Reality: A New Paranasal Sinus Surgery Simulator. *Laryngoscope* **120,** 420–426 (2010).

266.   Ujiie, H., Sato, K., Onda, H., Oikawa, A., Kagawa, M., Takakura, K. & Kobayashi, N. Clinical analysis of incidentally discovered unruptured aneurysms. *Stroke* **24,** 1850–1856 (1993).

267.   Ustun, C., Uston, C. & Willis, T. NEUROwords Dr. Thomas Willis' famous eponym: the circle of Willis. *J Hist Neurosci* **14,** 16–21 (2005).

268.   Vaillant, R., Barthe, L., Guennebaud, G., Cani, M.-P., Rohmer, D., Wyvill, B., Gourmel, O. & Paulin, M. Implicit Skinning: Real-time Skin Deformation with Contact Modeling. *ACM Trans. Graph.* **32,** 125:1–125:12 (2013).

269.   Van Beurden, M. H. P. H., Ijsselsteijn, W. A. & de Kort, Y. A. W. in *Gesture and Sign Language in Human-Computer Interaction and Embodied Communication* 36–47 (Springer Berlin Heidelberg, 2012).

270.   Van Det, M. J., Meijerink, W. J., Hoff, C., Totte, E. R. & Pierie, J. P. Optimal Ergonomics for Laparoscopic Surgery in Minimally Invasive Surgery Suites: A Review and Guidelines. *Surg Endosc* **23,** 1279–1285 (2009).

271.   Vilanova Bartroli, A., Wegenkittl, R., Konig, A. & Gröller, E. *Nonlinear virtual colon unfolding* in *Proc. of Visualization* (2001), 411–579.

272.   Vlak, M. H., Algra, A., Brandenburg, R. & Rinkel, G. J. Prevalence of unruptured intracranial aneurysms, with emphasis on sex, age, comorbidity, country, and time period: a systematic review and meta-analysis. *Lancet Neurol* **10,** 626–636 (2011).

273. Voß, S., **Saalfeld**, **P.**, Saalfeld, S., Beuing, O., Janiga, G. & Preim, B. *Impact of Gradual Vascular Deformations on the Intra-aneurysmal Hemodynamics* in *Proc. of Workshop Bildverarbeitung für die Medizin* (2018), 359–364.

274. Wade, L. & Parent, R. E. Automated generation of control skeletons for use in animation. *The Visual Computer* **18,** 97–110 (2002).

275. Wang, M., Fei, G., Xin, Z., Zheng, Y. & Li, X. *3D Freehand Canvas* in *Proc. of Technologies for E-Learning and Digital Entertainment* (2008), 602–612.

276. Ware, C., Arthur, K. & Booth, K. S. *Fish Tank Virtual Reality* in *Proc. of ACM SIGCHI conference on Human factors in computing systems (CHI)* (1993), 37–42.

277. Weichert, F., Bachmann, D., Rudak, B. & Fisseler, D. Analysis of the accuracy and robustness of the leap motion controller. *Sensors (Basel)* **13,** 6380–6393 (2013).

278. Wigdor, D. & Wixon, D. *Brave NUI world: designing natural user interfaces for touch and gesture* (Elsevier, 2011).

279. Williams, D., Grimm, S., Coto, E., Roudsari, A. & Hatzakis, H. Volumetric Curved Planar Reformation for Virtual Endoscopy. *IEEE Transactions of Visualization and Computer Graphics (TVCG)* **14,** 109–119 (2008).

280. Wills, G. J. *NicheWorks — Interactive visualization of very large graphs* in *Graph Drawing* (1997), 403–414.

281. Witmer, B. G. & Singer, M. J. Measuring Presence in Virtual Environments: A Presence Questionnaire. *Presence: Teleoperators and Virtual Environments* **7,** 225–240 (3 1998).

282. Wong, G. K., Tan, H.-B., Kwan, M. C., Ng, R. Y., Yu, S. C., Zhu, X.-L. & Poon, W.-S. Evolution of intracranial aneurysm treatment: From Hunterian ligation to the flow diverter. *Surgical Practice* **15,** 16–20 (2011).

283. Wu, E., Liu, Y. & Liu, X. An Improved Study of Real-time Fluid Simulation on GPU: Research Articles. *Comput. Animat. Virtual Worlds* **15,** 139–146 (2004).

284. Wu, J., Wei, M., Li, Y., Ma, X., Jia, F. & Hu, Q. Scale-adaptive Surface Modeling of Vascular Structures. *BioMedical Engineering OnLine* **9,** 1–16 (2010).

285. Wyvill, B., McPheeters, C. & Wyvill, G. Animating Soft Objects. *The Visual Computer* **2,** 235–242 (1986).

286. Xu, X., Liu, W., Jin, X. & A, Z. S. *Sketch-based User Interface for Creative Tasks* in *Proc. of Asia Pacific Conference on Computer Human Interaction* (2002), 560–570.

287. Yang, L., Zhang, L., Dong, H., Alelaiwi, A. & Saddik, A. E. Evaluating and Improving the Depth Accuracy of Kinect for Windows v2. *IEEE Sensors Journal* **15,** 4275–4285 (2015).

288. Yureidini, A., Kerrien, E., Dequidt, J., Duriez, C. & Cotin, S. in *Proc. of Medical Image Computing and Computer-Assisted Intervention (MICCAI)* 553–560 (Springer, 2012).

289. Zhu, B., Iwata, M., Haraguchi, R., Ashihara, T., Umetani, N., Igarashi, T. & Nakazawa, K. *Sketch-based Dynamic Illustration of Fluid Systems* in *Proc. of the SIGGRAPH Asia Conference* (ACM, 2011), 134:1–134:8.